



LUND UNIVERSITY

The Many Facets of bicoid Gradient Formation in Drosophila

Cai, Xiaoli

2017

Document Version:
Publisher's PDF, also known as Version of record

[Link to publication](#)

Citation for published version (APA):
Cai, X. (2017). *The Many Facets of bicoid Gradient Formation in Drosophila*. [Doctoral Thesis (compilation), Faculty of Medicine]. Lund University: Faculty of Medicine.

Total number of authors:
1

General rights

Unless other specific re-use rights are stated the following general rights apply:
Copyright and moral rights for the publications made accessible in the public portal are retained by the authors and/or other copyright owners and it is a condition of accessing publications that users recognise and abide by the legal requirements associated with these rights.

- Users may download and print one copy of any publication from the public portal for the purpose of private study or research.
- You may not further distribute the material or use it for any profit-making activity or commercial gain
- You may freely distribute the URL identifying the publication in the public portal

Read more about Creative commons licenses: <https://creativecommons.org/licenses/>

Take down policy

If you believe that this document breaches copyright please contact us providing details, and we will remove access to the work immediately and investigate your claim.

LUND UNIVERSITY

PO Box 117
221 00 Lund
+46 46-222 00 00

The Many Facets of *bicoid* Gradient Formation in *Drosophila*

Xiaoli Cai



LUND
UNIVERSITY

DOCTORAL DISSERTATION

by due permission of the Faculty of medicine, Lund University, Sweden.
To be defended at the lecture hall ‘Segerfalksalen’ at BMC, Sölvegatan 19, Lund
on December 5th 2017 at 13:00.

Faculty opponent

Docent Anne Uv

Göteborg, Sweden

The Many Facets of *bicoid* Gradient Formation in *Drosophila*

Xiaoli Cai



LUND
UNIVERSITY

Coverphoto: Analysis of Bicoid movement in *Drosophila* embryos exposed to hypoxia and different drugs, and monitored using heat-maps.

Copyright: Xiaoli Cai

Faculty of Medicine
Department of Experimental Medical Science

Lund University, Faculty of Medicine Doctoral Dissertation Series 2017:178
ISBN 978-91-7619-560-4
ISSN 1652-8220

Printed in Sweden by Media-Tryck, Lund University, Lund 2017



Table of Contents

ABSTRACT	7
LIST OF PAPERS	9
ABBREVIATIONS	11
1 INTRODUCTION	13
1.1 Overview of the <i>Drosophila</i> life cycle	14
1.2 Overview of early <i>Drosophila</i> development	15
1.3 Genes that govern the <i>Drosophila</i> body plan	15
1.3.1 Maternal-effect genes	15
1.3.2 <i>bicoid</i> , a maternal effect gene determines the AP axis	17
1.3.3 Analysis of the Bcd sequence and its functional domains	18
1.3.4 The homeo-domain-less Bicoid protein (small Bicoid)	20
1.3.5 Large Bcd as a transcription and translation factor	20
1.4 The recent origin of <i>bcd</i> during insect radiation	22
1.5 Two controversial models of Bcd gradient formation	22
1.5.1 The SDD model and its paradox	22
1.5.2 The ARTS model	24
1.6 The cornerstones behind the ARTS model	25
1.6.1 The secondary structure of the <i>bcd</i> 3'UTR and its respective roles	25
1.6.2 <i>bcd</i> mRNA localization in oocytes	26
1.6.3 Cortical MT network at blastoderm embryos	27
1.7 MT organizing center	28
1.7.1 Golgi complex as an aMTOC	28
1.8 Other factors regulating <i>bcd</i> activity	30
1.8.1 Regulation of poly(A) tail length	30
1.8.2 Cyclins	31
1.8.3 Egg activation	32
1.8.4 Drug treatment of actin and MTs	32
1.8.5 Hypoxia in <i>Drosophila</i> embryos	35
1.9 The GAL4-UAS system for inducible gene expression in <i>Drosophila</i> research	35

2 PRESENT INVESTIGATIONS	37
2.1 Paper I: α Tubulin 67C and Ncd are essential for establishing a cortical microtubular network and formation of the <i>bicoid</i> mRNA gradient in <i>Drosophila</i>	37
2.2 Paper II: Cortical movement of Bicoid in early <i>Drosophila</i> embryos is actin- and microtubule-dependent and disagrees with the SDD diffusion model	38
2.3 Paper III: Genetic analysis of factors influencing <i>bicoid</i> gradient formation in <i>Drosophila</i>	40
2.4 Paper IV: Segmentation gene expression patterns in <i>Bactrocera dorsalis</i> and related insects: regulation and shape of the blastoderm and larval cuticle	41
3 ACKNOWLEDGEMENTS	43
4 REFERENCES	45
PAPER I-IV	54

ABSTRACT

In *Drosophila*, the Bicoid protein serves as paradigm as the first identified morphogen, whose concentration gradient provides the initial positional information in the anterior half of the embryo. There, it differentially activates segmentation genes, in particular the gap genes. Insofar, there are two mainly prevailing models to explain how the Bicoid protein concentration gradient forms: 1) the SDD (Synthesis, Diffusion and Degradation) model proposing that the *bicoid* mRNA is located at the anterior pole of the embryo at all times. The mRNA then serves as a source for translation of the Bicoid protein, followed by diffusion of the protein to the posterior, combined with uniform degradation. 2) the ARTS (Active RNA Transport and Synthesis) model proposing that the mRNA is transported at the cortex along microtubules to form the mRNA gradient, which serves as template for the production of Bicoid. Hence, there are clear differences between the SDD and the ARTS model.

To corroborate the ARTS model, we used several approaches: 1) we investigated on the transport mechanism of *bicoid* mRNA. To this end, we detected a cortical microtubular network that was present in the anterior half of the early *Drosophila* embryos, which was only active during metaphase and early anaphase. We found that *αTubulin67C* is crucial for establishing the cortical microtubular network and that cortical *bicoid* mRNA transport is compromised in *αTubulin67C* mutants. We defined a motor protein, *nonclaret disjunctional (ncd)* to be a critical motor for *bicoid* mRNA transport and demonstrated that *ncd* interacts genetically with *αTubulin67C*. This data suggested that *ncd* required *αTubulin67C* for cortical *bicoid* mRNA transport, also demonstrated by colocalization of *αTubulin67C* with Ncd. 2) we chose one special fly stock that expresses 3 times more Bicoid and treated the embryos with hypoxia to challenge the validity of the SDD model. Our data showed that under hypoxic conditions, the Bicoid protein did not move into the interior, but rather moved along the cortex, even during long exposures. 3) Combining hypoxia with drugs that disturb the formation of microtubules, we could observe interior movement of Bicoid, while the mRNA strictly remained at the tip. When actin was compromised, little cortical Bicoid movement was observed. This data suggested that Bicoid requires an intact cytoarchitecture for cortical movement. Finally, we revealed several factors that played distinct roles in

bicoid mRNA gradient formation, including *trans*-Golgi proteins, the poly(A) polymerase Wispy, CyclinB and egg-activation genes.

Apart from studying the mechanism of *bicoid* gradient transport, we explored the expression patterns of *bicoid*-downstream genes in *Bactrocera dorsalis*, which is the oriental fruit fly with high relatedness to *Drosophila*, however lacking *bicoid*. When comparing the segmentation gene expression patterns between *Drosophila* and *Bactrocera*, *bicoid* downstream genes showed a strong shift of expression towards the posterior suggesting that the positioning of the segmental anlagen along the anterior-posterior axis changed during evolution.

LIST OF PAPERS

This thesis is based on the following papers, which are referred to in the text with their Roman numerals.

- I Fahmy, K., Akber, M., **Cai, X.**, Koul, A., Hayder, A. and Baumgartner, S. (2014) **AlphaTubulin 67C and Ncd are essential for establishing a cortical microtubular network and formation of the *bicoid* mRNA gradient in *Drosophila*.** PloS One. 2014 Nov 12; 9(11): e112053.
- II **Cai, X.**, Spirov, A., Akber, M. and Baumgartner, S. (2017). **Cortical movement of Bicoid in early *Drosophila* embryos is actin- and microtubule-dependent and disagrees with the SDD diffusion model.** PloS One 2017 Oct 3; 12(10):e0185443.
- III **Cai, X.**, Fahmy, K. and Baumgartner, S. **Genetic analysis of factors influencing *bicoid* gradient formation in *Drosophila*.** (manuscript: deleted as per Lund University library request)
- IV Suksuwan, W., **Cai, X.**, Ngernsiri, L., Baumgartner, S. (2017) **Segmentation gene expression patterns in *Bactrocera dorsalis* and related insects: regulation and shape of the blastoderm and larval cuticle.** Int. J. Dev. Biol. 61(6-7): 439-450. doi: 10.1387/ijdb.160277sb.

ABBREVIATIONS

aa	amino acid
aMTOC	acentriolar microtubule organizing center
AP	anterior-to-posterior
<i>asl</i>	<i>asterless</i>
<i>bcd</i>	<i>bicoid</i>
bp	base pair
<i>cnn</i>	<i>centrosomin</i>
<i>chb</i>	<i>chromosome bow</i>
CLASP	cytoplasmic linker-associated protein
CNS	central nervous system
<i>dpp</i>	<i>decapentaplegic</i>
DV	dorsal-to-ventral
<i>ems</i>	<i>empty spiracles</i>
<i>en</i>	<i>engrailed</i>
<i>eve</i>	<i>even-skipped</i>
FGF	fibroblast growth factor
<i>hb</i>	<i>hunchback</i>
<i>Kr</i>	<i>Krüppel</i>
MT	microtubule
MTOC	microtubule organizing center
<i>nos</i>	<i>nanos</i>
nt	nucleotide
<i>osk</i>	<i>oskar</i>
<i>otd</i>	<i>orthodenticle</i>
PA	posterior-to-anterior
PAP	Poly(A) polymerase
PCM	pericentriolar material
PEST	proline (P), glutamic acid (E), serine (S) and threonine (T)
RNP	ribonuclear protein
SID	self-inhibitory domain
<i>spd-2</i>	<i>spindle defective 2</i>
TGN	<i>trans</i> -Golgi network
γ -TURC	γ -tubulin ring complex
wg	wingless

1 INTRODUCTION

“Developmental biology deals with the process by which the genes in the fertilized egg control cell behavior in the embryo and so determine its pattern, its form, and much of its behavior... differential gene activity controls development” (Wolpert, 1998).

Mice, frogs, zebrafish, *C. elegans* or *Drosophila melanogaster*? Each idealized animal model has its own strength and weakness. Critics have mainly questioned whether those animal models are qualified to represent the rest of the animal species, since the requirements of those animals as study models were subject to the bias of their life cycles and developmental advantage.

Thanks to the pioneering genetic studies of Thomas Hunt Morgan beginning in 1910, the history of using *Drosophila* as an animal organism in modern biological sciences spans a century. Executed as a pilot study before sequencing the human genome, *Drosophila* was the first complex animal to have its entire genome sequenced (Adams et al., 2000). Regardless of the different developmental patterns, the highly conserved genes and regulatory mechanisms that *Drosophila* shares among all the animals draw more scientific attention (Reiter et al., 2001). In *Drosophila*, there are approximately 15,600 genes within a genome of 144 million base pairs. The genes associated with known diseases that range from the central nervous system to cardiovascular diseases, from cancer to metabolic disorders, share nearly 77% similarity with their human counterparts (Kornberg and Krasnow, 2000; Pandey and Nichols, 2011). For instance, the major components of the Ras signaling pathway in the fly visual system have been found to be highly conserved in mammalian cells (Cagan, 2009; Nagaraj and Banerjee, 2004), which contribute the research of cancer biology. As a model for neurodegenerative diseases, when the CNS of the flies was transfected with Parkinson’s disease-associated genes, flies displayed similar symptoms with those from human Parkinson’s patients (Feany and Bender, 2000; Whitworth, 2011).

1.1 Overview of the *Drosophila* life cycle

The life journey of *Drosophila* begins with the fertilized egg, which undergoes its embryogenesis within the first 24 hours. Afterwards, a first instar larva hatches out of the egg. This larva eats to increase its size during the next 4.5 days, while going through two more instars. At day 5.5, the larva forms the pupa by secreting a pupal case. During the pupal stage, a significant phase called metamorphosis takes place resulting in the formation of the adult structures. The last step is the hatching of the adult fly, which completes the life cycle. The life cycle of *Drosophila* takes 9 days at 25° C and is demonstrated in Fig. 1.

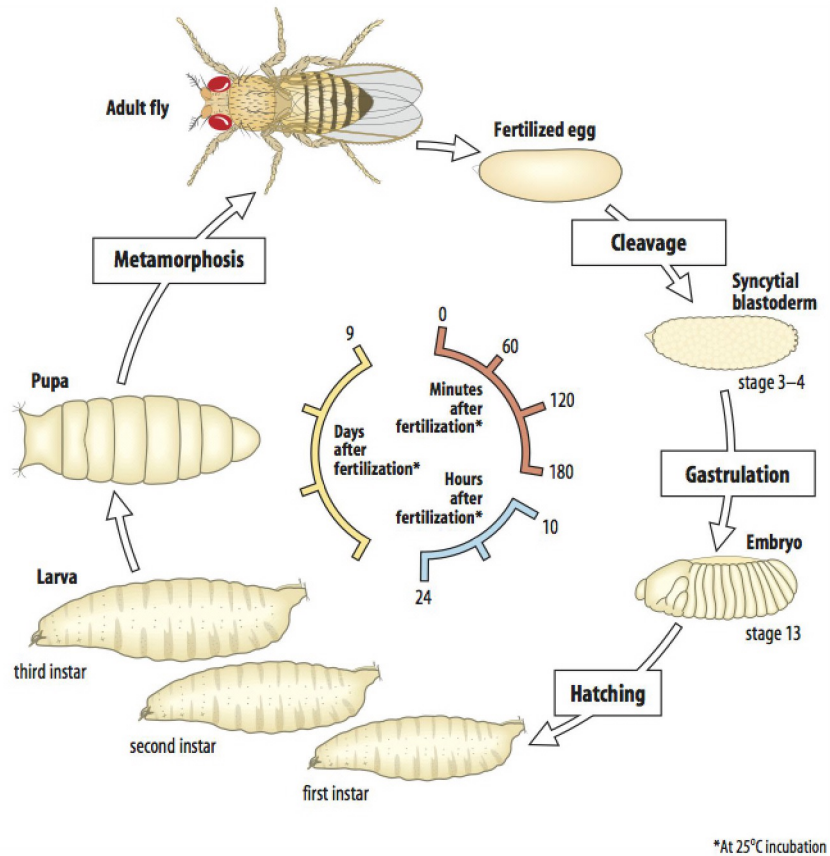


Fig. 1 Life cycle of *Drosophila melanogaster*

The life cycle of the fruit fly takes approximately 9 days at 25° C. Image taken from the book "Principles of Development", Wolpert et. al. , 5th ed. (2015), Sinauer, ISBN 978-0-19-967814-3

1.2 Overview of early *Drosophila* development

The early stage of *Drosophila* embryogenesis is represented by 14 nuclear cycles during the first 3 hours, in the absence of cytokinesis. The first nuclear cycle (nc) occurs after the fusion of the male and female pronuclei, whereby the syncytial cycles are initiated. The first 7 nuclear divisions occur at the center along the anterior-posterior axis. From the 8th division on, the nuclei start to migrate toward the periphery of the embryos. During the period of nc 9, approximately five nuclei move to the posterior pole and become enveloped by cell membranes. These give rise to pole cells that later will become the gametes of the adult. The remaining nuclei distribute along the cortex from nc 10 on, and complete the last 4 divisions. During the 14th nuclear cycle, cell membranes encapsule the nuclei, forming the cellular blastoderm. Fig. 2 shows the cleavage stages of *Drosophila* embryos.

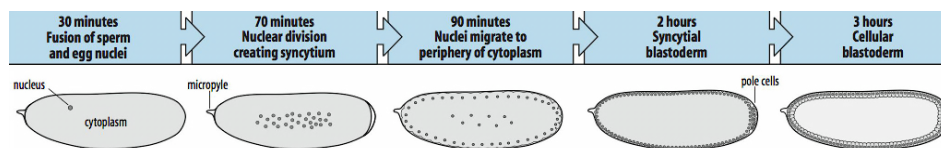


Fig. 2 *Drosophila melanogaster*: early embryogenesis

After the first 3 hours and 14 nuclear divisions, the embryo is at the cellular blastoderm stage, which contains approximately 6,000 nuclei at the embryonic surface. Image taken from the book "Principles of Development", Wolpert et. al. , 5th ed. (2015), Sinauer, ISBN 978-0-19-967814-3

1.3 Genes that govern the *Drosophila* body plan

The commitment of *Drosophila* body patterning consists of two steps: specification and determination. The specification of the cell fate depends on signals provided by protein gradients that originate from maternal genes, and can still be influenced in response to other cells. The specified cell fate is transformed into an irreversible determination by zygotic genes, categorized as segmentation genes (gap genes, pair-rule genes, and segment polarity genes), and becomes cell-intrinsic.

1.3.1 Maternal-effect genes

(Marlow, 2010) describes: "Maternal genes are those genes whose products, RNA or protein, are produced or deposited in the oocyte or are present in the fertilized egg or embryo before expression of zygotic genes is initiated." During the early

embryonic stage in *Drosophila*, maternal genes that are dumped from nurse cells to oocytes, are responsible for programming the early embryogenesis, specifically in regards to the formation of the body axes: the AP and DV axes (Fig. 3).

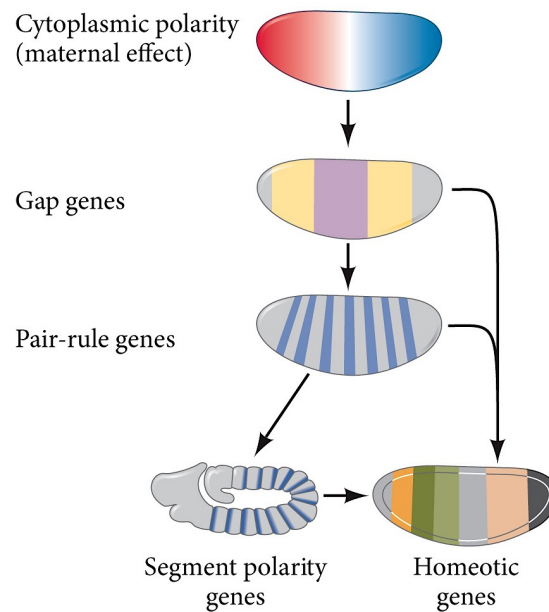


Fig. 3 Maternal effect genes on body pattern establishment

The establishment of the body pattern is subject to products of the maternal genes that form gradients and regions of morphogenetic proteins. Positional information provided by these morphogens activates a series of zygotic genes. The first ones are the gap genes, whose mutations cause body portions to disappear. The gap genes then enable the expression of pair-rule genes, which regulate the formation of body segments. The segment polarity genes decide the cells fate in each parasegment. Together, the interactions of all those genes regulate the homeotic selector genes and decide upon the characteristic structures of each segment. Image taken from the book “Developmental Biology”, Gilbert and Barresi, 11th ed. (2016), Sinauer, ISBN 978-1605354705

One of the most important maternal genes is *bicoid* (*bcd*), the first identified morphogen found in a maternal-effect mutation screen (Frohnhof et al., 1986). Bcd is known to affect multiple maternal and zygotic genes by initiating expression patterns in relation to the AP axis (Fig. 4).

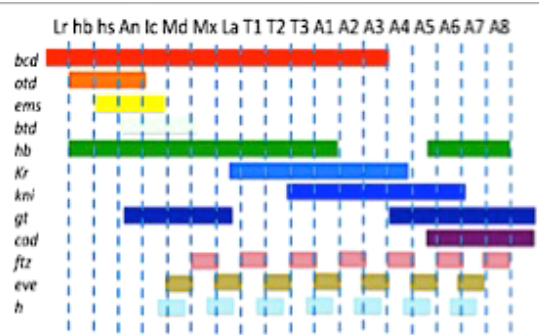


Fig. 4 Segmental cascade initiated by maternal genes along the AP axis

Once the Bcd morphogen provides pattern information, the downstream genes are activated sequentially and spatially. Segments: Lr, labral; hb, preantennal domain (head blob of wingless); hs, preantennal domain (head spot of engrailed); An, antennal; lc, intercalary; Md, mandibular; Mx, maxillar; La, labial; T1-3, thoracic segments; A1-9, abdominal segments. bcd, bicoid; otd, orthodenticle; ems, empty spiracles; btd, bottonhead; hb, hunchback; Kr, Krüppel; kni, knirps; gt, giant; cad, caudal; ftz, fushi tarazu; eve, even-skipped; h, hairy.

Image credit: Adapted from Dmitri Papatsenko

(<https://bspace.berkeley.edu/access/content/user/247388/index.html>)

1.3.2 *bicoid*, a maternal effect gene determines the AP axis

bcd belongs to the homeobox gene family and stems from an ancestral Hox3 gene. An interspecific comparison between *D. melanogaster* and *D. pseudoobscura* was carried out by (Seeger and Kaufman, 1990) identifying conserved functional domains of *bcd* in *Drosophila*. In the past 30 years, numerous studies on Bcd have been carried out at the molecular, cellular and physical level, all devoted to uncover the DNA and protein structure, and to determine the fundamental roles and the mechanism of Bcd. Many studies have provided experimental data that Bcd was the first true morphogen, playing a role via its protein concentration gradient along the AP axis during *Drosophila* embryonic development (Fig. 5) (Crauk and Dostatni, 2005; Little et al., 2013; Porcher and Dostatni, 2010; Wieschaus, 2016).

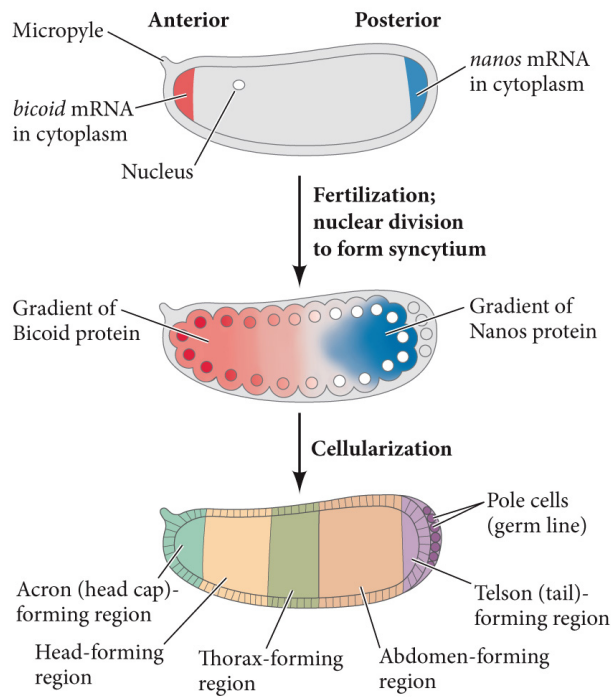


Fig. 5 Genetic pathways of *bcd* to form the AP axis

In oogenesis, *bcd* mRNA is synthesized in the nurse cells, then dumped into the oocyte and finally transported to the anterior tip. After egg activation, *bcd* mRNA is translated into proteins during the syncytial blastoderm. With the positional signal provided from the Bcd protein gradient, the anterior zygotic genes are up- or down-regulated to form the AP axis. Image taken from the book “Developmental Biology”, Gilbert and Barresi, 11th ed. (2016), Sinauer, ISBN 978-1605354705

1.3.3 Analysis of the Bcd sequence and its functional domains

(Berleth et al., 1988) was the first report that determined the sequence of *bcd*. The study also identified a shorter isoform containing only exons 1 and 4, which arises through alternative splicing. Compared to the length of the current known Bcd (large Bcd), the product of the 1.4 kb isoform was later designated ‘small Bicoid’ (Fig. 6B).

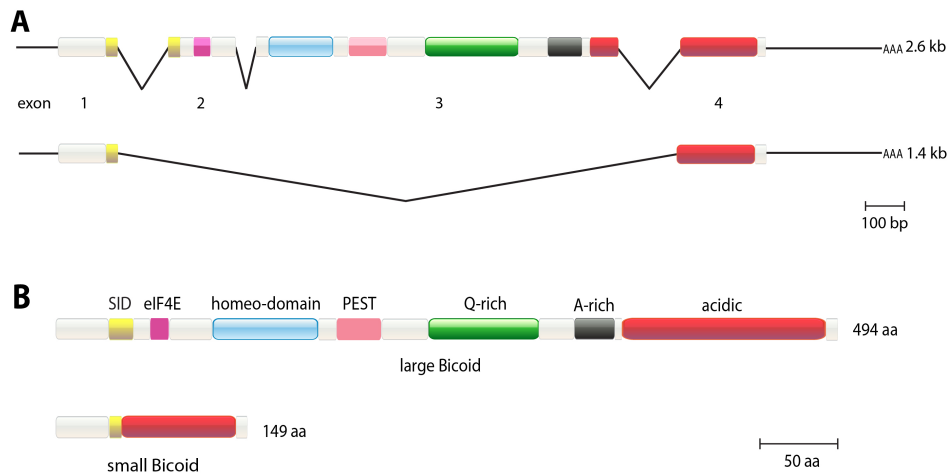


Fig. 6 Gene structure and functional domains of Bicoid

Compared to the large Bcd (494 aa), the splice event generates a 1.4 kb fragment that loses the activity of the SID domain (self-inhibitory domain, yellow), the homeo-domain (light blue), the PEST domain (pink), the Q-rich (green), the A-rich (dark) and other domains with unknown functions. Note that the majority of the acidic domain (red) is maintained in small Bcd. Image drawn by Cai, X.

The Bcd protein (494 aa) is divided into 7 independent domains (Fig. 6B). The main functional domain of Bcd, also called the homeo-domain, resides in the amino-terminal part and is responsible for facilitating its morphogenic activity by binding DNA or RNA in a sequence specific manner (Baird-Titus et al., 2006; Rivera-Pomar et al., 1996). Homeo-domains are evolutionarily-conserved domains encompassing exactly 60 amino acids that regulate developmental processes during embryonic pattern formation in many multicellular organisms. Interestingly, the Bcd homeo-domain is considered to be unique. (Baird-Titus et al., 2006; Dave et al., 2000) demonstrated that the homeo-domain of Bcd contains not only a lysine residue at the critical position 50 (K50), but also has an arginine residue at position 54 (R54). With this flexibility, *bcd* is enabled to re-program its recognition codes corresponding to consensus or non-consensus target-binding sites, and alternates its role as a transcriptional and translational regulator. Further functional and structural studies demonstrated that the helix 3 of Bcd adopts multiple conformations when bound to different targets. Further, it was proposed that the conformational heterogeneity of the homeo-domain could play an important role in admitting Bcd to read its various binding zones (Adhikary et al., 2017; Dave et al., 2000).

Immediately after the homeo-domain, a domain between aa 170 and 203 constitutes a PEST domain, which regulates the degradation of Bcd and results in a half-time of Bcd shorter than 30 min (Driever and Nusslein-Volhard, 1988).

Approximately 80 aa upstream of the carboxy-terminal end of Bcd, an acidic motif was found, which was also identified as the main domain of small Bcd. Studies of (Driever and Nusslein-Volhard, 1989; Struhl et al., 1989) concluded that the acidic domain was not required for mediating the transcriptional activity of Bcd, but to maximize *bcd* activity.

1.3.4 The homeo-domain-less Bicoid protein (small Bicoid)

The small Bicoid (smBcd) lacks the homeo-domain, the PEST domain, the Q- and A-rich domain as well as other domains of unknown function, and is thought to modulate the transcriptional activity of the main Bcd protein (large Bcd) (Zhao et al., 2003). It has been reported that the other important maternal gene *osk* in *Drosophila* encodes two protein isoforms, termed long Osk and short Osk (Ephrussi and Lehmann, 1992; Hurd et al., 2016; Markussen et al., 1995; Vanzo et al., 2007). Both isoforms together regulate the downstream genes at the posterior end, and determines the germ cell fate and the posterior polarity. Between the two, the short Osk is part of the germ plasm and is indispensable for the formation of functional primordial germ cells. However, in contrast to Osk, there is sparse structural and functional information on smBcd, because this isoform was largely neglected.

Current studies reveal that smBcd lacks the most important functional domain, the homeo-domain. Moreover, the splice event leads a truncated SID domain (self-inhibitory domain, see Fig. 6B) that contains a particular 10 amino acid stretch identified for modulating the transcriptional activity of large Bcd (Zhao et al., 2002). Interestingly, exon 1 of smBcd ends exactly within the 6 amino acids important for this function. Mutational studies have shown that, by altering the last 4 amino acids of the SID in the large Bcd (located on exon 2 and thus absent in small Bcd), the transcriptional activity of Bcd is lowered by a factor of 100 in CAT-assays (Zhao et al., 2003), indicating a particular function ascribed to smBcd.

1.3.5 Large Bcd as a transcription and translation factor

Due to its flexible binding ability to both DNA and RNA, scientists have identified more than 40 zygotic target genes and 66 enhancers that are directly mediated in a Bcd-dependent manner (Chen et al., 2012; Driever and Nusslein-Volhard, 1989; Howard and Struhl, 1990; Kantorovitz et al., 2009; Riddihough and Ish-Horowicz,

1991; Struhl et al., 1989; Xu et al., 2014). Bcd regulates its target genes in both positive and negative ways. One well-studied example is the establishment of the expression pattern of *hunchback* (*hb*). *hb* contains at least 8 Bcd binding sites and highly depends on Bcd to maintain its domain of transcriptional activity in the anterior half of the embryo (Driever and Nusslein-Volhard, 1989; Lucas et al., 2013). (Niessing et al., 1999) revealed that the PEST motif of Bcd participates in the translational repression of *caudal* (*cad*) through binding to the 3' untranslated region (3'UTR) of the *cad* mRNA in the anterior part of the embryo. Furthermore, (Rodel et al., 2013) added that Bcd binds to the *cad* 3'UTR together with the help of the miR-2 microRNA. (Lasko, 2012) described that the Nanos gradient along the PA axis is achieved through translational-repressing activity of Bcd. Fig. 7 shows the interaction domains between Bcd and its target genes (McGregor, 2005).

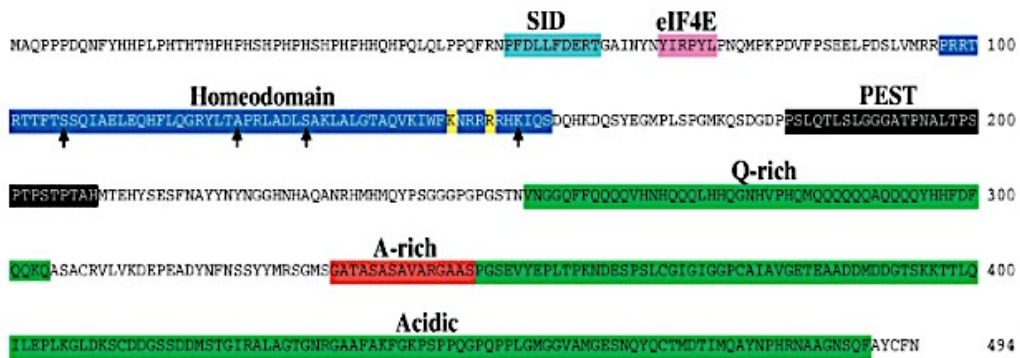


Fig. 7 The functional domains of Bcd

The homeo-domain is shown in dark blue with the lysine and arginine residues at positions 50 and 54, respectively, and highlighted in yellow. Amino acids involved in cooperative Bcd binding are indicated by arrows. The SID, which can reduce the transcriptional activity of Bcd is shown in cyan. The eIF4E-binding domain (shown in purple) blocks the initiation of the translation complex at the 5'-cap of *cad* transcripts. The PEST domain (shown in black) also contributes to the repression of *cad* translation as well as in transcriptional activation and Ubiquitin-dependent protein degradation. The glutamine (Q)-rich transcriptional activation domain (shown in green) can be down-regulated by the alanine (A)-rich transcriptional repression domain (shown in red). The C-terminal acidic region (shown in green) is also a transcriptional activation domain. Image from (McGregor, 2005).

1.4 The recent origin of *bcd* during insect radiation

As a member of the homeobox genes, *bcd* was considered to be as conserved as other homeobox genes in animal evolution. However, *bcd* homologs are rarely found in other species, apart from *Drosophila melanogaster*, and were found only in the family of dipterans, such as *Megaselia* (Stauber et al., 1999; Stauber et al., 2000), *Musca* and *Lucilia* (Shaw et al., 2001). On this basis, it was suggested that *bcd* evolved recently and was derived from the ancestral *Hox3* gene during insect evolution (Stauber et al., 1999; Stauber et al., 2002). This suggestion is peculiar, leading to questions of how the *bcd* gene evolved and adopted its unique function in organizing its patterning activity along the AP axis, and how other insects would execute this task without *bcd*.

1.5 Two controversial models of Bcd gradient formation

Regardless of its function as a transcriptional or a translational factor, the Bcd protein gradient along the AP axis is an important information source at the early stage of embryonic development. The mechanisms behind the establishment of this concentration gradient have attracted the attention of scientists across many disciplines. At present, there are two opposing, but well investigated models.

1.5.1 The SDD model and its paradox

Since its discovery in 1988, the Bcd gradient has been analyzed extensively by various methods (Ephrussi and St Johnston, 2004). By utilizing various antibodies against the Bcd protein, an anterior exponential gradient reaching > 50% egg length was detected (Driever and Nusslein-Volhard, 1988). To explain the occurrence of the gradient, a simple cellular mechanism was put forward: Bcd is synthesized from a local source of mRNA, followed by diffusion and uniform degradation. This mechanism would generate non-uniform distribution of Bcd along the AP axis to regulate pattern formation (Driever and Nusslein-Volhard, 1988; Fradin, 2017; Gregor et al., 2007) (Fig. 8), also termed the SDD model (synthesis, diffusion and degradation). As one member of the morphogen family, it was reasonable to propose diffusion as the mode of transport of the Bcd (Turing, 1952). In fact, several well-studied morphogen gradients including those of Dpp, Wg and Fgf8, largely satisfy the principle of the diffusion model (Grimm et al., 2010; Kicheva et al., 2007).

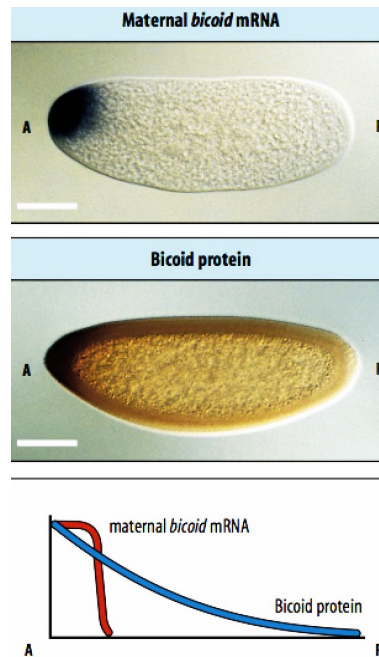


Fig. 8 The SDD model

Image taken from the book “Principles of Development”, Wolpert et. al. , 3th ed. (2007), Sinauer, ISBN 978-0-19-927537-3

Even though the SDD model can be extended to several other morphogens, the model recently encountered a critical challenge. Combining the diffusion equation to estimate the diffusion coefficient (D) of Bcd and the framework of SDD model, it was expected that D should be approximately $2 \mu\text{m}^2/\text{s}$ to reach a stable concentration along the cortex within 90 minutes. However, results from Fluorescence Recovery After Photobleaching (FRAP) identified that the $D_{(FRAP)}$ was stable at approximately $0.3 \mu\text{m}^2/\text{s}$, which is at least one order of magnitude lower than expected (Gregor et al., 2008; Gregor et al., 2007). This fact questions the possibility that the gradient could be established so rapidly (i. e. within 90 minutes).

(Abu-Arish et al., 2010; Porcher et al., 2010) measured the Bcd coefficient using Fluorescence Correlation Spectroscopy (FCS) and found that the diffusion coefficient ($D_{FCS} \sim 7 \mu\text{m}^2/\text{s}$) was too high to be consistent with the SDD diffusion model. In their studies, D_{FRAP} was measured as well, and parameters were close to $1 \mu\text{m}^2/\text{s}$. (Sigaut et al., 2014) explained the results from both diffusion efficient (D_{FCS} and D_{FRAP}) by proposing that the results could be compatible, if one considers the interaction of Bcd with slowly-moving binding sites.

Already in 1986, the presence of an mRNA gradient had been shown (Frigerio et al., 1986), adding further to the inconsistencies within the SDD model. However, this report lacked a detailed analysis and hence the results were neglected for at least two decades. However, research has resumed once again in recognition of the importance of the mRNA gradient along the anterior-posterior axis.

1.5.2 The ARTS model

In 2009, (Spirov et al., 2009) published a seminal article demonstrating that the mRNA itself forms a concentration gradient along the embryonic cortex (Fig. 9), in accordance with the previous findings of the existence of a mRNA gradient 3 decades ago (Frigerio et al., 1986). This mRNA gradient decrease exponentially from the anterior pole of the embryo at the syncytial blastoderm stage and at all stages precisely parallels that of the Bcd protein distribution.

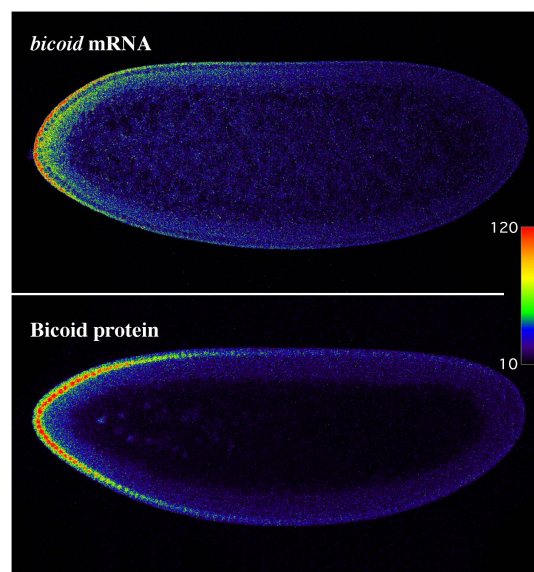


Fig. 9 The *bcd* mRNA (top) and Bcd protein gradient (bottom).

Image taken from the book "Developmental Biology", Gilbert and Barresi, 11th ed. (2016), Sinauer, ISBN 978-1605354705

In order to achieve the rapid transport of the *bcd* mRNA within the time limitations, active and fast transport of the mRNA along a cortical network of microtubules (MTs) was proposed, a model referred to as the ARTS model (active

RNA transport and synthesis (Spirov et al., 2009). The ARTS model differs dramatically from the SDD model and provides a reasonable explanation for the paradoxical results, that the diffusion of the Bcd protein was too slow by one order of magnitude (Gregor et al., 2007).

1.6 The cornerstones behind the ARTS model

1.6.1 The secondary structure of the *bcd* 3'UTR and its respective roles

How is the active transport of the *bcd* mRNA achieved at the molecular level? It is presumed that the *bcd* mRNA localization is highly dependent on its 3'UTR, which folds into a particular secondary structure showing three arms (Fig. 10). Two arms, domains IV and V, are responsible for the localization of the mRNA by binding to Staufen, a RNA-binding protein (Ferrandon et al., 1994). The third arm, domain III, is responsible for dimerization (Wagner et al., 2004). Approximate 40 nt downstream of the stop codon, a degradation motif was identified (Surdej and Jacobs-Lorena, 1998) providing a tool to regulate the amount of *bcd* mRNA. The Staufen-mRNA complex, along with other proteins, is thought to bind Dynein or Kinesin, two motor proteins, which allow rapid movement of the complex along microtubules (MTs). In essence, it is this large *bcd* ribonuclear protein (RNP) complex that migrates along MTs at the cortex of the embryo to form the *bcd* mRNA gradient.

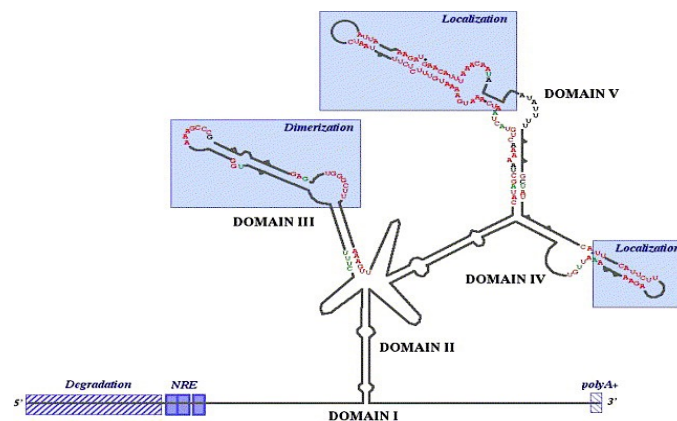


Fig. 10 Secondary structure of the *bcd* 3' UTR

The structure shows the elements for localization, dimerization and degradation. Image from (Brunel and Ehresmann, 2004)

1.6.2 *bcd* mRNA localization in oocytes

In the *Drosophila* oocyte, the process for *bcd* mRNA microtubule-dependent localization was demonstrated (Chang et al., 2011; Khuc Trong et al., 2015; Stephenson and Pokrywka, 1992). In the oocyte, at stage 10b and onwards, the γ -tubulin ring complex (γ -TURC) as the microtubule organizing center (MTOC) assembles microtubular tracts for *bcd* mRNA transportation (Weil et al., 2006). MTs are nucleated or anchored at the cortex and spread from the periphery into the interior. More importantly, cortical MTs follow a decreasing concentration gradient along the cortex, consistent with the distribution of the *bcd* mRNA (Weil et al., 2010). According to their model (Fig. 11) and supported by experimental data, distinct roles of Staufen and Dynein were proposed during late *Drosophila* oogenesis. It was described that both Staufen and Dynein were closely associated with the *bcd* mRNA to form the *bcd* RNP. The *bcd* RNP moved along specialized MTs at the anterior pole, maintained by the cortical actin cytoskeleton. Together, localization of *bcd* mRNA along the embryonic cortex is a complex process including transacting factors (e.g. Staufen), molecular motor proteins (e.g. Kinesin and Dynein) and cytoskeletal components (e.g. microtubules) that remodel extensively during the lifetime of the mRNA.

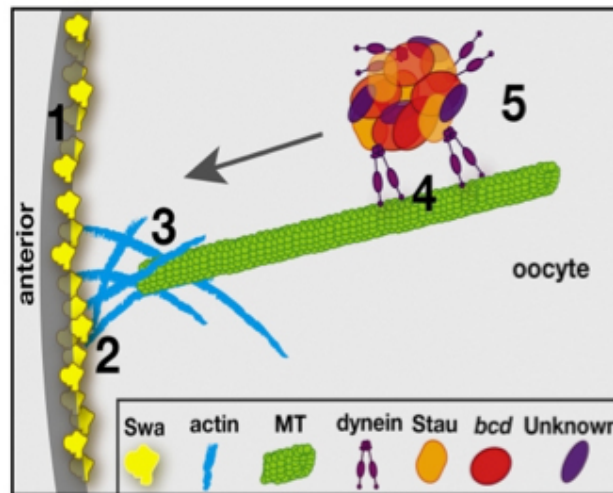


Fig. 11 Model for *bcd* mRNA localization in late oogenesis

MTs (green) are localized by actin (blue), and *bcd* mRNA (red) moves along the MTs with the help of dynein (purple) as a RNP complex. Image from *Development* 137, 169-176 (2010)

More recent studies suggested that the anchoring of the *bcd* mRNA after being transported to the anterior was not MT-dependent. (Trovisco et al., 2016)

depolymerized microtubules by incubating the embryos in the presence of Colcemid. However, a large percentage of the *bcd* mRNA remained stable. In addition, microtubules were stained with the minus-end binding protein Patronin. The result showed that the *bcd* mRNA and the MT minus-ends do not overlap, even though both proteins are strongly localized at the anterior pole of the oocyte. Considering all these significant findings, it was proposed that only the delivery of *bcd* mRNA towards the anterior pole needed MTs as tracts. However, as for anchoring the *bcd* mRNA, MTs would be required to cooperate with other components to specifically anchor the RNA along the anterior cortex.

The mechanisms of *bcd* mRNA transport during oocyte development shed promising light on how the Bcd protein gradient formation could occur during early *Drosophila* embryogenesis. Most importantly, however, it should be taken into account that all MT arrays are disassembled into short and un-oriented MT filaments through the late stage of oogenesis (Steinhauer and Kalderon, 2006; Theurkauf and Hawley, 1992; Theurkauf et al., 1992). This means that the embryo after fertilization needs to build up a fresh MT network.

1.6.3 Cortical MT network at blastoderm embryos

In contrast to the wealth of information on the *bcd* mRNA transport during oogenesis, information in regards to the cortical MT network for *bcd* mRNA transportation during embryogenesis was sparse. Most reports focused on detecting how the MTs cooperate with other microfilaments such as actin for the development of the cytoskeleton during the syncytial blastoderm (Karr and Alberts, 1986; McCartney et al., 2001; Rodriguez et al., 2003; Sullivan and Theurkauf, 1995).

(Fahmy et al., 2014) detected a peculiar cortical MT network in the anterior half of early nuclear cycle 1-6 embryos. The study also showed that when the cortical MT network or the motor protein was compromised, e.g. through mutations in the respective gene, *bcd* mRNA transport was not established along the cortex anymore.

Since it was shown that the cortical MT network is indispensable to the formation of *bcd* mRNA gradient during early embryogenesis, an important question comes up: where are the cortical MT arrays nucleated?

1.7 MT organizing center

The centrosome is the conventional microtubule organizing center (MTOC) in cells and is mainly involved in the process of meiosis and mitosis. MT arrays organized from the centrosome are astral, whose minus-ends are embedded in the centrosome, while the highly dynamic plus-ends stretch outwards.

It has been shown that MT arrays can also be nucleated from centrosome-independent centers, termed acentriolar microtubule organizing centers (aMTOCs) (Baumbach et al., 2015; Moutinho-Pereira et al., 2009). The MT arrays that are assembled by aMTOCs are asymmetric. (Yvon and Wadsworth, 1997) found non-centrosomal acting MTs that emanated from the peripheral lamella of human kidney cells that behaved dynamically at each end. (Khodjakov et al., 2000) deactivated one or two centrosomes, respectively, and still could find largely functional MTs. (Nguyen et al., 2011) showed that in *Drosophila* neurons, MT arrays were formed independently of the centrosome and did not require centrosomes for maintenance of those MTs. In *Drosophila* somatic cells, monopolar spindle MTs were assembled with the assistance of aMTOCs, but without recruitment of centrosomal- and chromatin-MTs (Mottier-Pavie et al., 2011). Likewise, in others specialized cell types, a number of aMTOCs have been detected, among these are melanosomes in the pigments cells (Malikov et al., 2004), the plasma membrane of polarized epithelial cells (Reilein and Nelson, 2005), and nuclear envelope in myotubes (Bugnard et al., 2005). However, studies have showed that MT nucleation of aMTOC to a certain degree relies on the known centrosomal pericentriolar material (PCM) with the assistances of Asterless (Asl) serving as a member of mother centrioles. In parallel, Centrosomin (Cnn) and Spindle defective 2 (Spd-2) serve as PCM scaffolding proteins (Baumbach et al., 2015).

1.7.1 Golgi complex as an aMTOC

In addition to the above, numerous reports showed that MT-assembling structures could emanate from Golgi membranes (Chabin-Brion et al., 2001; Sanders and Kaverina, 2015; Stephens, 2012; Zhu and Kaverina, 2013) (Fig. 12). A role of MTs nucleated at the Golgi complex was ascribed to help to maintain the integrity of the Golgi stacks (Miller et al., 2009), and stabilizing the position of the Golgi complex within cells (Derby et al., 2007; Efimov et al., 2007).

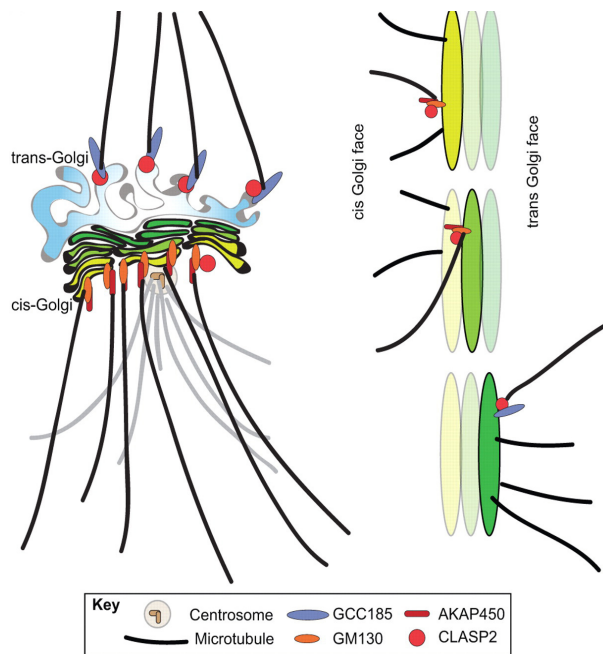


Fig. 12 Golgi as an aMTOC.

Golgi complex is as an aMTOC to nuclear MTs via both *cis*- and *trans*-golgins. Image from (Stephens, 2012)

Image credit: (Stephens, 2012)

The golgins, a family of large coiled-coil proteins thought to function as tethers are associated with the cytoplasmic surface of the Golgi complex (Nozawa et al., 2005). dGM130 and dGM210 are localized within the *cis*-Golgi, while the GRIP domain-containing golgins (dGolgin-97, dGolgin-245, dGCC88, and dGCC185, all decorate the surface of the *trans*-Golgi network (TGN). Most of them have binding sites for the Rab family GTPases for the purpose of anchoring to the Golgi membranes (Sinka et al., 2008; Yadav and Linstedt, 2011), see also Table 1.

Table 1 Golgi binding sites of GTPases

Proteins	Localization	GTPases	Interactions
dGM130	<i>cis</i> -Golgi	Rab1, Rab30	
dGMAP210	<i>cis</i> -Golgi	Rab2	MTs
dGolgin-97	<i>trans</i> -Golgi	Rab6, Arl1/3	
dGolgin-245	<i>trans</i> -Golgi	Rab2, Arl1/3	
dGCC88	<i>trans</i> -Golgi	Rab6, Arl1/3	
dGCC185	<i>trans</i> -Golgi	Rab2, Arl1	MTs

In nocodazole wash-out hepatic cells, Golgi-dependent MTs are reconstituted and anchored, together with the participation of γ -tubulin (Chabin-Brion et al., 2001). Later, it was shown that a *cis*-Golgi MT binding protein, GMAP-210 was involved in tethering γ -tubulin to the Golgi membranes in mammalian cells (Rios et al., 2004). GM130 captures nascent MTs directly with the exception of GMAP-210 (Wei et al., 2015). Following up with prior research, (Efimov et al., 2007; Goud and Gleeson, 2010) subsequently demonstrated that the TGN plays an important role in both MT recruitment and stabilization. They found that on the surface of TGN, a MT plus-end binding protein, cytoplasmic linker-associated protein (CLASP), is trapped to the TGN and which recruits the MTs, with assistance of dGCC185.

Apart from the Golgi complex as a potent aMTOC in *Drosophila* embryos, the MT minus-end protein, Patronin, was reported to be involved in capping MTs. This finding by (Goodwin and Vale, 2010) showed that purified Patronin was sufficient to cap and protect the minus-end of MTs against depolymerization in *Drosophila* S2 cells. In Patronin-deficient cells, free MT arrays were found moving through the cytoplasm. (Nashchekin et al., 2016; Takeichi and Toya, 2016) elucidated that in *Drosophila* oocytes, Patronin was located along the cortex by interacting with a cortical anchor, named ‘Short stop’, for the recruitment of noncentrosomal MTs to establish the AP axis.

1.8 Other factors regulating *bcd* activity

1.8.1 Regulation of poly(A) tail length

When comparing the *bcd* mRNA and protein patterns, it is obvious that the protein gradient reaches more posterior areas than the mRNA gradient. While the latter could be due to lack of sensitivity to detect a longer mRNA gradient, it does not exclude the possibility that there is post-transcriptional control involved that allows to stretch the gradient further to the posterior.

Previous reports have shown that the translational efficiency of Bcd strongly depends on the length of the poly(A) tail of the *bcd* mRNA (Salles et al., 1994), see also Fig. 13.

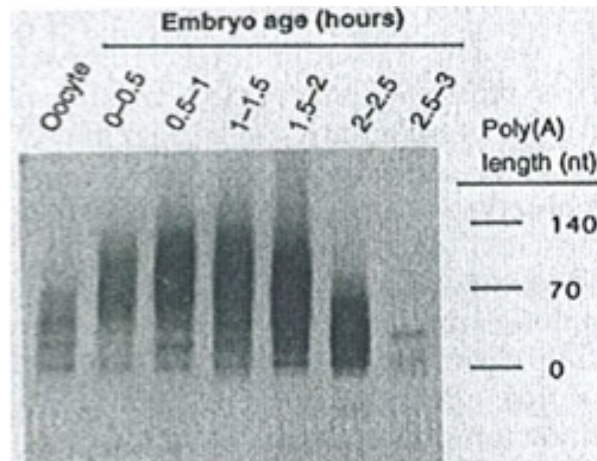


Fig. 13 poly(A) tail length analysis

Tests show that the poly(A) tail changes with time and is highest at the time of nc 14 Image from (Salles et al., 1994).

The *Drosophila* genome harbors two poly(A) polymerase (PAP), *wispy* and *pap2*. Overexpression of *PAP2* level leads to a substantial increase of *bcd* protein concentration (Juge et al., 2002). In the oocyte, during mid to late oogenesis, *wispy* assists *gurken* mRNA localization at the dorsal-anterior corner through its role of polyadenylation (Derrick and Weil, 2017; Norvell et al., 2015). Before egg activation, the poly(A) tail length of *bcd* was short, preventing translation of Bcd (Eichhorn et al., 2016). Moreover, embryos from *wispy* mothers failed to go through oocyte maturation due to defects with MT-based events, which are essential for *bcd*, *nos* or *osk* mRNA localization to either pole (Brent et al., 2000). In summary, both *PAP2* and *wispy* are required sequentially in cytoplasmic polyadenylation of *Drosophila* oogenesis and in the early developmental stage. *PAP2* is responsible during the mid-oogenesis, while *wispy* is active from the late oogenesis to early embryogenesis (Benoit et al., 2008).

1.8.2 Cyclins

In syncytial *Drosophila* embryos, the “wait-until-ready” mechanism of spindle assembly checkpoint (SAC) coordinating the mitotic events in slower-dividing nuclei from nc 13 on appears inappropriate and dispensable (Yuan and O’Farrell,

2015). For this reason, a cyclin-based intrinsic timer was adopted. There are three mitotic cyclins (A, B, and B3) that function and timely control the phase-phase transition in syncytial embryos. The sequential degradation of CyclinA, CyclinB and CyclinB3 is responsible for the timing and coordination of mitotic events. CyclinA is degraded prior to the metaphase-anaphase transition and is responsible for sister chromosome disjunction, while CyclinB3 is degraded during anaphase and facilitates the restoration of the interphase nucleus. In contrast, the degradation of CyclinB contributes to the transition from metaphase to anaphase (Parry and O'Farrell, 2001; Yuan and O'Farrell, 2015). Interestingly, CyclinB is a target of Wispy (Cui et al., 2013). Due to the fact that the activity of the cortical MT threads for *bcd* mRNA transport are cell-cycle-dependent and are detected during metaphase and early anaphase only (Fahmy et al., 2014), it is reasonable to hypothesize that CyclinB could regulate the occurrence of the cortical MTs. Hence, CyclinB could play a role in *bcd* mRNA gradient formation.

1.8.3 Egg activation

Translational recruitment of maternal mRNAs is an essential process in most biological systems. Activation of mature oocytes could therefore serve as a switch for subsequent translational activities after *Drosophila* meiotic arrest. Two genes, *cortex* and *grauzone*, which were identified in a screen for female-sterile mutations, play roles in translation and poly(A) tail length determination of *bcd* mRNA (Harms et al., 2000; Page and Orr-Weaver, 1996; Schupbach and Wieschaus, 1989). Embryos laid by either *cortex* or *grauzone* mutant mothers contain a shorter poly(A) tail of *bcd* mRNA (~ 80 nucleotides versus ~140 nucleotides in wild type embryos), and the post-translational activity of *bcd* mRNA is disturbed (Lieberfarb et al., 1996). (Horner et al., 2006) reported that *bcd* mRNA translation is repressed in eggs laid by *sarah* mutant mothers (*sarah* encodes the *Drosophila* calcipressin involved in egg activation) by interrupting the polyadenylation machinery, as well.

1.8.4 Drug treatment of actin and MTs

Actin participates in protein-protein interactions more than any other recorded protein. If *Drosophila* oocytes were bathed in the actin-depolymerizing drug cytochalasin D, *bcd* mRNA localization at the anterior tip was compromised and stable actin-dependent anchoring of the mRNA was no longer possible (Weil et al., 2006; Weil et al., 2008). There are various actin-targeting drugs used in basic research (Allingham et al., 2006; Spector et al., 1999). Of note are the latrunculins, an actin-destabilizing drug similar to cytochalasin D used in the past to disrupt filamentous actin (F-actin) in early *Drosophila* embryos. Phalloidin, a F-actin-

stabilizing drug is used predominantly as a tool to visualize F-actin in combination with fluorescent phalloidin-derivatives.

Small commonly-used molecular MT-binding drugs (Florian and Mitchison, 2016), summarized in Table 2, have made significant impacts in both in medicine and basic research (Dostal and Libusova, 2014), (Fig. 14). The use of drugs that assemble or destroy MT arrays, such as Taxol, Vinblastine, Colcemid and Colchicine has been important in studying the mechanism of the MT network for transportation of *bcd* mRNA (Fahmy et al., 2014; Weil et al., 2010). However, the waxy layer that encompasses the vitelline membrane of the *Drosophila* eggshell poses a challenge as to the use of drugs, by reducing the permeability. Fortunately, several methods for permeabilizing the embryos still in their vitelline membrane were described (Rand et al., 2010; Schulman et al., 2013).

Table 2 Summary of drugs acting on MTs

Drug	Binding site	Textbook mechanism of action	Effects on MT array
Colchicine	Colchicine	Inhibits neutrophil migration	Inhibits MTs polymerization
Colcemid	Colchicine		Inhibits MTs polymerization
Combretastatin A4	Colchicine	Antiangiogenic	Inhibits MTs polymerization
Nocodazole	Colchicine(?)		Inhibits MTs polymerization
Benomyl			Inhibits MTs polymerization
T138067	Binds covalently to Cys-239 of β -Tubulin		Inhibits MTs polymerization
Vinblastine	Vinca	Antimitotic	Inhibits MTs polymerization
Vincristine	Vinca	Antimitotic	Inhibits MTs polymerization
Paclitaxel	Taxane	Antimitotic	Polymerizes MTs
Docetaxel	Taxane	Antimitotic	Polymerizes MTs
Eribulin	Vinca	Antimitotic	Inhibits MTs polymerization

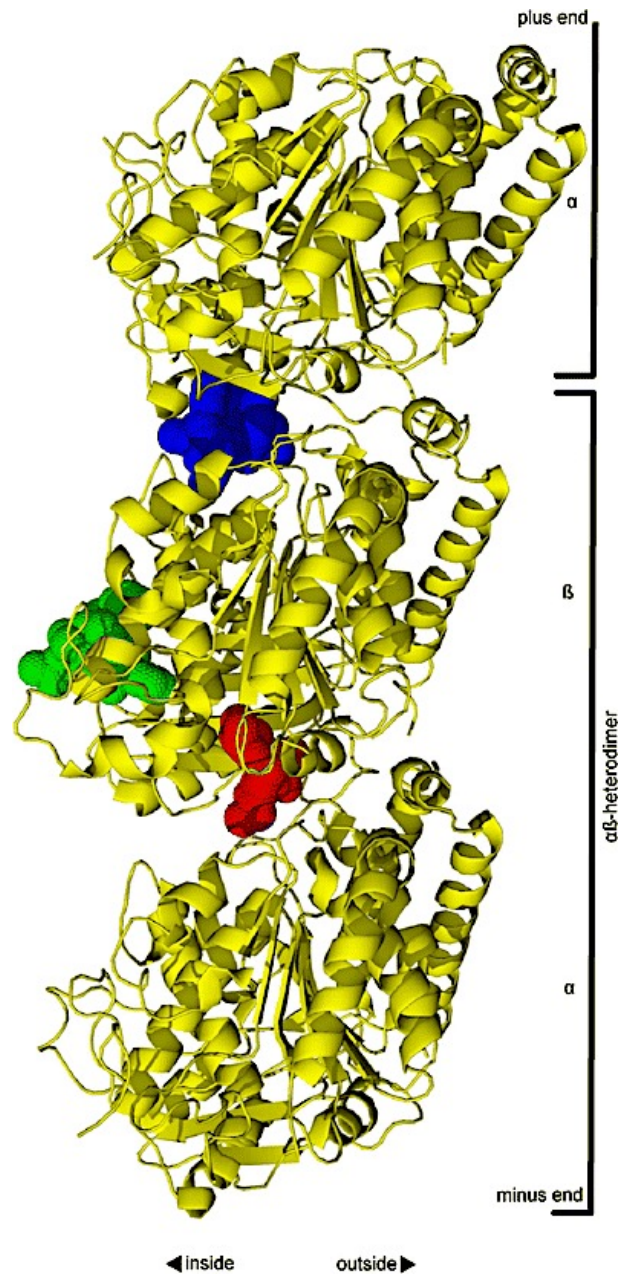


Fig. 14 Binding sites for main MT drugs

Binding site of Colchicine is shown in the red zone. The blue zone is the binding site of Vinca, and the green zone is responsible for binding of Taxane, respectively. Image from (Dostal and Libusova, 2014)

1.8.5 Hypoxia in *Drosophila* embryos

The reaction to low-O₂ environment is diverse among animals. Some species in the invertebrate kingdom, as exemplified by *Drosophila*, are capable of being exposed to hypoxic conditions for prolonged periods without apparent tissue injury. During the hypoxic state, *Drosophila* embryos stop development and enter into an arrested or a “sleeping” phase that can be reversed upon being exposed in oxygen again (Haddad et al., 1997). However, (Heinrich et al., 2011) reported that the growth rate and the body size are affected, generating smaller-sized thoraces and wings by multiple mechanisms at various developmental stages.

1.9 The GAL4-UAS system for inducible gene expression in *Drosophila* research

Manipulation of gene expression is an important tool for studying the function of a gene. A binary expression system is a popular and efficient strategy to up- or down-regulate a target gene (Riabinina and Potter, 2016; Viktorinova and Wimmer, 2007). In *Drosophila*, the GAL4-UAS system has been an extraordinarily efficient tool to dissect gene function in subsets of cells within a given tissue (Brand and Perrimon, 1993; Fischer et al., 1988). The working principle of the system is: an enhancer-driven *GAL4* gene that encodes a yeast transcriptional activator will specifically bind to a region where the *UAS* (upstream activating sequence) is located. The cDNA sequence of a targeted gene *X* is placed downstream of *UAS* (Fig. 16) (St Johnston, 2002). In *Drosophila*, the binary system is achieved by crossing one strain carrying the *GAL4* driver to another strain carrying the *UAS*-gene *X* construct (Fig. 15). Combined with extensive RNA interference (RNAi) stock collections and classical genetic mutations, the GAL4-UAS system has proven itself as a very good tool to directly assess the effects of altering the activity of a single gene in most developing tissues.

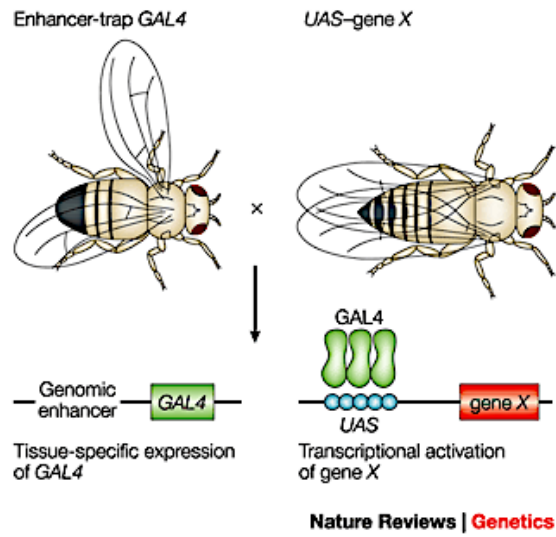


Fig. 15 The GAL4-UAS system.

The yeast transcriptional activator GAL4 can be used to regulate gene expression in *Drosophila* by inserting the upstream activating sequence (UAS) to which it binds next to a gene of interest (gene X). The GAL4 gene has been inserted at random positions in the *Drosophila* genome to generate 'enhancer-trap' lines that express GAL4 under the control of nearby genomic enhancers. Therefore, the expression of gene X can be driven in any of these patterns by crossing the appropriate GAL4 enhancer-trap line to flies that carry the UAS-gene X transgene. Image from (St Johnston, 2002)

2 PRESENT INVESTIGATIONS

2.1 Paper I: α Tubulin 67C and Ncd are essential for establishing a cortical microtubular network and formation of the *bicoid* mRNA gradient in *Drosophila*

Aim and results

The Bcd protein serves as a paradigm for morphogen gradient formation in textbooks and has been studied during more than 3 decades. Two competing models of how the gradient arises are available: the SDD model (Synthesis, Diffusion and Degradation) and the ARTS model (Active RNA Transport and Synthesis). The SDD model proposes that the Bcd protein is synthesized from an anteriorly-localized *bcd* mRNA, and subsequently diffuses throughout the embryos to establish the gradient, combined with uniform degradation (Driever and Nusslein-Volhard, 1988). In contrast, the ARTS model proposes that the *bcd* mRNA is actively transported along the cortex to the posterior to form an mRNA gradient that serves as a template for Bcd synthesis (Spirov et al., 2009). The existence of a *bcd* mRNA gradient was first identified by (Frigerio et al., 1986). The SDD model recently encountered a big challenge (Gregor et al., 2007), so the question of how the *bcd* mRNA gradient up to 40% EL (Fig. 1A , B) forms was answered in this paper.

Using a monoclonal antibody YL_{1,2} made against freshly-assembled Tubulin, a cortical and omnidirectional MT network was detected that appeared only in the anterior half of the embryos during metaphase and early anaphase of nc 1-6 embryos (Fig.1C, F). The network was not built up in unfertilized eggs (Fig. 1D, E). Moreover, as embryonic development proceeded, the cortical MTs became more and more numerous. At nc 6, the MT threads were detected to extend 20 μ m from the cortex (Fig. 1H, H'). At nc 11, the threads became denser below the nuclear monolayer (Fig. 1J, K). At nc 13, vigorous MT activity was found showing long extensions up to 30 μ m into the interior (Fig. 1L). At nc 14, threads extended further into the yolk with a length up to 50 μ m (Fig. 1M). Interestingly, the majority of those long threads were also detected using an antibody against α Tubulin 67C (Fig. 1O), a maternal Tubulin known to contribute to long MTs.

Given the fact that α Tubulin 84B and α Tubulin 84D preferred to be associated with MTs that embrace the nuclei (Fig. 1P), it was proposed that the composition of α Tubulins in the different cellular sub-compartments varies in space and time. Furthermore, a study between the relationship of actin and the MT network revealed that the two networks were independent of each other (Fig. 2).

Furthermore, among all 4 *α Tubulin* genes, the expression profile of *α Tub67C* was remarkably similar to that of *bcd* mRNA (Attrill et al., 2016). Thus, we explored the role of *α Tub67C* for the cortical MT network. We stained eggs of *kavar^{null}/Df* hemizygous mothers (a complete knock-down) and found many short MTs without orientation (Fig. 4A, B). Next, we looked at the role of *α Tub67C* for *bcd* mRNA transport and showed that in *α Tub67C* mutants, instead of being transported along the cortex, *bcd* mRNA moved in the interior of the embryos (Fig. 4C). In search for specific motor proteins associated with *α Tub67C*, we found that *nonclaret disjunctional (ncd)* encoding an unconventional minus-end Kinesin interacted genetically with *α Tub67C*. Analyses from both strong and weak *ncd* alleles showed similar *bcd* mRNA movement as seen in *kavar^{null}* mutations (Fig. 4F). To corroborate an involvement of *ncd* in the transport of *bcd* mRNA together with *α Tub67C*, we stained embryos with antibodies specific for each protein alone. A clear colocalization between Ncd and *α Tub67C* was demonstrated in the periplasm and perinuclear areas of nc 14 embryos (Fig. 4P, Q), suggesting that indeed these two proteins interact with each other.

2.2 Paper II: Cortical movement of Bicoid in early *Drosophila* embryos is actin- and microtubule-dependent and disagrees with the SDD diffusion model

Aim and results

Following the work in 2014 (Fahmy et al., 2014), the ARTS model strongly challenged the SDD model. In the ARTS model, the *bcd* mRNA is transported along the cortical MT network to generate the mRNA gradient, which then serves as template for translation of the Bcd protein. To further provide evidence in support for the ARTS model, we developed a sensitive assay to monitor the movement of Bcd during early nuclear cycles.

The SDD model predicts diffusion of the protein from the anterior tip throughout the embryo, including the cortex as well as the interior yolk. To achieve a high sensitivity, we used a sensitive antibody against Bcd, combined with a strain that expresses 3 times more Bcd protein than in wild-type embryos, *bcd⁺⁵⁺⁸*. As

expected, the Bcd protein gradient formed gradually from stage of nc 6 to stage of nc 9 (Fig. 1A to D). However, we observed that the Bcd gradient always remained along the cortex and no traces of Bcd were found in the interior of the embryo. To further investigate the movement and the path of Bcd along the cortex, we exposed embryos to hypoxic conditions, which would inactivate the mRNA transportation system without affecting the viability of embryos. We chose nc 6 as a reference time-point to evaluate Bcd migration from the position where hypoxic conditions were applied. Embryos collected from different time periods of hypoxic treatment revealed that the Bcd movement was still at the cortex, but its movement was remarkably sparse (Fig. 1E to I). In contrast, the *bcd* mRNA remained tightly located at the tip with virtually no movement (Fig. 1K, L). We then analyzed the developmental consequences of the extra movement of Bcd under hypoxia. The majority of embryos exhibited an enlargement of anterior segments with squeezed posterior segments (Fig. 1M), in contrast to a smaller portion of embryos missing several segments (Fig. 1N). Interestingly, the formation of pole cells was suppressed (Fig. 1Q). To investigate whether Bcd movement is MT-dependent or not, we combined our water-based hypoxic treatment with drug application. Embryos exposed to hypoxia and the MT-destabilizing drug mixture colchicine/colcemid (CC) displayed extensive interior movement during the developmental stages (Fig. 3A-C). Embryos treated with the MT-stabilizing drug taxol maintained the Bcd movement along the cortex (Fig. 3E, F). Surprisingly, when embryos were treated with the drug vinblastine, Bcd was distributed throughout the embryos (Fig. 3K). This data indicates that indeed the SDD model could be simulated experimentally, but only if the yolk was modified. To rule out that the Bcd protein movement resulted from movement of the mRNA, we stained all the different treatments for the presence of *bcd* mRNA (Fig. 3D, H, L). In all cases, we detected little movement, i. e. a similar distribution with that of hypoxia-only treated embryos (Fig. 1K).

To investigate whether actin participates in the movement of Bcd, we subjected *bcd*⁺⁵⁺⁸ embryos to drugs that disturb the formation of actin filaments. Embryos exposed to the actin-destabilizing drug latrunculin B (Fig. 4A-C) revealed sparse cortical movement with no interior Bcd movement. Embryos treated with the actin-stabilizing drug phalloidin (Fig. 4E-G) behaved like *bcd*⁺⁵⁺⁸ embryos with a minor fraction of protein moving to the interior. As expected, the *bcd* mRNA from treated embryos with either drug stayed at the tip with little or no movement (Fig. 4D, H).

In addition to investigating the roles of cytoskeleton actin and MTs, we analyzed the behaviour of Bcd and Stauf protein (as a read-out system of *bcd* mRNA) in unfertilized embryos during short time intervals to monitor their movements. Our results indicated that the Bcd protein followed an interior path, which paralleled that of the pattern of *bcd* mRNA (Fig. 5). Our data suggested that an internal MT

network exists in unfertilized embryos that served as a transportation path for the *bcd* mRNA, while the cortical MT network and cortical mRNA transport would be established only after fertilization.

2.3 Paper III: Genetic analysis of factors influencing *bicoid* gradient formation in *Drosophila*

Aim and results

Substantial evidence was shown that *bcd* mRNA gradient formation underlies the Bcd protein formation during *Drosophila* embryogenesis. The transport mechanism of *bcd* mRNA in embryos is MT-based and one motor protein was identified (Fahmy et al., 2014). However, knowledge on other factors that influence *bcd* mRNA gradient formation is sparse. Given our previous and current studies, we investigated four groups of factors, *trans*-Golgi proteins, poly(A) polymerases, Cyclins and egg activation genes, in order to pave a fundamental path to the mechanisms of *bcd* mRNA gradient formation.

We stained MTs with a MT-plus end marker, Chromosome bows (Chb), formerly called Mast/Orbit/CLASP. We could show that Chb was associated with cortical MTs in *Drosophila* embryos (Fig. 1). Since Chb was shown to serve as an aMTOC, in concert with *trans*-Golgi proteins in vertebrates, we investigated whether some of the proteins from the *trans*-Golgi compartment were involved in cortical MT-network establishment in *Drosophila*, as well. Using genetic approaches to over-express and down-regulate candidate proteins, we analyzed the effects by monitoring the patterns of *bcd*-downstream genes such as the gap gene *empty spiracles* (*ems*) and the pair-rule gene *even-skipped* (*eve*). We analyzed 4 *trans*-Golgi genes, *dGCC88*, *dGolgin97*, *dGCC185* and *dGolgin245* and could demonstrate that 3 of them affect the Bcd gradient. Summarizing the cuticle patterns in the 4 *trans*-Golgins (Fig. 2), we could observe that all four mutations revealed head-defects, likely caused by altered Bcd activity. Furthermore, the embryos from the partial loss-of-function of *dGCC185*^{c03845}/*Df(3R)08155* showed defective germband retraction (Fig. 2H). A small portion of *dGolgin97* embryos exhibited an interesting phenotype of distinct regional nuclear density at nc 14 (Fig. 4E, insert), which showed two sets of nuclear density along the AP axis.

To investigate the relationship between the length of the poly(A) tail of the *bcd* mRNA and gradient establishment, we targeted two poly(A) polymerases, Wispy and PAP2. Due to the lethality of *pap2* overexpression, we were only able to obtain information from *wispy* overexpression (Fig. 5). The poly(A) polymerase

gene *wispy*, presumably acting on the poly(A) tail length of the *bcd* mRNA was found to shift the Eve stripes mainly to the posterior. Due to the effect caused by Wispy acting on various other segmentation genes, the embryos displayed various segmental defects (Fig. 5J, K, L). Furthermore, we performed a study on the cell-cycle gene *CyclinB*. When overexpressed, CyclinB was shown to affect the segmental anlagen primarily in the anterior part (Fig. 6). Finally, to determine the link between egg activation and Bcd gradient formation, we analyzed 3 egg activation genes. Due to high mortality of egg from *cortex* mothers, we could not execute statistical analyses. Two egg-activating genes (*grauzone* and *sarah*) were shown to affect the Bcd gradient by shifting the majority of the Eve stripes to the posterior.

In summary: we have provided evidence of the existence of factors with diverse cellular functions that regulate Bcd gradient formation. Our data reveals a larger complexity of the mechanisms for Bcd gradient formation than initially anticipated.

2.4 Paper IV: Segmentation gene expression patterns in *Bactrocera dorsalis* and related insects: regulation and shape of the blastoderm and larval cuticle

Aim and results

Previous studies revealed that *bcd* diverged recently from the *Hox3* gene in the course of insect evolution, instead of being conserved as the other *Hox* class genes in animals (Stauber et al., 1999; Stauber et al., 2002). It is well known that *bcd* is the most important anterior determinant for the generation of the AP polarity in *Drosophila* embryos. However, *bcd* is not detected in many other flies, and plays its role only in higher dipterans (Bonneton, 2003; McGregor, 2005). One interesting avenue was therefore to investigate is how the AP patterns look like in other flies where *bcd* was absent.

In this study, we explored the expression patterns of the *bcd* target genes in the oriental fruit fly *Bactrocera dorsalis*. Phylogenetically, *B. dorsalis* is a member of the family *Tephritidae* that is located immediately adjacent of that of *Drosophilidae* (Geib et al., 2014). The (at that time) unpublished data showed that the *bcd* gene was lacking in the *B. dorsalis* genome. Since the embryology of *B. dorsalis* was not described in detail, we first undertook a comparison of its embryology to that of *Drosophila*. This showed that the embryogenesis of *B. dorsalis* was very similar to that of *Drosophila*, except that the overall shape of the

embryo was quite different (Fig. 1 and 7B). Next, we examined the expression patterns of selected *bcd*-downstream target genes in *Drosophila* that were also expressed in *B. dorsalis*, including the gap genes *hb*, *otd* and *Kr*, the pair-rule gene *eve*, and the segment polarity gene *engrailed* (*en*). Interestingly, the onset of expression of all segmentation genes was detected one nc later, compared to their *Drosophila* counterparts. Moreover, while the transcription of *otd* continued in *Drosophila*, *otd* transcripts in *B. dorsalis* ceased after the extended germband stage. Among those expression patterns of the genes, the way that the *eve* stripes were aligned along the AP axis was particularly conspicuous. It was perpendicular to the AP axis (Fig. 5), suggesting a distinct control. Furthermore, 3 extra stripes of *en* were observed in *B. dorsalis*, which were not found in *Drosophila* (Fig. 6). Finally, a comparative expression analysis revealed a distinct interpretation of the gap gene (*Kr*) signal at the pair-rule level (*eve*) between *B. dorsalis*, *Drosophila* and a third fly, the blow fly *Lucilia sericata* (Fig. 7).

3 ACKNOWLEDGEMENTS

There is an ancient Chinese saying: as one fence needs three stakes, a good guy needs three fellows. Here, I would like to express my sincerest gratitude to those who have supported, encouraged me to a successful PhD.

Stefan Baumgartner: my supervisor. ‘Please do not call me Dear Professor Baumgartner, just Stefan.’ I will always fondly remember you and **Ulrike** picking me up at the airport. I recalled being so exhausted but immediately felt comfortable in the way you spoke that it put me such at ease while introducing me to an unfamiliar town. For one who is used to the hierarchial system, instinct told me that my PhD life in your group would be more enjoyable, which it has been proved to be during my 4 years. With your patience, tolerance, and kindness, I adapted myself well and walked the track of studying this discipline more smoothly. Despite my uninformed questions at times, you have always had time to explain them as detailed as possible, providing corresponding solutions. Regardless of my errors, you have always smiled and said: ‘learn it next time.’ Undeterred by unexpected results, you have always taken the most optimistic viewpoint. You keep the working environment both professional and friendly, not only in the lab, but your cordial attitude extends to neighboring labs and even the entire floor. Under such conditions, have I been more relaxed and more efficient. Thank you for offering me such a constructive working environment to satisfy my curiosity in developmental biology as a discipline. More importantly, thank you for being a good life mentor, I have learned a lot from you, both academically and socially. Whatever lies in store for the future, let this not be goodbye.

Sol Da Rocha Baez: techniques tutor. ‘I do not trust people with a 24-hour smile.’ Even though it was not a judgment about me, I was worried if I could ‘survive’ under your military-like working style. Happily, I did. With your help and guidance, I have greatly improved my experimental skills, and have become more rigorous. By the way, I kept that Swedish pizza menu translation that you wrote the first time for our routine Friday weekly lunches. After so many years, it has greatly assisted me when ordering food.

Udo Häcker (co-supervisor) and Martina Schneider: my *Drosophila* neighbors. Without your company, I am pretty sure that our flies would feel too lonely in the BMC. Thank you for making us happy. Thank you for sharing your wisdom to us. Because of your presence, I have learned a lot about the German logic and

precision. Because of your presence, I have also been familiarized with the ‘not-funny-at-all’ German humor.

Edgar Pera: the Frog. ‘You guys are so anti-social. You have to put Fika on the top of your daily schedule. That is the priority on Wednesday.’ Ha-ha, too much pressure from your friendly fly-friends, but so much fun for us to just tease your group that way.

Maria Climent: my dear JieJie. The first time I met you, you simply gave me a big and sweet smile. From that moment, I knew if I had any problems, you were the person I could go to for help. You brought the Spanish sunshine to my first dark winter here. It was so grateful that you invited me to spend Christmas with your and also my Spanish family together. I am so happy to have a sister like you.

Linda and Thomas Blom, Sara Andersson: ‘Linda, Linda, listen-listen to me!’ Thank you for your generously revising my thesis and transcripts and more transcripts and then thesis again! Thank you for sharing your fruit basket with such a ‘poor student’. I hope soon Linda will manage her Swedish, otherwise it would definitely be the fault of Thomas and Sara! Ha-ha!

Time flies. Within those 4-years, so many people have come and gone. **Khalid Fahmy** (your delicious baklava and broad knowledge of insects), **Worramin** (my Thai sister and your awesome Oriental Fruit Fly), **Lukas** (‘guinea pig’ of my food experiments), **Inge** (finally my ‘labor’), **Nadège** (wondering what could knock you down), **Franziska** (the first German with blue eyes) and **Cibely** (Brazil sunshine and nice host in Barcelona).

Some became friends, some were just passersby. But, whatever their roles are, they played a very important part through a certain stages of my life. I am so grateful that I have met all of you guys. I am a life-experience collector. Those precious memories will be kept close at reach and close to my heart.

4 REFERENCES

- Abu-Arish, A., Porcher, A., Czerwonka, A., Dostatni, N., Fradin, C., 2010. High mobility of bicoid captured by fluorescence correlation spectroscopy: implication for the rapid establishment of its gradient. *Biophysical journal* 99, L33-35.
- Adams, M.D., Celniker, S.E., Holt, R.A., Evans, C.A., Gocayne, J.D., Amanatides, P.G., Scherer, S.E., Li, P.W., Hoskins, R.A., Galle, R.F., George, R.A., Lewis, S.E., Richards, S., Ashburner, M., Henderson, S.N., Sutton, G.G., Wortman, J.R., Yandell, M.D., Zhang, Q., Chen, L.X., Brandon, R.C., Rogers, Y.H., Blazej, R.G., Champe, M., Pfeiffer, B.D., Wan, K.H., Doyle, C., Baxter, E.G., Helt, G., Nelson, C.R., Gabor, G.L., Abril, J.F., Agbayani, A., An, H.J., Andrews-Pfannkoch, C., Baldwin, D., Ballew, R.M., Basu, A., Baxendale, J., Bayraktaroglu, L., Beasley, E.M., Beeson, K.Y., Benos, P.V., Berman, B.P., Bhandari, D., Bolshakov, S., Borkova, D., Botchan, M.R., Bouck, J., Brokstein, P., Brottier, P., Burtis, K.C., Busam, D.A., Butler, H., Cadieu, E., Center, A., Chandra, I., Cherry, J.M., Cawley, S., Dahlke, C., Davenport, L.B., Davies, P., de Pablos, B., Delcher, A., Deng, Z., Mays, A.D., Dew, I., Dietz, S.M., Dodson, K., Doup, L.E., Downes, M., Dugan-Rocha, S., Dunkov, B.C., Dunn, P., Durbin, K.J., Evangelista, C.C., Ferraz, C., Ferriera, S., Fleischmann, W., Fosler, C., Gabrielian, A.E., Garg, N.S., Gelbart, W.M., Glasser, K., Glodek, A., Gong, F., Gorrell, J.H., Gu, Z., Guan, P., Harris, M., Harris, N.L., Harvey, D., Heiman, T.J., Hernandez, J.R., Houck, J., Hostin, D., Houston, K.A., Howland, T.J., Wei, M.H., Ibegwam, C., Jalali, M., Kalush, F., Karpen, G.H., Ke, Z., Kennison, J.A., Ketchum, K.A., Kimmel, B.E., Kodira, C.D., Kraft, C., Kravitz, S., Kulp, D., Lai, Z., Lasko, P., Lei, Y., Levitsky, A.A., Li, J., Li, Z., Liang, Y., Lin, X., Liu, X., Mattei, B., McIntosh, T.C., McLeod, M.P., McPherson, D., Merkulov, G., Milshina, N.V., Mobarry, C., Morris, J., Moshrefi, A., Mount, S.M., Moy, M., Murphy, B., Murphy, L., Muzny, D.M., Nelson, D.L., Nelson, D.R., Nelson, K.A., Nixon, K., Nusskern, D.R., Pacleb, J.M., Palazzolo, M., Pittman, G.S., Pan, S., Pollard, J., Puri, V., Reese, M.G., Reinert, K., Remington, K., Saunders, R.D., Scheeler, F., Shen, H., Shue, B.C., Siden-Kiamos, I., Simpson, M., Skupski, M.P., Smith, T., Spier, E., Spradling, A.C., Stapleton, M., Strong, R., Sun, E., Svirskas, R., Tector, C., Turner, R., Venter, E., Wang, A.H., Wang, X., Wang, Z.Y., Wassarman, D.A., Weinstock, G.M., Weissenbach, J., Williams, S.M., Woodage, T., Worley, K.C., Wu, D., Yang, S., Yao, Q.A., Ye, J., Yeh, R.F., Zaveri, J.S., Zhan, M., Zhang, G., Zhao, Q., Zheng, L., Zheng, X.H., Zhong, F.N., Zhong, W., Zhou, X., Zhu, S., Zhu, X., Smith, H.O., Gibbs, R.A., Myers, E.W., Rubin, G.M., Venter, J.C., 2000. The genome sequence of *Drosophila melanogaster*. *Science* 287, 2185-2195.
- Adhikary, R., Tan, Y.X., Liu, J., Zimmermann, J., Holcomb, M., Yvellez, C., Dawson, P.E., Romesberg, F.E., 2017. Conformational Heterogeneity and DNA Recognition by the Morphogen Bicoid. *Biochemistry*.

- Allingham, J.S., Klenchin, V.A., Rayment, I., 2006. Actin-targeting natural products: structures, properties and mechanisms of action. *Cell Mol Life Sci* 63, 2119-2134.
- Attrill, H., Falls, K., Goodman, J.L., Millburn, G.H., Antonazzo, G., Rey, A.J., Marygold, S.J., FlyBase, C., 2016. FlyBase: establishing a Gene Group resource for *Drosophila melanogaster*. *Nucleic Acids Res* 44, D786-792.
- Baird-Titus, J.M., Clark-Baldwin, K., Dave, V., Caperelli, C.A., Ma, J., Rance, M., 2006. The solution structure of the native K50 Bicoid homeodomain bound to the consensus TAATCC DNA-binding site. *J Mol Biol* 356, 1137-1151.
- Baumbach, J., Novak, Z.A., Raff, J.W., Wainman, A., 2015. Dissecting the function and assembly of acentriolar microtubule organizing centers in *Drosophila* cells in vivo. *PLoS Genet* 11, e1005261.
- Benoit, P., Papin, C., Kwak, J.E., Wickens, M., Simonelig, M., 2008. PAP- and GLD-2-type poly(A) polymerases are required sequentially in cytoplasmic polyadenylation and oogenesis in *Drosophila*. *Development* 135, 1969-1979.
- Berleth, T., Burri, M., Thoma, G., Bopp, D., Richstein, S., Frigerio, G., Noll, M., Nusslein-Volhard, C., 1988. The role of localization of bicoid RNA in organizing the anterior pattern of the *Drosophila* embryo. *EMBO J* 7, 1749-1756.
- Bonneton, F., 2003. [Extreme divergence of a homeotic gene: the bicoid case]. *Med Sci (Paris)* 19, 1265-1270.
- Brand, A.H., Perrimon, N., 1993. Targeted Gene-Expression as a Means of Altering Cell Fates and Generating Dominant Phenotypes. *Development* 118, 401-415.
- Brent, A.E., MacQueen, A., Hazelrigg, T., 2000. The *Drosophila* wispy gene is required for RNA localization and other microtubule-based events of meiosis and early embryogenesis. *Genetics* 154, 1649-1662.
- Brunel, C., Ehresmann, C., 2004. Secondary structure of the 3' UTR of bicoid mRNA. *Biochimie* 86, 91-104.
- Bugnard, E., Zaal, K.J., Ralston, E., 2005. Reorganization of microtubule nucleation during muscle differentiation. *Cell Motil Cytoskeleton* 60, 1-13.
- Cagan, R., 2009. Principles of *Drosophila* eye differentiation. *Curr Top Dev Biol* 89, 115-135.
- Chabin-Brion, K., Marceiller, J., Perez, F., Settegrana, C., Drechou, A., Durand, G., Pous, C., 2001. The Golgi complex is a microtubule-organizing organelle. *Mol Biol Cell* 12, 2047-2060.
- Chang, C.W., Nashchekin, D., Wheatley, L., Irion, U., Dahlgaard, K., Montague, T.G., Hall, J., St Johnston, D., 2011. Anterior-posterior axis specification in *Drosophila* oocytes: identification of novel bicoid and oskar mRNA localization factors. *Genetics* 188, 883-896.
- Chen, H., Xu, Z., Mei, C., Yu, D., Small, S., 2012. A system of repressor gradients spatially organizes the boundaries of Bicoid-dependent target genes. *Cell* 149, 618-629.
- Crauk, O., Dostatni, N., 2005. Bicoid determines sharp and precise target gene expression in the *Drosophila* embryo. *Curr Biol* 15, 1888-1898.

- Cui, J., Sartain, C.V., Pleiss, J.A., Wolfner, M.F., 2013. Cytoplasmic polyadenylation is a major mRNA regulator during oogenesis and egg activation in *Drosophila*. *Dev Biol* 383, 121-131.
- Dave, V., Zhao, C., Yang, F., Tung, C.S., Ma, J., 2000. Reprogrammable recognition codes in bicoid homeodomain-DNA interaction. *Mol Cell Biol* 20, 7673-7684.
- Derby, M.C., Lieu, Z.Z., Brown, D., Stow, J.L., Goud, B., Gleeson, P.A., 2007. The trans-Golgi network golgin, GCC185, is required for endosome-to-Golgi transport and maintenance of Golgi structure. *Traffic* 8, 758-773.
- Derrick, C.J., Weil, T.T., 2017. Translational control of gurken mRNA in *Drosophila* development. *Cell Cycle* 16, 23-32.
- Dostal, V., Libusova, L., 2014. Microtubule drugs: action, selectivity, and resistance across the kingdoms of life. *Protoplasma* 251, 991-1005.
- Driever, W., Nusslein-Volhard, C., 1988. A gradient of bicoid protein in *Drosophila* embryos. *Cell* 54, 83-93.
- Driever, W., Nusslein-Volhard, C., 1989. The Bicoid Protein Is a Positive Regulator of Hunchback Transcription in the Early *Drosophila* Embryo. *Nature* 337, 138-143.
- Efimov, A., Kharitonov, A., Efimova, N., Loncarek, J., Miller, P.M., Andreyeva, N., Gleeson, P., Galjart, N., Maia, A.R., McLeod, I.X., Yates, J.R., 3rd, Maiato, H., Khodjakov, A., Akhmanova, A., Kaverina, I., 2007. Asymmetric CLASP-dependent nucleation of noncentrosomal microtubules at the trans-Golgi network. *Dev Cell* 12, 917-930.
- Eichhorn, S.W., Subtelny, A.O., Kronja, I., Kwasniewski, J.C., Orr-Weaver, T.L., Bartel, D.P., 2016. mRNA poly(A)-tail changes specified by deadenylation broadly reshape translation in *Drosophila* oocytes and early embryos. *Elife* 5.
- Ephrussi, A., Lehmann, R., 1992. Induction of germ cell formation by oskar. *Nature* 358, 387-392.
- Ephrussi, A., St Johnston, D., 2004. Seeing is believing: the bicoid morphogen gradient matures. *Cell* 116, 143-152.
- Fahmy, K., Akber, M., Cai, X., Koul, A., Hayder, A., Baumgartner, S., 2014. alphaTubulin 67C and Ncd are essential for establishing a cortical microtubular network and formation of the Bicoid mRNA gradient in *Drosophila*. *PLoS One* 9, e112053.
- Feany, M.B., Bender, W.W., 2000. A *Drosophila* model of Parkinson's disease. *Nature* 404, 394-398.
- Ferrandon, D., Elphick, L., Nusslein-Volhard, C., St Johnston, D., 1994. Stauf protein associates with the 3'UTR of bicoid mRNA to form particles that move in a microtubule-dependent manner. *Cell* 79, 1221-1232.
- Fischer, J.A., Giniger, E., Maniatis, T., Ptashne, M., 1988. GAL4 activates transcription in *Drosophila*. *Nature* 332, 853-856.
- Florian, S., Mitchison, T.J., 2016. Anti-Microtubule Drugs. *Methods Mol Biol* 1413, 403-421.
- Fradin, C., 2017. On the importance of protein diffusion in biological systems: The example of the Bicoid morphogen gradient. *Biochim Biophys Acta*.

- Frigerio, G., Burri, M., Bopp, D., Baumgartner, S., Noll, M., 1986. Structure of the segmentation gene paired and the *Drosophila* PRD gene set as part of a gene network. *Cell* 47, 735-746.
- Frohnhofer, H.G., Lehmann, R., Nusslein-Volhard, C., 1986. Manipulating the anteroposterior pattern of the *Drosophila* embryo. *Journal of embryology and experimental morphology* 97 Suppl, 169-179.
- Geib, S.M., Calla, B., Hall, B., Hou, S., Manoukis, N.C., 2014. Characterizing the developmental transcriptome of the oriental fruit fly, *Bactrocera dorsalis* (Diptera: Tephritidae) through comparative genomic analysis with *Drosophila melanogaster* utilizing modENCODE datasets. *BMC Genomics* 15, 942.
- Goodwin, S.S., Vale, R.D., 2010. Patronin regulates the microtubule network by protecting microtubule minus ends. *Cell* 143, 263-274.
- Goud, B., Gleeson, P.A., 2010. TGN golgins, Rab and cytoskeleton: regulating the Golgi trafficking highways. *Trends Cell Biol* 20, 329-336.
- Gregor, T., McGregor, A.P., Wieschaus, E.F., 2008. Shape and function of the Bicoid morphogen gradient in dipteran species with different sized embryos. *Dev Biol* 316, 350-358.
- Gregor, T., Wieschaus, E.F., McGregor, A.P., Bialek, W., Tank, D.W., 2007. Stability and nuclear dynamics of the bicoid morphogen gradient. *Cell* 130, 141-152.
- Grimm, O., Coppey, M., Wieschaus, E., 2010. Modelling the Bicoid gradient. *Development* 137, 2253-2264.
- Haddad, G.G., Sun, Y., Wyman, R.J., Xu, T., 1997. Genetic basis of tolerance to O₂ deprivation in *Drosophila melanogaster*. *Proc Natl Acad Sci U S A* 94, 10809-10812.
- Harms, E., Chu, T., Henrion, G., Strickland, S., 2000. The only function of Grauzone required for *Drosophila* oocyte meiosis is transcriptional activation of the cortex gene. *Genetics* 155, 1831-1839.
- Heinrich, E.C., Farzin, M., Klok, C.J., Harrison, J.F., 2011. The effect of developmental stage on the sensitivity of cell and body size to hypoxia in *Drosophila melanogaster*. *J Exp Biol* 214, 1419-1427.
- Horner, V.L., Czank, A., Jang, J.K., Singh, N., Williams, B.C., Puro, J., Kubli, E., Hanes, S.D., McKim, K.S., Wolfner, M.F., Goldberg, M.L., 2006. The *Drosophila* calcipressin sarah is required for several aspects of egg activation. *Curr Biol* 16, 1441-1446.
- Howard, K.R., Struhl, G., 1990. Decoding positional information: regulation of the pair-rule gene hairy. *Development* 110, 1223-1231.
- Hurd, T.R., Herrmann, B., Sauerwald, J., Sanny, J., Grosch, M., Lehmann, R., 2016. Long Oskar Controls Mitochondrial Inheritance in *Drosophila melanogaster*. *Dev Cell* 39, 560-571.
- Juge, F., Zaessinger, S., Temme, C., Wahle, E., Simonelig, M., 2002. Control of poly(A) polymerase level is essential to cytoplasmic polyadenylation and early development in *Drosophila*. *EMBO J* 21, 6603-6613.

- Kantorovitz, M.R., Kazemian, M., Kinston, S., Miranda-Saavedra, D., Zhu, Q., Robinson, G.E., Gottgens, B., Halfon, M.S., Sinha, S., 2009. Motif-blind, genome-wide discovery of cis-regulatory modules in *Drosophila* and mouse. *Dev Cell* 17, 568-579.
- Karr, T.L., Alberts, B.M., 1986. Organization of the cytoskeleton in early *Drosophila* embryos. *J Cell Biol* 102, 1494-1509.
- Khodjakov, A., Cole, R.W., Oakley, B.R., Rieder, C.L., 2000. Centrosome-independent mitotic spindle formation in vertebrates. *Curr Biol* 10, 59-67.
- Khuc Trong, P., Doerflinger, H., Dunkel, J., St Johnston, D., Goldstein, R.E., 2015. Cortical microtubule nucleation can organise the cytoskeleton of *Drosophila* oocytes to define the anteroposterior axis. *Elife* 4.
- Kicheva, A., Pantazis, P., Bollenbach, T., Kalaidzidis, Y., Bittig, T., Julicher, F., Gonzalez-Gaitan, M., 2007. Kinetics of morphogen gradient formation. *Science* 315, 521-525.
- Kornberg, T.B., Krasnow, M.A., 2000. The *Drosophila* genome sequence: implications for biology and medicine. *Science* 287, 2218-2220.
- Lasko, P., 2012. mRNA localization and translational control in *Drosophila* oogenesis. *Cold Spring Harb Perspect Biol* 4.
- Lieberfarb, M.E., Chu, T., Wreden, C., Theurkauf, W., Gergen, J.P., Strickland, S., 1996. Mutations that perturb poly(A)-dependent maternal mRNA activation block the initiation of development. *Development* 122, 579-588.
- Little, S.C., Tikhonov, M., Gregor, T., 2013. Precise developmental gene expression arises from globally stochastic transcriptional activity. *Cell* 154, 789-800.
- Lucas, T., Ferraro, T., Roelens, B., De Las Heras Chanes, J., Walczak, A.M., Coppey, M., Dostatni, N., 2013. Live imaging of bicoid-dependent transcription in *Drosophila* embryos. *Curr Biol* 23, 2135-2139.
- Malikov, V., Kashina, A., Rodionov, V., 2004. Cytoplasmic dynein nucleates microtubules to organize them into radial arrays in vivo. *Mol Biol Cell* 15, 2742-2749.
- Markussen, F.H., Michon, A.M., Breitwieser, W., Ephrussi, A., 1995. Translational control of oskar generates short OSK, the isoform that induces pole plasma assembly. *Development* 121, 3723-3732.
- Marlow, F.L., 2010. *Maternal Control of Development in Vertebrates: My Mother Made Me Do It!*, San Rafael (CA).
- McCartney, B.M., McEwen, D.G., Grevenkoed, E., Maddox, P., Bejsovec, A., Peifer, M., 2001. *Drosophila* APC2 and Armadillo participate in tethering mitotic spindles to cortical actin. *Nat Cell Biol* 3, 933-938.
- McGregor, A.P., 2005. How to get ahead: the origin, evolution and function of bicoid. *Bioessays* 27, 904-913.
- Miller, P.M., Folkmann, A.W., Maia, A.R., Efimova, N., Efimov, A., Kaverina, I., 2009. Golgi-derived CLASP-dependent microtubules control Golgi organization and polarized trafficking in motile cells. *Nat Cell Biol* 11, 1069-1080.
- Mottier-Pavie, V., Cenci, G., Verni, F., Gatti, M., Bonaccorsi, S., 2011. Phenotypic analysis of misato function reveals roles of noncentrosomal microtubules in *Drosophila* spindle formation. *J Cell Sci* 124, 706-717.

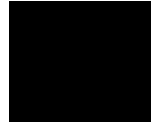
- Moutinho-Pereira, S., Debec, A., Maiato, H., 2009. Microtubule cytoskeleton remodeling by acentriolar microtubule-organizing centers at the entry and exit from mitosis in *Drosophila* somatic cells. *Mol Biol Cell* 20, 2796-2808.
- Nagaraj, R., Banerjee, U., 2004. The little R cell that could. *Int J Dev Biol* 48, 755-760.
- Nashchekin, D., Fernandes, A.R., St Johnston, D., 2016. Patronin/Shot Cortical Foci Assemble the Noncentrosomal Microtubule Array that Specifies the *Drosophila* Anterior-Posterior Axis. *Dev Cell* 38, 61-72.
- Nguyen, M.M., Stone, M.C., Rolls, M.M., 2011. Microtubules are organized independently of the centrosome in *Drosophila* neurons. *Neural Dev* 6, 38.
- Niessing, D., Dostatni, N., Jackle, H., Rivera-Pomar, R., 1999. Sequence interval within the PEST motif of Bicoid is important for translational repression of caudal mRNA in the anterior region of the *Drosophila* embryo. *Embo Journal* 18, 1966-1973.
- Norvell, A., Wong, J., Randolph, K., Thompson, L., 2015. Wispy and Orb cooperate in the cytoplasmic polyadenylation of localized *gurken* mRNA. *Dev Dyn* 244, 1276-1285.
- Nozawa, K., Fritzler, M.J., Chan, E.K., 2005. Unique and shared features of Golgi complex autoantigens. *Autoimmun Rev* 4, 35-41.
- Page, A.W., Orr-Weaver, T.L., 1996. The *Drosophila* genes *grauzone* and *cortex* are necessary for proper female meiosis. *J Cell Sci* 109 (Pt 7), 1707-1715.
- Pandey, U.B., Nichols, C.D., 2011. Human disease models in *Drosophila melanogaster* and the role of the fly in therapeutic drug discovery. *Pharmacol Rev* 63, 411-436.
- Parry, D.H., O'Farrell, P.H., 2001. The schedule of destruction of three mitotic cyclins can dictate the timing of events during exit from mitosis. *Curr Biol* 11, 671-683.
- Porcher, A., Abu-Arish, A., Huart, S., Roelens, B., Fradin, C., Dostatni, N., 2010. The time to measure positional information: maternal *hunchback* is required for the synchrony of the Bicoid transcriptional response at the onset of zygotic transcription. *Development* 137, 2795-2804.
- Porcher, A., Dostatni, N., 2010. The bicoid morphogen system. *Curr Biol* 20, R249-254.
- Rand, M.D., Kearney, A.L., Dao, J., Clason, T., 2010. Permeabilization of *Drosophila* embryos for introduction of small molecules. *Insect Biochem Mol Biol* 40, 792-804.
- Reilein, A., Nelson, W.J., 2005. APC is a component of an organizing template for cortical microtubule networks. *Nat Cell Biol* 7, 463-473.
- Reiter, L.T., Potocki, L., Chien, S., Gribskov, M., Bier, E., 2001. A systematic analysis of human disease-associated gene sequences in *Drosophila melanogaster*. *Genome Res* 11, 1114-1125.
- Riabinina, O., Potter, C.J., 2016. The Q-System: A Versatile Expression System for *Drosophila*. *Methods Mol Biol* 1478, 53-78.
- Riddihough, G., Ish-Horowicz, D., 1991. Individual stripe regulatory elements in the *Drosophila* hairy promoter respond to maternal, gap, and pair-rule genes. *Genes Dev* 5, 840-854.
- Rios, R.M., Sanchis, A., Tassin, A.M., Fedriani, C., Bornens, M., 2004. GMAP-210 recruits gamma-tubulin complexes to cis-Golgi membranes and is required for Golgi ribbon formation. *Cell* 118, 323-335.

- Rivera-Pomar, R., Niessing, D., Schmidt-Ott, U., Gehring, W.J., Jackle, H., 1996. RNA binding and translational suppression by bicoid. *Nature* 379, 746-749.
- Rodel, C.J., Gilles, A.F., Averof, M., 2013. MicroRNAs act as cofactors in bicoid-mediated translational repression. *Curr Biol* 23, 1579-1584.
- Rodriguez, O.C., Schaefer, A.W., Mandato, C.A., Forscher, P., Bement, W.M., Waterman-Storer, C.M., 2003. Conserved microtubule-actin interactions in cell movement and morphogenesis. *Nat Cell Biol* 5, 599-609.
- Salles, F.J., Lieberfarb, M.E., Wreden, C., Gergen, J.P., Strickland, S., 1994. Coordinate initiation of *Drosophila* development by regulated polyadenylation of maternal messenger RNAs. *Science* 266, 1996-1999.
- Sanders, A.A., Kaverina, I., 2015. Nucleation and Dynamics of Golgi-derived Microtubules. *Front Neurosci* 9, 431.
- Schulman, V.K., Folker, E.S., Baylies, M.K., 2013. A method for reversible drug delivery to internal tissues of *Drosophila* embryos. *Fly (Austin)* 7, 193-203.
- Schupbach, T., Wieschaus, E., 1989. Female sterile mutations on the second chromosome of *Drosophila melanogaster*. I. Maternal effect mutations. *Genetics* 121, 101-117.
- Seeger, M.A., Kaufman, T.C., 1990. Molecular analysis of the bicoid gene from *Drosophila pseudoobscura*: identification of conserved domains within coding and noncoding regions of the bicoid mRNA. *EMBO J* 9, 2977-2987.
- Shaw, P.J., Salameh, A., McGregor, A.P., Bala, S., Dover, G.A., 2001. Divergent structure and function of the bicoid gene in Muscoidea fly species. *Evolution & development* 3, 251-262.
- Sigaut, L., Pearson, J.E., Colman-Lerner, A., Ponce Dawson, S., 2014. Messages do diffuse faster than messengers: reconciling disparate estimates of the morphogen bicoid diffusion coefficient. *PLoS computational biology* 10, e1003629.
- Sinka, R., Gillingham, A.K., Kondylis, V., Munro, S., 2008. Golgi coiled-coil proteins contain multiple binding sites for Rab family G proteins. *J Cell Biol* 183, 607-615.
- Spector, I., Braet, F., Shochet, N.R., Bubb, M.R., 1999. New anti-actin drugs in the study of the organization and function of the actin cytoskeleton. *Microsc Res Tech* 47, 18-37.
- Spirov, A., Fahmy, K., Schneider, M., Frei, E., Noll, M., Baumgartner, S., 2009. Formation of the bicoid morphogen gradient: an mRNA gradient dictates the protein gradient. *Development* 136, 605-614.
- St Johnston, D., 2002. The art and design of genetic screens: *Drosophila melanogaster*. *Nat Rev Genet* 3, 176-188.
- Stauber, M., Jackle, H., Schmidt-Ott, U., 1999. The anterior determinant bicoid of *Drosophila* is a derived Hox class 3 gene. *Proc Natl Acad Sci U S A* 96, 3786-3789.
- Stauber, M., Prell, A., Schmidt-Ott, U., 2002. A single Hox3 gene with composite bicoid and *zerknüllt* expression characteristics in non-Cyclorrhaphan flies. *Proc Natl Acad Sci U S A* 99, 274-279.
- Stauber, M., Taubert, H., Schmidt-Ott, U., 2000. Function of bicoid and hunchback homologs in the basal cyclorrhaphan fly *Megaselia* (Phoridae). *Proc Natl Acad Sci U S A* 97, 10844-10849.

- Steinhauer, J., Kalderon, D., 2006. Microtubule polarity and axis formation in the *Drosophila* oocyte. *Dev Dyn* 235, 1455-1468.
- Stephens, D.J., 2012. Functional coupling of microtubules to membranes - implications for membrane structure and dynamics. *J Cell Sci* 125, 2795-2804.
- Stephenson, E.C., Pokrywka, N.J., 1992. Localization of bicoid message during *Drosophila* oogenesis. *Current topics in developmental biology* 26, 23-34.
- Struhl, G., Struhl, K., Macdonald, P.M., 1989. The gradient morphogen bicoid is a concentration-dependent transcriptional activator. *Cell* 57, 1259-1273.
- Sullivan, W., Theurkauf, W.E., 1995. The cytoskeleton and morphogenesis of the early *Drosophila* embryo. *Curr Opin Cell Biol* 7, 18-22.
- Surdej, P., Jacobs-Lorena, M., 1998. Developmental regulation of bicoid mRNA stability is mediated by the first 43 nucleotides of the 3' untranslated region. *Mol Cell Biol* 18, 2892-2900.
- Takeichi, M., Toya, M., 2016. Patronin Takes a Shot at Polarity. *Dev Cell* 38, 12-13.
- Theurkauf, W.E., Hawley, R.S., 1992. Meiotic spindle assembly in *Drosophila* females: behavior of nonexchange chromosomes and the effects of mutations in the nod kinesin-like protein. *J Cell Biol* 116, 1167-1180.
- Theurkauf, W.E., Smiley, S., Wong, M.L., Alberts, B.M., 1992. Reorganization of the cytoskeleton during *Drosophila* oogenesis: implications for axis specification and intercellular transport. *Development* 115, 923-936.
- Trovisco, V., Belaya, K., Nashchekin, D., Irion, U., Sirinakis, G., Butler, R., Lee, J.J., Gavis, E.R., St Johnston, D., 2016. bicoid mRNA localises to the *Drosophila* oocyte anterior by random Dynein-mediated transport and anchoring. *eLife* 5.
- Turing, A.M., 1952. The Chemical Basis of Morphogenesis. *Philos T Roy Soc B* 237, 37-72.
- Vanzo, N., Oprins, A., Xanthakis, D., Ephrussi, A., Rabouille, C., 2007. Stimulation of endocytosis and actin dynamics by Oskar polarizes the *Drosophila* oocyte. *Dev Cell* 12, 543-555.
- Viktorinova, I., Wimmer, E.A., 2007. Comparative analysis of binary expression systems for directed gene expression in transgenic insects. *Insect Biochem Mol Biol* 37, 246-254.
- Wagner, C., Ehresmann, C., Ehresmann, B., Brunel, C., 2004. Mechanism of dimerization of bicoid mRNA: initiation and stabilization. *J Biol Chem* 279, 4560-4569.
- Wei, J.H., Zhang, Z.C., Wynn, R.M., Seemann, J., 2015. GM130 Regulates Golgi-Derived Spindle Assembly by Activating TPX2 and Capturing Microtubules. *Cell* 162, 287-299.
- Weil, T.T., Forrest, K.M., Gavis, E.R., 2006. Localization of bicoid mRNA in late oocytes is maintained by continual active transport. *Dev Cell* 11, 251-262.
- Weil, T.T., Parton, R., Davis, I., Gavis, E.R., 2008. Changes in bicoid mRNA anchoring highlight conserved mechanisms during the oocyte-to-embryo transition. *Curr Biol* 18, 1055-1061.

- Weil, T.T., Xanthakis, D., Parton, R., Dobbie, I., Rabouille, C., Gavis, E.R., Davis, I., 2010. Distinguishing direct from indirect roles for bicoid mRNA localization factors. *Development* 137, 169-176.
- Whitworth, A.J., 2011. *Drosophila* models of Parkinson's disease. *Adv Genet* 73, 1-50.
- Wieschaus, E., 2016. Positional Information and Cell Fate Determination in the Early *Drosophila* Embryo. *Curr Top Dev Biol* 117, 567-579.
- Wolpert, L., 1998. Principles of development. *Current Biology* ; Oxford University Press, London ; New York Oxford ; New York.
- Xu, Z., Chen, H., Ling, J., Yu, D., Struffi, P., Small, S., 2014. Impacts of the ubiquitous factor Zelda on Bicoid-dependent DNA binding and transcription in *Drosophila*. *Genes Dev* 28, 608-621.
- Yadav, S., Linstedt, A.D., 2011. Golgi positioning. *Cold Spring Harb Perspect Biol* 3.
- Yuan, K., O'Farrell, P.H., 2015. Cyclin B3 Is a Mitotic Cyclin that Promotes the Metaphase-Anaphase Transition. *Current Biology* 25, 811-816.
- Yvon, A.M., Wadsworth, P., 1997. Non-centrosomal microtubule formation and measurement of minus end microtubule dynamics in A498 cells. *J Cell Sci* 110 (Pt 19), 2391-2401.
- Zhao, C., Fu, D., Dave, V., Ma, J., 2003. A composite motif of the *Drosophila* morphogenetic protein bicoid critical to transcription control. *The Journal of biological chemistry* 278, 43901-43909.
- Zhao, C., York, A., Yang, F., Forsthoefel, D.J., Dave, V., Fu, D., Zhang, D., Corado, M.S., Small, S., Seeger, M.A., Ma, J., 2002. The activity of the *Drosophila* morphogenetic protein Bicoid is inhibited by a domain located outside its homeodomain. *Development* 129, 1669-1680.
- Zhu, X., Kaverina, I., 2013. Golgi as an MTOC: making microtubules for its own good. *Histochem Cell Biol* 140, 361-367.

Paper I





αTubulin 67C and *Ncd* Are Essential for Establishing a Cortical Microtubular Network and Formation of the *Bicoid* mRNA Gradient in *Drosophila*

Khalid Fahmy^{1†}, Mira Akber², Xiaoli Cai, Aabid Koul, Awais Hayder, Stefan Baumgartner*

Department of Experimental Medical Sciences, Lund University, Lund, Sweden

Abstract

The Bicoid (Bcd) protein gradient in *Drosophila* serves as a paradigm for gradient formation in textbooks. To explain the generation of the gradient, the ARTS model, which is based on the observation of a *bcd* mRNA gradient, proposes that the *bcd* mRNA, localized at the anterior pole at fertilization, migrates along microtubules (MTs) at the cortex to the posterior to form a *bcd* mRNA gradient which is translated to form a protein gradient. To fulfil the criteria of the ARTS model, an early cortical MT network is thus a prerequisite. We report hitherto undiscovered MT activities in the early embryo important for *bcd* mRNA transport: (i) an early and omnidirectional MT network exclusively at the anterior cortex of early nuclear cycle embryos showing activity during metaphase and anaphase only, (ii) long MTs up to 50 μm extending into the yolk at blastoderm stage to enable basal-apical transport. The cortical MT network is not anchored to the actin cytoskeleton. The posterior transport of the mRNA via the cortical MT network critically depends on maternally-expressed *αTubulin67C* and the minus-end motor *Ncd*. In either mutant, cortical transport of the *bcd* mRNA does not take place and the mRNA migrates along another yet undisclosed interior MT network, instead. Our data strongly corroborate the ARTS model and explain the occurrence of the *bcd* mRNA gradient.

Citation: Fahmy K, Akber M, Cai X, Koul A, Hayder A, et al. (2014) *αTubulin 67C* and *Ncd* Are Essential for Establishing a Cortical Microtubular Network and Formation of the *Bicoid* mRNA Gradient in *Drosophila*. PLoS ONE 9(11): e112053. doi:10.1371/journal.pone.0112053

Editor: Christian Bökel, Technische Universität Dresden, Germany

Received: July 8, 2014; **Accepted:** October 10, 2014; **Published:** November 12, 2014

Copyright: © 2014 Fahmy et al. This is an open-access article distributed under the terms of the Creative Commons Attribution License, which permits unrestricted use, distribution, and reproduction in any medium, provided the original author and source are credited.

Data Availability: The authors confirm that all data underlying the findings are fully available without restriction. All relevant data are within the paper and its Supporting Information files.

Funding: SB received funding from the Swedish Research Council, the Eric Philippp Sörensen Stiftelse, the Olle Engkvist Foundation, and the Medical Faculty of Lund. KF received funding from the Swedish Research Council and Hereditas. The funders had no role in study design, data collection and analysis, decision to publish, or preparation of the manuscript.

Competing Interests: The authors have declared that no competing interests exist.

* Email: Stefan.Baumgartner@med.lu.se

† Current address: Department of Genetics, Faculty of Agriculture, Ain Shams University, Cairo, Egypt

‡ These authors contributed equally to this work.

Introduction

The Bicoid (Bcd) protein is a paradigm for morphogen gradient formation taught in textbooks and studied for more than two decades. The hallmark of the Bcd morphogen is its spectacular gradient along the anterior-posterior axis of the early *Drosophila* blastoderm egg [1]. In the past, two models were put forward to explain the formation of the gradient, the ARTS model [2–4] and the SDD model [1,5]. The SDD (Synthesis, Diffusion and Degradation) model proposes that the gradient arises through translation of an anteriorly-localized *bcd* mRNA source, followed by diffusion of Bcd throughout the embryo, and uniform degradation. In contrast, the ARTS (Active RNA Transport and Synthesis) model proposes that the *bcd* mRNA is actively transported along the cortex in a posterior direction from its anterior pole to form an mRNA gradient which serves as template for the synthesis of Bcd.

Recently, the SDD model encountered some severe difficulties: the diffusion coefficient of Bcd was found to be two orders of magnitude too low to establish a steady-state Bcd gradient by the blastoderm stage [5]. Subsequently, other reports measured higher

diffusion rates [6,7], calculated to be high enough to explain the SDD diffusion model, and corroborated by a recent biophysical model analysis [8]. Unfortunately, as a major drawback, all the above analyses comprised measurements of diffusion during late nuclear cycles (nc) 10–14 and at the peripheral cytoplasm of the embryo. However, we should bear in mind that the time window from fertilization up to nc 10 is the important time interval where the SDD model predicts long-range diffusion of Bcd. Arguably, the diffusion properties of proteins in the dense yolk are different from those of the cytoplasm surrounding the cortical nuclei at 10–14 which make predictions of the diffusion coefficient problematic. It is thus important to note here that, although these above experimental and theoretical data permit to explain the SDD model, it would be premature to imply *a priori* that the SDD model is the correct one. Furthermore, the model still lacks a direct proof of the existence of long-range Bcd diffusion, e. g. by tracking single Bcd molecules during the early nuclear cycles. Equally important to note: the ARTS model does not argue against a high diffusion coefficient of Bcd, it is only largely irrelevant for the model.

The existence of a *bcd* mRNA gradient, which is the hallmark of the ARTS model, was first described in 1986 [2]. In 2009, the SDD model was challenged by a detailed analysis of the *bcd* mRNA distribution during early *Drosophila* embryogenesis [3], which confirmed previous data [2]. On the other hand, the ARTS model, which is based on this demonstration, raises the question of how the *bcd* mRNA gradient forms from a *bcd* mRNA source that at fertilization is strictly localized to the anterior pole of the embryo.

Plenty of information is meanwhile available on the transport of the *bcd* mRNA during oogenesis, using *in vivo* imaging of the movement of the *bcd* mRNA [9,10]. These data showed that the dumping of the *bcd* mRNA by the nurse cells into the oocyte starts at stage 10b, accompanied by an active cytoplasmic movement within the oocyte (also referred to as “ooplasmic streaming” [9]). During subsequent developmental stages (stages 10b-13), the *bcd* mRNA behaves very dynamic [10], however, a microtubule (MT)-based transport, with the help of the minus-end motor *dynein*, begins to accumulate the mRNA at the anterior pole [9,10] such that at the end of oogenesis, the *bcd* mRNA is confined completely to the anterior pole, anchored by the actin cytoskeleton. Recent measurements showed that *Drosophila* females produce around 7.4×10^7 *bcd* mRNA molecules which are dumped into the egg as maternal supply [11].

As far as the MT network in the oocyte is concerned, several conflicting models were published how MTs are organized and how they transport maternal factors to the anterior or posterior ends of the oocyte [12–17]. More recently, however, using *in vivo* imaging, Parton et al. resolved many issues of the conflicting models and reported highly dynamic MTs that are organized with a biased random polarity that increased toward the posterior [18]. However, it is important to note that at the end of oogenesis, all MTs are completely degraded again [19–21], implying that fertilized embryos need to start to build up the MTs from the beginning.

The ARTS model postulated a mechanism based on MTs that transport the *bcd* mRNA [3]. Yet, so far convincing evidence for such a postulated network of MTs has been lacking. A plethora of information on the content and appearance of *Drosophila* Tubulin is available, but most reports are devoted to the blastoderm stage, while data on MT architecture in early nc embryos are scarce. [22,23] reported the existence of an extensive cortical network throughout the embryo. However, there is a major problem with these reports, as Taxol was used to stabilize the MTs which gives an altered picture of the native MT architecture. Hence our quest for a technique that would allow to preserve the native appearance of cortical MTs of early nc embryos.

Using a modified permeabilization and fixation method to rapidly fix and preserve cortical MT structures, we detected MT activity in early nc embryos and demonstrate that (i) there is an extensive MT network exclusively in the anterior half, (ii) this MT network is only formed at the cortex, and (iii) Taxol induces artefacts giving the impression that the egg contains a dense and ubiquitous network of cortical MTs. Further, we show that *αTubulin67C* and the kinesin-like minus-end motor *ncd* are critically important for transport of the *bcd* mRNA in the oocyte and along the embryonic cortex to establish the mRNA gradient.

Results

The bicoid mRNA gradient

We recently reported the existence of a *bcd* mRNA gradient in *Drosophila* [3] that corroborated earlier data [2]. Typical examples of an mRNA gradient are shown in an embryo at nc

1444 min. (Fig. 1A, B, Fig. S1B) where the posterior extent of the gradient reaches about 40% egg length (EL). At this stage, the majority of the mRNA is transported from the basal to apical side of the nuclei and thus accumulates at the periplasm, before rapid degradation commences [3]. At fertilization, however, the mRNA is tightly associated with the tip of the embryo (Fig. S1A). Hence, to convert the pattern at fertilization to that at nc 14, a transportation system was proposed involving cortical MTs which is one of the facets of the ARTS model [3]. In the large blowfly *Lucilia sericata*, the gradient appears very similar (Fig. S1C, D), suggesting that the mRNA gradient as well as the ARTS model are universal among Diptera. Moreover, recent large-scale analysis of cryo-sliced embryos confirms the existence of a long *bcd* mRNA gradient showing transcripts up to 40% EL [24]; FlyBase).

A cortical MT network in the anterior half of early nuclear cycle embryos

In search for a method to stain native MTs without the necessity to use Taxol for stabilization, we utilized an efficient permeabilization protocol that avoids heptane [25] and adapted it using high concentrations of formaldehyde to “freeze” the cortical MTs as fast as possible. This fixation technique, along with monoclonal antibody YL_{1,2} against tyrosinated tubulin (i. e. against freshly-assembled Tubulin [26], allowed for the staining of a cortical and omnidirectional MT network (Fig. 1C, Video S1). The network can also be visualized by using a more conventional 27% formaldehyde/heptane fixation protocol, but with a somewhat poorer preservation of the MTs. Interestingly, this network was confined exclusively to the anterior half of the embryo and appeared only during metaphase and anaphase of nc 1–6 embryos (Fig. 1C, insert), i. e. during short nuclear phases of 1 minute each [27]. Moreover, the threads were found in the outermost 20 μm of the cortex only (Fig. 1H). Attempts to live-image the network using *αTubulin84B-GFP* embryos failed, due to the weakness of the signal and the dynamics of the MTs (data not shown). The network was not detected in unfertilized embryos (Fig. 1D, E), but became apparent from nc 1 onwards, exemplified by a nc 1 (Fig. 1C) or a nc 4 embryo (Fig. 1F). From nc 6 on, it was present throughout all nuclear phases, e. g. during interphase (Fig. 1H, H'), while still being absent in the posterior half (Fig. 1I). At nc 7, when cortical migration commences, the posterior half showed cortical MT activity also (data not shown). At nc 11, tyrosinated tubulin is detected as a dense network below the nuclear layer originating from long astral MTs that surround the nuclei (Fig. 1J, K). Notably, these astral MTs showed Staufen-mediated *bcd* mRNA binding activity [28]. At nc 13, strong MT activity was detected showing long extensions up to 30 μm into the yolk (Fig. 1L, insert) and even longer ones in nc 14 embryos (Fig. 1M, N, up to 50 μm). These threads resemble those on the drawings by [29]. The majority of these long MTs could also be stained using antibodies against *αTubulin 67C* (*αTub67C*; Fig. 1O), a maternal Tubulin known to contribute to long MTs and which is expressed mainly in oocytes and in early embryos [30,31]. nc 14 embryos also revealed a striking regionalization of Tubulin; if stained with mab DM1A which detects both *αTubulin 84B* and *αTubulin 84D* (Fig. 1P; [31]), then these two Tubulins are preferentially associated with MTs that embrace the nuclei (Fig. 1P, green channel), compared to *αTub67C* which also accumulates in the periplasm (Fig. 1O, green channel). Hence, the composition of *αTubulins* in the different cellular sub-compartments varies in space. Since the lengths of these threads by far exceed the observed lengths of MTs of previous reports [22] despite Taxol being used in these studies which favours long MTs, we concluded

sagittal section of the same embryo, supplemented with the signal from the nuclear stain using DAPI (blue) and an antibody against γ Tubulin (green). A dense network is detected around the nuclei. (L) confocal mid-sagittal section of a nc 13 embryo, along with the signals from the nuclear stain using DAPI (blue) and an antibody against γ Tubulin (green). An extensive MT network ranging deeply into the yolk is visible (insert, thickness about 30 μ m). (M) and (N) confocal mid-sagittal section of a nc 14+10 min. embryo, along with the signals from the nuclear stain DAPI (blue) and an antibody against Minispindles (green). (N) high magnification of the insert in (M) showing an extensive MT network ranging deeply into the yolk (insert, about 50 μ m deep). (O) colocalization of mab YL_{1,2} to polyclonal α Tub67C antibody in a cellularised nc 14 embryo, along with DAPI staining. Most YL_{1,2}-positive threads are also positive for α Tub67C. (P) colocalization of mabYL_{1,2} to mab DM1A in a nc 14+18 min. embryo, along with DAPI staining. Most YL_{1,2} threads are co-localized with DM1A at perinuclear MTs, while the periplasm is virtually free from α Tub84B & D. Stages of embryos are denoted in yellow and follow the nomenclature of [61] and [3]. doi:10.1371/journal.pone.0112053.g001

that the long MTs in Fig. 1J–M were preserved owing to the improved fixation method.

Independence of the MT network from actin

To determine whether or not a link exists between the cortical MT network and actin, we examined their relative distribution patterns in early embryos. In the anterior tip of a nc 2 embryo, the actin formed a dense layer (Fig. 2A) which was not in contact with the MT network (Fig. 2B, C). At later stages (nc 6), the situation remained unchanged (Fig. 2D–F). A 3-D visualization technique of the two confocal stacks in Fig. 2A and B allowed us to visualize the relationship of the MT threads to actin more explicitly (Fig. 2G, H; Video S2 & S3). Evidently, at no location of the scanned area, the MT network was associated with the actin sheet, rather it resided immediately next to it at the inner cortex.

Taxol induces artefacts

Previous analyses of MT activity reported a cortical network of short MT [22,23,32,33], but many of these investigations used the MT-stabilizing drug Taxol. We therefore repeated these experiments with Taxol and noted that the MT threads could even be detected in unfertilized embryos (Fig. 3A, B). Furthermore, the threads were found uniformly distributed in the posterior half. Fertilized embryos showed the same distribution, as shown in a nc 5 embryo, although the density of threads was somewhat increased, while no difference in length was detected (Fig. 3C, D). When a mixture of Colchicine and Colcemide, drugs known to destabilize MT threads, was applied, we found that the drug treatment led to complete degradation of all MT threads (Fig. 3E, F). Our data from Taxol treatments suggest that the Tubulin monomers are present throughout the embryo, but under normal conditions they polymerize only in the anterior half.

α Tubulin67C and *ncd* are critically important for cortical MT formation and *bcd* mRNA transport

Of the α Tubulin genes [34] that would be critical for cortical mRNA transport, we considered α Tub67C a good candidate since it showed maternal expression and an expression profile similar to that of *bcd* mRNA [34,35]. The α Tub67C locus is represented by the α Tub67C mutant alleles [30,36] and by the independently isolated dominant female-sterile *Kavar* mutants [31,37]. We stained eggs of *kavar^{mut}*-hemizygous mothers (a complete loss-of-function (LOF) mutation) [37] for the presence of the cortical network and found a network of short MTs without directionality (Fig. 4A, B), consistent with the notion that α Tub67C is required for the formation of long MTs [31,37]. If assayed for *bcd* mRNA transport, embryos do not show any cortical transport, rather the mRNA formed a long streak in the interior of the embryo in parallel to the A-P axis (Fig. 4C). Next, we assayed the behaviour of the mRNA in oocytes of homozygous α Tub67C³ females, the weakest available allele. In a stage 10 α Tub67C³ oocyte, the mRNA did not localize to the anterior pole, residing instead at the edge (Fig. 4D). In a late stage 14 oocyte, the aberrant lateral

localization was even more pronounced showing a shallow anterior distribution (Fig. 4E), demonstrating a vital role for α Tub67C³ allele in anterior localization of the *bcd* mRNA during oogenesis, in contrast to the *null* alleles, see below. In α Tub67C³ embryos, the mRNA shows a shallow gradient from the time of fertilization on, similar to the profile in late oogenesis (Fig. 4E, data not shown). However, when α Tub67C³ embryos were assayed for the presence of the cortical network using mab YL_{1,2}, we noted a dense network of MTs (Fig. S2C). A larger area showed the MTs assembled in aster-like structures (asterisks), surprisingly without any nuclei in their centers, previously detected in α Tub67C² and α Tub67C¹ alleles [30]. The remaining area showed a dense network, similar to Taxol-treated embryos (Fig. 3A–D). The other α Tub67C alleles behaved similar to the LOF allele, with α Tub67C⁴, α Tub67C², *Kavar^{21C}* and *Kavar^{18C}* showing the mRNA streak (Fig. S2A, B, D, E). Interestingly, α Tub67C³ was the only allele that showed a specific effect on mRNA transport and localization in the oocyte (Fig. 4D, E), while the *null* allele showed the mRNA accumulated largely normal at the anterior pole during oogenesis (Fig. S2H). This notion is supported by data from [38] that demonstrated that *kavar^{mut}* mutants show almost normal ooplasmic streaming.

In search for specific motor proteins associated with α Tub67C, we noted the *nonclaret disjunctional* (*ncd*) locus encoding an unconventional Kinesin which transports cargos to the minus-end [39] and which interacts genetically with α Tub67C [40,41]. We first analysed a strong *ncd* allele, *ncd¹* which again showed a large *bcd* mRNA streak (Fig. 4F), similar to that in *kavar^{mut}* mutant embryos (Fig. 4C). A semi-lethal allele, *ncd⁵⁸⁸⁹*, showed this streak less pronounced and some cortical movement was observed (Fig. S2F). Next, we analysed oocytes from *ncd¹/ncd⁰* homozygous females, a weak semi-dominant female sterile allele [42] and noted that in stage 10 oocytes, the *bcd* mRNA accumulated laterally (Fig. 4G), although not as severe as in α Tub67C³ oocytes (Fig. 4D). Consequently, due to the lateral localization in oocytes, in early nc 6 *ncd¹/ncd⁰* embryos, the *bcd* mRNA appeared more posterior (Fig. 4H), compared to wild-type embryos of the same stage, while in nc 13 embryos, this aberrant localization appeared largely corrected to wild-type distribution (Fig. 4I). In oocytes of homozygous α Tub67C³ *ncd⁰* mothers, anterior mRNA transport in oocytes appeared rather normal (Fig. 4J), suggesting that *ncd⁰* ameliorates the α Tub67C³ phenotype. However, when embryos derived from homozygous α Tub67C³ *ncd⁰* mothers were assayed, they again revealed complete absence of cortical *bcd* mRNA transport (Fig. 4K). Rather, the mRNA followed a path towards the aberrantly-looking nuclei in the center of the yolk, reminiscent to the situation in *kavar^{mut}* or *ncd¹* embryos (Fig. 4C, F), however less pronounced. In α Tub67C³/*ncd⁰*/*ncd⁰* embryos [41], the mRNA followed a similar path to the center (Fig. 4L), consistent with the dominant phenotype of α Tub67C mutations [30,37].

To further corroborate an involvement of *ncd* in the transport of *bcd* mRNA, we over-expressed Ncd during oogenesis using the maternal driver V32. A stage 10 oocyte showed lateral accumulation of the mRNA (Fig. 4M), similar to α Tub67C³ oocytes

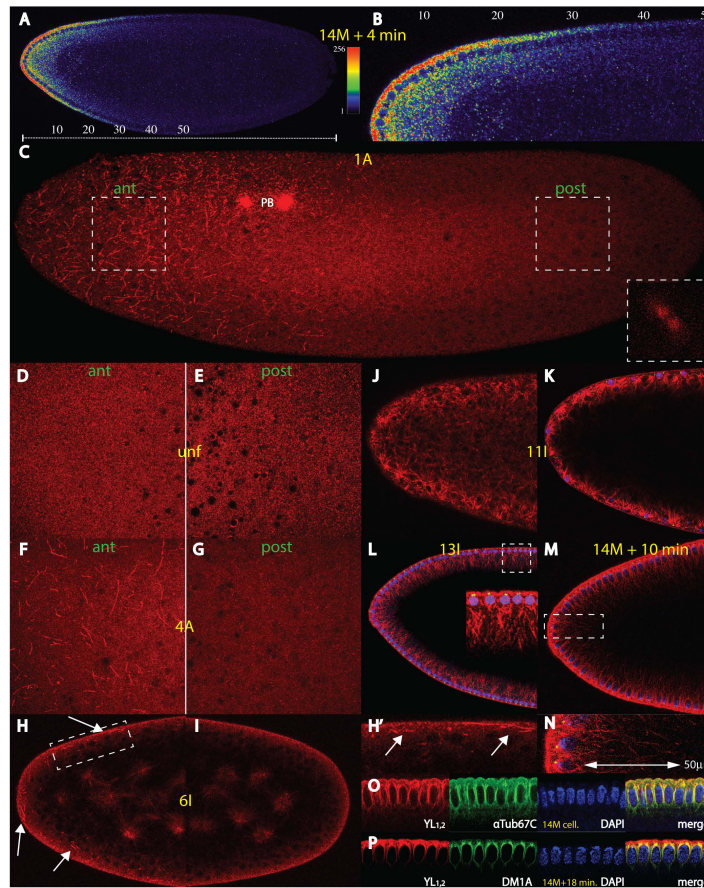


Figure 1. The *bicoid* mRNA gradient and an anterior cortical microtubular network. (A) A single confocal section of a nuclear cycle (nc) 14+4 min, *Drosophila* embryo showing a typical *bicoid* mRNA gradient extending up to 50% of egg length (EL, scale bar below embryo). Fluorescence intensities, reflecting *bicoid* mRNA concentrations were converted to a colour scale shown at the right (cf. Material and Methods). (B) High magnification of the dorsal region of embryo in (A), numbers of EL above the embryo. (C) Confocal analysis at the surface of a nc 1 embryo at anaphase (insert on lower right) using mab YL₁₂ against tyrosinated microtubules (MT), showing a network exclusively in the anterior half of the embryo, along with the polar bodies (PB). Two adjacent confocal sections 2.48 μm apart and maximal intensity projection were used. White areas denote magnifications of corresponding anterior (ant) regions and posterior (post) regions used in (D–G). (D) and (E) magnification of anterior (D) and posterior (E) portions on the surface of an unfertilized embryo. No network is visible. (F) and (G) magnification of anterior (F) and posterior (G) portions on the surface of an embryo at nc 4. The network is visible at the anterior half, but is absent in the posterior half. (H), (H') and (I) sagittal confocal sections of the anterior (H) and the posterior (I) half of an embryo at nc 6. (H') is a magnification of the area indicated in (H). The MT threads are exclusively at the anterior cortex (arrows). In the interior, asters of interphase nuclei are seen. (J) confocal section just below the nuclear layer of a nc 11 embryo and (K) mid-

sagittal section of the same embryo, supplemented with the signal from the nuclear stain using DAPI (blue) and an antibody against γ Tubulin (green). A dense network is detected around the nuclei. (L) confocal mid-sagittal section of a nc 13 embryo, along with the signals from the nuclear stain using DAPI (blue) and an antibody against γ Tubulin (green). An extensive MT network ranging deeply into the yolk is visible (insert, thickness about 30 μ m). (M) and (N) confocal mid-sagittal section of a nc 14+10 min. embryo, along with the signals from the nuclear stain DAPI (blue) and an antibody against Minispindles (green). (N) high magnification of the insert in (M) showing an extensive MT network ranging deeply into the yolk (insert, about 50 μ m deep). (O) colocalization of mab YL_{1,2} to polyclonal α Tub67C antibody in a cellularised nc 14 embryo, along with DAPI staining. Most YL_{1,2}-positive threads are also positive for α Tub67C. (P) colocalization of mabYL_{1,2} to mab DM1A in a nc 14+18 min. embryo, along with DAPI staining. Most YL_{1,2} threads are co-localized with DM1A at perinuclear MTs, while the periplasm is virtually free from α Tub84B & D. Stages of embryos are denoted in yellow and follow the nomenclature of [61] and [3]. doi:10.1371/journal.pone.0112053.g001

that the long MTs in Fig. 1J–M were preserved owing to the improved fixation method.

Independence of the MT network from actin

To determine whether or not a link exists between the cortical MT network and actin, we examined their relative distribution patterns in early embryos. In the anterior tip of a nc 2 embryo, the actin formed a dense layer (Fig. 2A) which was not in contact with the MT network (Fig. 2B, C). At later stages (nc 6), the situation remained unchanged (Fig. 2D–F). A 3-D visualization technique of the two confocal stacks in Fig. 2A and B allowed us to visualize the relationship of the MT threads to actin more explicitly (Fig. 2G, H; Video S2 & S3). Evidently, at no location of the scanned area, the MT network was associated with the actin sheet, rather it resided immediately next to it at the inner cortex.

Taxol induces artefacts

Previous analyses of MT activity reported a cortical network of short MT [22,23,32,33], but many of these investigations used the MT-stabilizing drug Taxol. We therefore repeated these experiments with Taxol and noted that the MT threads could even be detected in unfertilized embryos (Fig. 3A, B). Furthermore, the threads were found uniformly distributed in the posterior half. Fertilized embryos showed the same distribution, as shown in a nc 5 embryo, although the density of threads was somewhat increased, while no difference in length was detected (Fig. 3C, D). When a mixture of Colchicine and Colcemide, drugs known to destabilize MT threads, was applied, we found that the drug treatment led to complete degradation of all MT threads (Fig. 3E, F). Our data from Taxol treatments suggest that the Tubulin monomers are present throughout the embryo, but under normal conditions they polymerize only in the anterior half.

α Tubulin67C and *ncd* are critically important for cortical MT formation and *bcd* mRNA transport

Of the α Tubulin genes [34] that would be critical for cortical mRNA transport, we considered α Tub67C a good candidate since it showed maternal expression and an expression profile similar to that of *bcd* mRNA [34,35]. The α Tub67C locus is represented by the α Tub67C mutant alleles [30,36] and by the independently isolated dominant female-sterile *Kavar* mutants [31,37]. We stained eggs of *kavar^{mut}*-hemizygous mothers (a complete loss-of-function (LOF) mutation) [37] for the presence of the cortical network and found a network of short MTs without directionality (Fig. 4A, B), consistent with the notion that α Tub67C is required for the formation of long MTs [31,37]. If assayed for *bcd* mRNA transport, embryos do not show any cortical transport, rather the mRNA formed a long streak in the interior of the embryo in parallel to the A-P axis (Fig. 4C). Next, we assayed the behaviour of the mRNA in oocytes of homozygous α Tub67C³ females, the weakest available allele. In a stage 10 α Tub67C³ oocyte, the mRNA did not localize to the anterior pole, residing instead at the edge (Fig. 4D). In a late stage 14 oocyte, the aberrant lateral

localization was even more pronounced showing a shallow anterior distribution (Fig. 4E), demonstrating a vital role for α Tub67C³ allele in anterior localization of the *bcd* mRNA during oogenesis, in contrast to the *null* alleles, see below. In α Tub67C³ embryos, the mRNA shows a shallow gradient from the time of fertilization on, similar to the profile in late oogenesis (Fig. 4E, data not shown). However, when α Tub67C³ embryos were assayed for the presence of the cortical network using mab YL_{1,2}, we noted a dense network of MTs (Fig. S2C). A larger area showed the MTs assembled in aster-like structures (asterisks), surprisingly without any nuclei in their centers, previously detected in α Tub67C² and α Tub67C¹ alleles [30]. The remaining area showed a dense network, similar to Taxol-treated embryos (Fig. 3A–D). The other α Tub67C alleles behaved similar to the LOF allele, with α Tub67C⁴, α Tub67C², *Kavar^{21C}* and *Kavar^{18C}* showing the mRNA streak (Fig. S2A, B, D, E). Interestingly, α Tub67C³ was the only allele that showed a specific effect on mRNA transport and localization in the oocyte (Fig. 4D, E), while the *null* allele showed the mRNA accumulated largely normal at the anterior pole during oogenesis (Fig. S2H). This notion is supported by data from [38] that demonstrated that *kavar^{mut}* mutants show almost normal ooplasmic streaming.

In search for specific motor proteins associated with α Tub67C, we noted the *nonclaret disjunctional* (*ncd*) locus encoding an unconventional Kinesin which transports cargos to the minus-end [39] and which interacts genetically with α Tub67C [40,41]. We first analysed a strong *ncd* allele, *ncd¹* which again showed a large *bcd* mRNA streak (Fig. 4F), similar to that in *kavar^{mut}* mutant embryos (Fig. 4C). A semi-lethal allele, *ncd⁵⁸⁸⁹*, showed this streak less pronounced and some cortical movement was observed (Fig. S2F). Next, we analysed oocytes from *ncd¹/ncd⁰* homozygous females, a weak semi-dominant female sterile allele [42] and noted that in stage 10 oocytes, the *bcd* mRNA accumulated laterally (Fig. 4G), although not as severe as in α Tub67C³ oocytes (Fig. 4D). Consequently, due to the lateral localization in oocytes, in early nc 6 *ncd¹/ncd⁰* embryos, the *bcd* mRNA appeared more posterior (Fig. 4H), compared to wild-type embryos of the same stage, while in nc 13 embryos, this aberrant localization appeared largely corrected to wild-type distribution (Fig. 4I). In oocytes of homozygous α Tub67C³ *ncd⁰* mothers, anterior mRNA transport in oocytes appeared rather normal (Fig. 4J), suggesting that *ncd⁰* ameliorates the α Tub67C³ phenotype. However, when embryos derived from homozygous α Tub67C³ *ncd⁰* mothers were assayed, they again revealed complete absence of cortical *bcd* mRNA transport (Fig. 4K). Rather, the mRNA followed a path towards the aberrantly-looking nuclei in the center of the yolk, reminiscent to the situation in *kavar^{mut}* or *ncd¹* embryos (Fig. 4C, F), however less pronounced. In α Tub67C³/*ncd⁰*/*ncd⁰* embryos [41], the mRNA followed a similar path to the center (Fig. 4L), consistent with the dominant phenotype of α Tub67C mutations [30,37].

To further corroborate an involvement of *ncd* in the transport of *bcd* mRNA, we over-expressed Ncd during oogenesis using the maternal driver V32. A stage 10 oocyte showed lateral accumulation of the mRNA (Fig. 4M), similar to α Tub67C³ oocytes

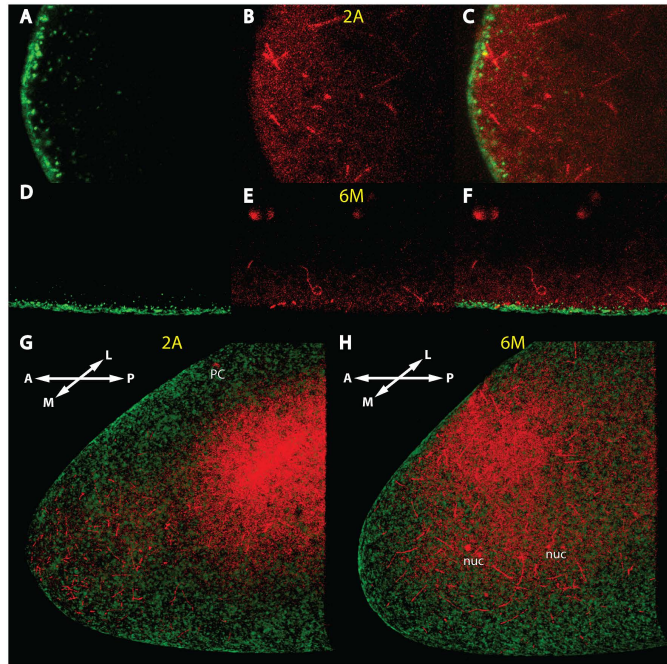


Figure 2. Independence of the early MT network from the actin sheet. (A)–(C) mid-sagittal confocal sections of the anterior tip of a nc 2 embryo stained with Phalloidin (A) to reveal the actin structure, with mab YL_{1,2} against tyrosinated Tubulin (B) and merge in (C). (D)–(F) mid-sagittal section of a ventral region about 50 μ m away from the anterior tip of a nc 6 embryo, stained with Phalloidin (D), mab YL_{1,2} (E) and merge in (F). (G) 3-D reconstruction of the confocal stack of the embryo of (A)–(C), view is from the middle (M) to the more lateral (L) part of the embryo. For film of 3D view, see Video S2. (H) 3-D reconstruction of the confocal stack of the embryo of (D)–(F), view is identical as in G. For film of 3D view, see Video S3. The red background on the inner “roof” of the embryos in (G) and (H) is excess of free tubulin which could not be removed during background subtraction of the 3D-program. Stages of embryos are denoted in yellow and follow the nomenclature of [61]. doi:10.1371/journal.pone.0112053.g002

(Fig. 4D) and to a lesser extent also to *ncd*^D oocytes (Fig. 4G). As a result of the aberrant lateral transport during oogenesis, a nc 6 embryo revealed the mRNA transported more posteriorly (Fig. 4N) compared to a wild-type embryo of the same stage, and even more posterior than an identical stage *ncd*^D/*ncd*^D embryo (Fig. 4H). In a nc 12 embryo, however, extended transport of the mRNA at the cortex well beyond the middle of the embryo was observed (Fig. 4O), demonstrating a vital role of *ncd* for the transport of the mRNA. We also noted a clear bias for accumulation of the *bcd* mRNA at the dorsal side in oocytes, exemplified by the position of the oocyte nucleus (Fig. 4G, M, inserts) which explains the skew of the *bcd* mRNA pool at the time of fertilization (Fig. 1B, insert).

α Tubulin67C and Ncd show colocalization

To perfect our analysis on the proposed molecular interaction of α Tub67C with *ncd* [40,41], we stained embryos with antibodies specific for each protein alone, along with a third antibody that recognized α Tub84B and α Tub84D (Fig. 4P–U). Ncd and α Tub67C showed colocalization in the periplasm and in perinuclear areas of nc 14 embryos (Fig. 4P, Q). Notably, the periplasm also showed strong *bcd* mRNA accumulation upon basal-apical transport (Fig. 1B; [3]), suggesting that α Tub67C and Ncd play also a role during basal-apical transport at nc 14. In contrast, α Tub84B and D localized immediately perinuclear, but were virtually absent from the periplasm, as evident in Fig. 4R. Consequently, only the perinuclear area was positive for all 3 proteins which stained in white (Fig. 4S). A pair-wise comparison of Ncd/ α Tub67C (Fig. 4T) and Ncd/ α Tub84B+D (Fig. 4U)

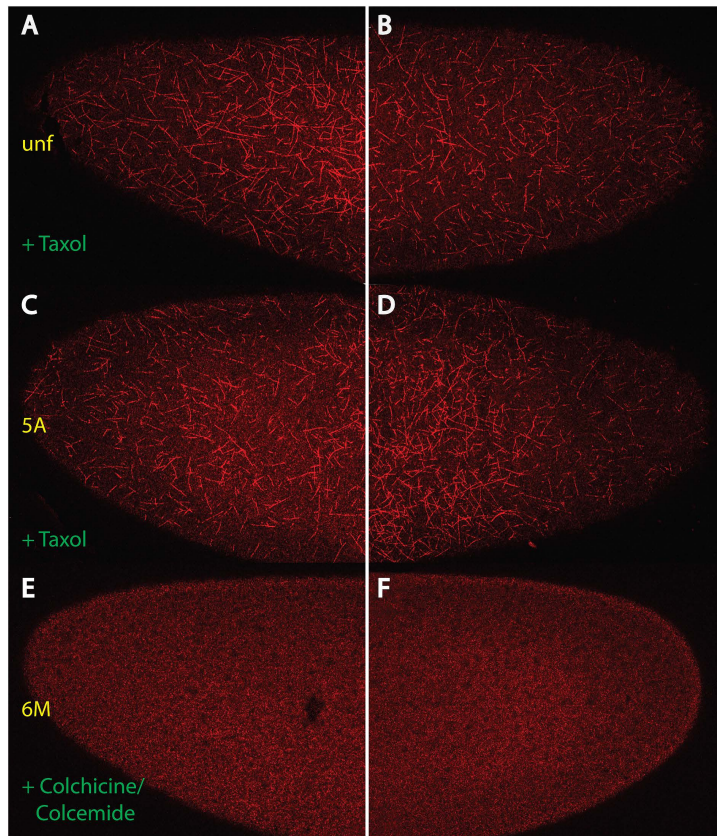


Figure 3. Behaviour of the MT threads upon treatment with drugs: use of Taxol results in artefacts. Anterior (A, C, E) and posterior (B, D, F) ends of embryos treated with Taxol (A–D) or Colchicine & Colcemide (E, F) stained with mAb γ L_{1,2} to reveal the MT network. (A, B) unfertilized embryo, (C, D) nc 5 embryo, (E, F) nc 6 embryo. Note that Taxol induces the formation of threads even in unfertilized embryos (compare to Fig. 1D, E) and even in posterior halves (B, D). Stages of embryos are denoted in yellow and follow the nomenclature of [61]. doi:10.1371/journal.pone.0112053.g003

corroborated this behaviour clearly. The above data suggested that Ncd preferentially associated with α Tub67C-positive MT bundles and define these two proteins as essential members of the *bcd* mRNA transport machinery.

Discussion

The ARTS model [3] predicted the presence of a cortical MT network in early staged *Drosophila* embryos where only sparse information of MT distributions was available. To visualize this network, two essential modifications of existing protocols were necessary: 1) a permeabilization and fixation protocol permitted to

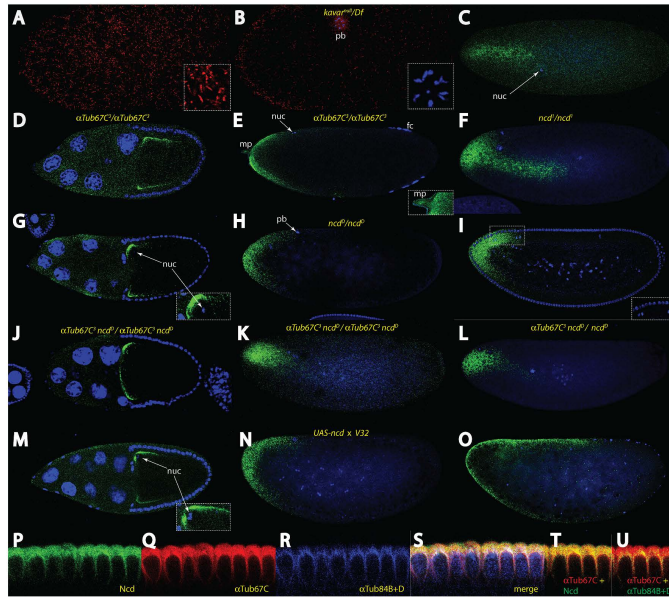


Figure 4. α tubulin 67C and ncd are essential for transport of the *bcd* mRNA. (A) surface confocal section of an anterior half of a *kavarin^{null}/Df(3L)55* embryo, stained with mab YL_{1,2} revealing a short omnidirectional MT network (insert). (B) more sagittal confocal section of the same embryo as in (A) to reveal the polar body (pb), stained along with DAPI to show the chromosomes (insert). Note the short MT threads at the cortex. (C) a *kavarin^{null}/Df(3L)55* embryo, stained for the *bcd* mRNA (green) along with DAPI (blue) to reveal the nucleus (nuc). (D) stage 10 and (E) stage 14 α Tub67C/ α Tub67C³ oocytes stained for *bcd* mRNA (green) and DAPI (blue). Insert in (E) denotes staining in the micropyle (mp). (F) nc 4 *ncd¹/ncd¹* embryo, stained for the *bcd* mRNA (green) along with DAPI (blue). (G–I) *ncd²/ncd²* stage 10 oocytes (G), *ncd²/ncd²* nc 6 embryo (H) and *ncd²/ncd²* nc 13 embryo (I), stained for *bcd* mRNA (green) and DAPI (blue). Insert in (G) denotes the position of the nucleus on the dorsal side. Insert in (I) denotes irregularities in the position of nuclei frequently seen in *ncd²/ncd²* embryos. (J–K) homozygous α Tub67C³ *ncd²* stage 10 oocyte (J) and nc 4 embryo (K) stained for *bcd* mRNA (green) along with DAPI (blue). (L) α Tub67C³ *ncd²/ncd²* nc 6 embryo stained for *bcd* mRNA (green) along with DAPI (blue). (M–O) *UAS-ncd* overexpression using maternal GAL-4 driver *V32*, stained for *bcd* mRNA (green) and DAPI (blue), stage 10 oocyte (M), nc 6 embryo (N) and nc 12 embryo (O). Insert in (M) denotes the position of the nucleus on the dorsal side. (P–U) mid-sagittal section of a nc14 embryos stained for Ncd (P), α Tub67C (Q), α Tub84B+D (R), and merge of P–Q, along with DAPI (S). Note that Ncd, α Tub67C and α Tub84B+D overlap only in MTs surrounding the nuclei (white). (T) Ncd staining together with α Tub67C. (U) α Tub67C staining together with α Tub84B+D. Note that Ncd overlaps with α Tub67C (T), in contrast to α Tub84B+D (U). fc follicle cells, nuc nuclei, mp micropyle, pb polar body.
doi:10.1371/journal.pone.0112053.g004

overcome the limitations of rapid fixation of MT structures in the *Drosophila* egg, and 2) an antibody with an excellent signal-to-noise ratio that detected tyrosinated Tubulin.

Initially, visibility of the cortical network was limited to a short 2 minute-window which let us conclude that it is a highly dynamic and short-lived MT network, consistent with the reported specificity of the mab against tyrosinated Tubulin [26]. The rapid fixation technique also disclosed MT activity with MT extensions as long as 50 μ m into the yolk at later stages (Fig. 1M, N). The MT threads likely serve to transport *bcd* mRNA molecules from the yolk to the apical side of the nuclei at early nc 14 [3]. Another possible function could be transporting lipid droplets, shown to be MT-based [43,44].

Freshly-synthesized Tubulin usually carries a COOH-terminal tyrosine residue as signature which is part of the epitope that is recognized by mab YL_{1,2}. Mature tubulin shows this terminal tyrosine cleaved off, often referred to as Glu-Tubulin, using an enzyme, Tubulin tyrosine carboxypeptidase (TTCp). If necessary, tyrosination of the de-tyrosinated end using an enzyme, Tubulin tyrosine ligase (TTL) could convert the COOH-end back to its original status (reviewed by [45]). As there is no true TTL detected in the *Drosophila* genome, we presume that tyrosinated Tubulin is provided to the egg via the pool of maternally-deposited Tubulin, or *de novo* synthesis.

Our Taxol experiments in Fig. 3 demonstrated that most previous descriptions of MT activity in the early nc embryo

[22,23,32,33] require a careful re-examination. The fact that Taxol could induce MT threads even in unfertilized embryos (Fig. 3A, B) suggested that the unfertilized egg was competent for MT thread assembly, but lacked an anteriorly-located trigger, or 'initiator' which is activated only after fertilization.

Attempts to counterstain the cortical MT threads with minus-end markers failed (data not shown), most likely because there is no 'conventional' microtubule organizing center (MTOC) at the cortex. Notably, the same minus-end markers usually detected the MTOCs associated with the internal nuclei without difficulty. Conversely, antibodies against plus-end markers do not stain well following our improved fixation method. We were also unable to stain the MT threads using Tubulin-GFP-constructs (unpublished), most likely due to the fact that the signal from their fine structures is difficult to detect within the autofluorescence of the yolk. The only protein that co-stains the cortical MT network is Chromosome bows (Chb), formerly called Mast/Orbit/CLASP [46,47], a MT-binding protein and a plus-end marker, which decorated the MT threads uniformly (data not shown). A recent survey in the literature revealed compelling evidence that MTs can form without functional centrosomes [48–53]. Of these, the observation that MTs can be nucleated at the *trans*-Golgi network with the help of vertebrate CLASP [53] attracted our attention. Indeed, Golgi network structures could be detected at the cortex of early nc 1–6 embryos [54,55].

As far as the velocity of the *bcd* mRNA transport is concerned, the velocity of Staufen-*bcd*-RNP complexes was measured in the oocyte, resulting in values of 0.36 to 2.15 $\mu\text{m}/\text{sec}$. [10]. As was argued in favour of the ARTS model [3], an omnidirectional MT network was predicted as a prerequisite for the transport system, due to the fact that an A-P directed MT network would have transported the *bcd* mRNA within minutes from the anterior to the posterior pole. As was discussed for the ARTS model [3], a slight directional bias of the MT network, as was observed in oocytes during *Stau-oskar* mRNA particle transport [17], represents a valid model for posterior transport, but only if the transport is mediated by both plus- and minus-end motors. However, what the ARTS model could not foresee was the fact that the transportation system would persist only during about 20% of the time of an early nuclear cycle.

An important facet is that all MT activities in the oocyte are abolished at the time of fertilization [19–21]. Hence, new MT structures need to be built up in the fertilized egg. Our data demonstrate the existence of at least two distinct and undiscovered MT networks in the early embryo: (i) the cortical network that relies critically on the process of fertilization and αTub67C (Figs. 1, 4), (ii) an internal network which rapidly transports the mRNA towards the interior of the embryos, but not requiring functional αTub67C nor Ncd. Since the latter MT network is located in the middle of the embryo, its detection proves difficult and hence still awaits visualization. Hints for its existence were shown in the initial inward movement of the *bcd* mRNA during nc 3–4, as noted by [3,56], before the cortical network comes into play which transports the mRNA to the cortex [3,56]. Interestingly, about 1–1.5% of all fertilized wild-type embryos show aberrant transport of the mRNA into the interior and towards the dividing nuclei (data not shown), suggesting that this network may correspond to that proposed for axial expansion of nuclei at nc 4–6 [57].

Fig. 1A, B corroborated earlier findings of a basal-to-apical transport of the mRNA during nc 14 and the existence of an apically-located *bcd* mRNA [2,3], before its final degradation takes place. This behaviour was negated in the analysis of [56]. Curiously, embryo G in Fig. S1 of the same report demonstrated

strong expression of an apical *bcd* mRNA, thus making the claim of a basal degradation of the mRNA without apical transport inconsistent. How do we reconcile these opposing results? We surmise that the discrepancy between our result demonstrating the presence of an apical mRNA and their result showing absence was caused by the fact that many embryos in the Little et al. analysis revealed poor preservation of the periplasm which appeared largely rubbed off, best exemplified in embryo E and F of their Fig. 5, respectively. Consequently, little or no fluorescent signal could emerge from the missing tissue. As far as the discrepancy of a long versus a short mRNA gradient is concerned, we surmise (i) a similar cause owing to the rubbed periplasm, and (ii) possibly a general loss of mRNA of the poorly-preserved embryos. Indeed, the long mRNA gradient was most conspicuous from the apical mRNA species [3]; Fig. 1A, B). The observed short mRNA gradient led Little et al. to conclude that diffusion of the Bcd protein is still an absolute requirement for fulfilment of the SDD model. On the other hand, our analyses [3]; this report and that of [24] demonstrated that the mRNA gradient reached a much more posterior extent that is sufficiently large to exclude the necessity to include long-range diffusion of the Bcd protein. To reconcile the difference of the posterior extent between the mRNA and the protein gradient, we propose that the poly(A) tail length of the mRNA and its control of the translation efficiency of Bcd [58] may represent another tool to extend the gradient to the posterior. Thus, we speculate that the length of the poly(A) tail of the *bcd* mRNA increases with posterior migration such that the posterior-most particles harbour the longest poly(A) tail. As a consequence, only few mRNA molecules would be required to efficiently translate the Bcd protein in more posterior regions, molecules that current *in situ* hybridization protocols are unable to detect. Interestingly, Wispy, a poly(A) polymerase was recently shown to be part of the *bcd* ribonucleoprotein particle [59]. Possibly, Wispy remains associated with the particle during the posterior migration, while simultaneously regulating the elongation of the poly(A) tail of the *bcd* mRNA. Like this, the poly(A) tail length of the *bcd* mRNA does not only vary with time [58], but may also vary with space.

To take up the question that was asked in the introduction: we demonstrate that the molecular structures which the ARTS model predicted exist and described two proteins that play critical roles for the transport machinery that form the *bcd* mRNA gradient. Further, we provide evidence of a long-range transport of *bcd* mRNA particles up to 40% EL [3] culminating in the mRNA gradient which largely dictates the protein gradient. Hence, the crucial question of the ARTS model concerning the mechanism by which the *bcd* mRNA gradient forms, is answered and confirms the earlier postulate of a MT-mediated transport [3].

Materials and Methods

Fly stocks

kavav^{X21}, referred to as *kavav^{null}*, the only known null allele of αTub67C is described in [37] and was used, together with *Df(3L)55*, to generate embryos without functional αTub67C activity [31,37]. The other *kavav* alleles were described in [37]. The αTub67C^2 , αTub67C^3 and αTub67C^4 alleles were described in [30], the *ncd⁰*, *ncd¹* and αTub67C^3 *ncd⁰* double mutants in [40,42], respectively. αTub67C^3 *ncd⁰/ncd⁰* embryos were obtained by crossing αTub67C^3 *ncd⁰* females to *ncd⁰/ncd⁰* males, as described by [41]. The semi-lethal *ncd⁰⁵³⁸⁴* allele and the over-expression *P[EPgy2]ncd^{ES103397}* allele were obtained from

Bloomington. The maternal GAL4-driver line *V32* was obtained from the Perrimon lab.

Fixation of embryos to visualize the microtubular network

In order to visualize the cortical network, we modified a recent permeabilization protocol without heptane [25] and fixed embryos for 15 minutes in 27% formaldehyde, followed by gentle devitellinization. The network can also be visualized by using a more conventional 27% formaldehyde/heptane fixation protocol, but with a somewhat poorer preservation of the MTs. Embryos in Fig. 2 were fixed like the other embryos, but were hand-devitellinized.

Drug treatments

After dechorionation, embryos were subjected to 10 µg/ml Taxol for 2 minutes, or to a 50 µg/ml Colcemide/20 µg/ml Colchicine mixture for 10 minutes in permeabilization buffer [25], before addition of 27% formaldehyde.

Antibodies

Mab YL_{1,2} against tyrosinated tubulin (Millipore) was used at 1:2000. Anti- α Tub67C rabbit polyclonal antibodies were made against a peptide from amino acids (aa) 35–61 of α Tub67C, affinity-purified and used at 1:400. Anti- α Tub84B/D guinea pig polyclonal antibodies were made against the last 15 aa including the tyrosine residue of the common COOH-termini of α Tub84B and α Tub84D, respectively, and used as crude serum at 1:300. DM1A was used as a FITC-conjugate (Sigma) at 1:50 sequentially to mab YL_{1,2} in Fig. 1P. Polyclonal goat antibodies against Ncd (dS-17) were purchased from Santa Cruz Biotechnology and used at 1:80. Polyclonal rabbit anti γ Tubulin and Msp antibodies were obtained from Y. Zheng and H. Ohkura, respectively, and were used both at 1:1000. For actin staining, we hand-devitellinized the embryos and used Phalloidin, coupled to Alexa 488 (Invitrogen) at 1:60. For YL_{1,2}, we preferentially used 2nd antibodies coupled to 594 nm fluorochromes to obtain an optimal signal-to-noise ratio. All pictures were recorded on a Zeiss LSM 710.

Western analysis

0–2 h extracts were separated on 12% PAGE and probed with Tubulin-specific mab's and a polyclonal antiserum using standard methods, as described in Figure S3.

In situ hybridization

Fluorescent *in situ* hybridization was used according to [3], except that RNA probes were used, combined with an Alexa Fluor 568 Signal-Amplification Kit (Invitrogen A11066). Care was taken to ensure preservation of the periplasm by gentle vortexing during the devitellinization step and proper fixation during the prehybridization steps to avoid poor preservation of the periplasm as in [56].

Colour conversion and 3D-analysis

For colour conversion and interpretation of signal intensities in Fig. 1A, B, the OsiriX DICOM program was used [60]. For 3D-analyses in Videos S2–S4, the ZEN 2009 program (Zeiss GmbH) was used. Note that due to the coverslip, the surface of the embryos does not appear not round, but rather flat.

Supporting Information

Figure S1 *bcd* mRNA gradients in Diptera. (A) a *Drosophila* embryo at fertilization hybridised with a *bcd* probe and alkaline phosphatase to reveal the strict accumulation of the mRNA at the anterior pole. (B) a *Drosophila* nc 14 embryo hybridised with a *bcd* probe and alkaline phosphatase showing an extended gradient. (C) a *Lucilia sericata* nc 14 embryo hybridised with a *bcd* probe and alkaline phosphatase showing an extended gradient. (D) a *Lucilia sericata* nc 14 embryo hybridised with a *bcd* probe using fluorescence. Methods and colour conversion as in Fig. 1A, B and [3]. (TIFF)

Figure S2 Mislocalization of the *bcd* mRNA in α Tub67C and motor protein mutants. (A) a nc 1 α Tub67C¹/ α Tub67C¹ embryo, stained for the *bcd* mRNA (green) along with DAPI (blue) to reveal a streak of the mRNA. (B) a nc 5 α Tub67C²/ α Tub67C² embryo, stained for the *bcd* mRNA (green), along with DAPI (blue). (C) 3-D reconstruction of the tip of a nc 5 α Tub67C²/ α Tub67C² embryo, stained with mab YL_{1,2} (red) and DAPI (blue) to reveal a dense MT network and aster-like MT bundles without nuclei (asterisks). The positions of the nuclei are indicated with yellow arrows, one normal metaphase nucleus is indicated with a white arrow. A movie of this 3-D construction is available as Video S4. (D) a nc 5 *Kavav*^{21C}/*+* embryo, stained for the *bcd* mRNA (green), along with DAPI (blue). (E) a nc 1 *Kavav*^{18C}/*+* embryo, stained for the *bcd* mRNA (green), along with DAPI (blue). (F) a nc 3 *ncd*⁶³⁸⁸⁷/*ncd*⁶³⁸⁸⁷ embryo, stained for the *bcd* mRNA (green) along with DAPI (blue). (G) wild-type stage 10 oocyte, stained for the *bcd* mRNA (green), along with DAPI (blue). (H) *kavav*^{mut}/*Df(3L)55* stage 10 oocyte, stained for the *bcd* mRNA (green), along with DAPI (blue). The anterior localization is largely normal. (TIFF)

Figure S3 Specificity of Tubulin antibodies. Western analysis of 0–2 h embryonic extracts (Fig. S3) showed that mab YL_{1,2} detected two Tubulin bands, in accordance with previous reports [62]. The upper band corresponded to α Tub67C, while the lower band corresponded to both α Tub84B and α Tub84D [31]. mab DM1A, another α Tubulin-specific mab specifically detected the lower α Tub84B/D band, in accordance with [31], while the α Tub67C-specific-antibody detected exclusively the upper band. (TIFF)

Video S1 An exclusive anterior MT network. Video of the 3D-reconstruction of the confocal stack used in Fig. 1C to reveal the MT network exclusively in the anterior half of a nc 1 embryo. (ZIP)

Video S2 Independence of the early MT network from the actin sheet in a nc 2 embryo. Video of the 3D-reconstruction of the confocal stack used in Fig. 2A–C, G. The MT network (red) is not in contact with the actin sheet (green) of a nc 2 embryo. (ZIP)

Video S3 Independence of the early MT network from the actin sheet in a nc 6 embryo. Video of the 3D-reconstruction of the confocal stack used in Fig. 2D–F, H. The MT network (red) is not in contact with the actin sheet (green) of a nc 6 embryo. (ZIP)

Video S4 Asters and intensive MT network activity at the cortex of α Tub67C² embryos. Video of the 3D-

50. Khodjakov A, Cole RW, Oakley BR, Rieder CL (2000) Centrosome-independent mitotic spindle formation in vertebrates. *Curr Biol* 10: 59–67.
51. Sawin KE, Fran PT (2006) Cytoplasmic microtubule organization in fission yeast. *Yeast* 23: 1001–1014.
52. Rogers CG, Russa NM, Pfeifer M, Rogers SL (2008) A multicomponent assembly pathway contributes to the formation of acentrosomal microtubule arrays in interphase *Drosophila* cells. *Mol Biol Cell* 19: 3163–3178.
53. Efimov A, Kharitonov A, Efimova N, Loncarek J, Miller PM, et al. (2007) Asymmetric CLASP-dependent nucleation of acentrosomal microtubules at the trans-Golgi network. *Dev Cell* 12: 917–929.
54. Bobiniec Y, Marcellou C, Morin X, Debrec A (2003) Dynamics of the endoplasmic reticulum during early development of *Drosophila melanogaster*. *Cell Motil Cytoskeleton* 54: 217–225.
55. Ripoché J, Link B, Yucel JK, Tokoyasu K, Malhotra V (1994) Location of Golgi membranes with reference to dividing nuclei in syncytial *Drosophila* embryos. *Proc Natl Acad Sci U S A* 91: 1878–1882.
56. Little SC, Tkacik G, Kneeland TB, Wieschaus EF, Gregor T (2011) The formation of the *Bicoid* morphogen gradient requires protein movement from anteriorly localized mRNA. *PLoS Biol* 9: e1000596.
57. Baker J, Theurkauf WE, Schubiger G (1993) Dynamic changes in microtubule configuration correlate with nuclear migration in the preblastoderm *Drosophila* embryo. *J Cell Biol* 122: 113–121.
58. Salles FJ, Lieberfarb ME, Wreden C, Gergen JP, Strickland S (1994) Coordinate initiation of *Drosophila* development by regulated polyadenylation of maternal messenger RNAs. *Science* 266: 1996–1999.
59. Cui J, Sartain CV, Pleiss JA, Wolfner MF (2013) Cytoplasmic polyadenylation is a major mRNA regulator during oogenesis and egg activation in *Drosophila*. *Dev Biol* 383: 121–131.
60. Rasset A, Spadola L, Ratih O (2004) OsiX: an open-source software for navigating in multidimensional DICOM images. *J Digit Imaging* 17: 203–216.
61. Foe VE, Alberts BM (1983) Studies of nuclear and cytoplasmic behaviour during the five mitotic cycles that precede gastrulation in *Drosophila* embryogenesis. *J Cell Sci* 61: 31–70.
62. Warn RM, Harrison A, Planques V, Robert-Nicoud N, Wehland J (1990) Distribution of microtubules containing post-translationally modified alpha-tubulin during *Drosophila* embryogenesis. *Cell Motil Cytoskeleton* 17: 34–45.

reconstruction of the confocal stack used in Fig. S2C. An intense MT activity with huge asters and a dense network is observed (red). Note that the internal nuclei (blue) are not associated with the asters.
(ZIF)

Acknowledgments

We thank Janos Szabad for providing the *kavar* alleles, Mark Biggin for rabbit anti-Bicoid antibodies, Yixian Zheng for γ Tubulin antibodies and Hiro Ohkura for Mps antibodies. We wish to thank the Institute of Molecular Life Sciences (Zürich, Switzerland) and the Kamprad Has/

References

- Driever W, Nüsslein-Volhard G (1988) A gradient of bicoid protein in *Drosophila* embryos. *Cell* 54: 83–93.
- Frigerio G, Burri M, Bopp D, Baumgartner S, Noll M (1986) Structure of the segmentation gene paired and the *Drosophila* PRD gene set as part of a gene network. *Cell* 47: 735–746.
- Spirow A, Fahmy K, Schneider M, Frei E, Noll M, et al. (2009) Formation of the bicoid morphogen gradient: an mRNA gradient dictates the protein gradient. *Development* 136: 605–614.
- Lipshitz HD (2009) Follow the mRNA: a new model for Bicoid gradient formation. *Nat Rev Mol Cell Biol* 10: 509–512.
- Gregor T, Wieschaus EF, McGregor AP, Bialek W, Tank DW (2007) Stability and nuclear dynamics of the bicoid morphogen gradient. *Cell* 130: 141–152.
- Castle BT, Howard SA, Odell DJ (2011) Assessment of Transport Mechanisms Underlying the Bicoid Morphogen Gradient. *Cell Mol Bioeng* 4: 116–121.
- Abu-Arish A, Forcher A, Czerwonka A, Dostani N, Pradig C (2010) High mobility of bicoid captured by fluorescence correlation spectroscopy: implication for the rapid establishment of its gradient. *Biophys J* 99: 133–35.
- Sigaut L, Pearson JE, Colman-Lerner A, Ponce Dawson S (2014) Messages do diffuse faster than messengers: reconciling disparate estimates of the morphogen bicoid diffusion coefficient. *PLoS Comput Biol* 10: e1003629.
- Wei TT, Forrest KM, Gavis ER (2006) Localization of bicoid mRNA in late oocytes is maintained by continual active transport. *Dev Cell* 11: 291–292.
- Wei TT, Parton R, Davis I, Gavis ER (2008) Changes in bicoid mRNA anchoring highlight conserved mechanisms during the oocyte-to-embryo transition. *Curr Biol* 18: 1055–1061.
- Ritkova MD, Little SC, Liu F, Gregor T (2014) Maternal origins of developmental reproducibility. *Curr Biol* 24: 1283–1288.
- Clark I, Gieger E, Ruohola-Baker H, Jan LY, Jan YN (1994) Transient posterior localization of a kinesin fusion protein reflects anteroposterior polarity of the *Drosophila* oocyte. *Curr Biol* 4: 289–300.
- Clark IE, Jan LY, Jan YN (1997) Reciprocal localization of Nod and kinesin fusion proteins indicates microtubule polarity in the *Drosophila* oocyte, epithelium, neuron and muscle. *Development* 124: 461–470.
- Theurkauf WE, Hazlrigg TI (1998) In vivo analyses of cytoplasmic transport and cytoskeletal organization during *Drosophila* oogenesis: characterization of a multi-step anterior localization pathway. *Development* 125: 3655–3666.
- Cha BJ, Koppeschtz BS, Theurkauf WE (2001) In vivo analysis of *Drosophila* bicoid mRNA localization reveals a novel microtubule-dependent axis specification pathway. *Cell* 106: 35–46.
- Januschke J, Gervais L, Gillet L, Keryer G, Bornens M, et al. (2006) The centrosome-nucleus complex and microtubule organization in the *Drosophila* oocyte. *Development* 133: 129–139.
- Zimyanin VL, Belaya K, Pecreaux J, Gilchrist MJ, Clark A, et al. (2008) In vivo imaging of oskar mRNA transport reveals the mechanism of posterior localization. *Cell* 134: 943–953.
- Parton RM, Hamilton RS, Ball G, Yang L, Cullen CE, et al. (2011) A PAR-1-dependent orientation gradient of dynamic microtubules directs posterior cargo transport in the *Drosophila* oocyte. *J Cell Biol* 194: 121–135.
- Theurkauf WE, Hawley RS (1992) Meiotic spindle assembly in *Drosophila* females: behavior of nonexchange chromosomes and the effects of mutations in the nod kinesin-like protein. *J Cell Biol* 116: 1167–1180.
- Theurkauf WE, Smiley S, Wong ML, Alberts BM (1992) Reorganization of the cytoskeleton during *Drosophila* oogenesis: implications for axis specification and intercellular transport. *Development* 115: 923–936.
- Page AW, Orr-Weaver TL (1996) The *Drosophila* genes *grauzone* and *cortex* are necessary for proper female meiosis. *J Cell Sci* 109 (Pt 7): 1707–1715.
- Karr TL, Alberts BM (1966) Organization of the cytoskeleton in early *Drosophila* embryos. *J Cell Biol* 102: 1494–1509.
- Callaini G, Riparbelli MG (1997) Patterns of microtubule assembly in taxol-treated early *Drosophila* embryos. *Cell Motil Cytoskeleton* 37: 300–307.
- Combs PA, Eisen MB (2013) Sequencing mRNA from cryo-sliced *Drosophila* embryos to determine genome-wide spatial patterns of gene expression. *PLoS One* 8: e71820.
- Rand MD, Kearney AL, Dao J, Clason T (2010) Permeabilization of *Drosophila* embryos for introduction of small molecules. *Insect Biochem Mol Biol* 40: 792–804.

Gunnar Nilsson Foundation (Lund, Sweden) for their generosity to use their excellently-maintained Zeiss LSM 710 confocal microscopes. We also thank Sol Da Rocha for excellent technical assistance, and Markus Noll and David Holloway for comments on the manuscript.

Author Contributions

Conceived and designed the experiments: KF SB. Performed the experiments: KF MA XC AK AH SB. Analyzed the data: KF MA XC AK AH SB. Contributed reagents/materials/analysis tools: KF MA XC AK AH SB. Contributed to the writing of the manuscript: KF SB.

- Weiland J, Willingham MC, Sandow IV (1993) A rat monoclonal antibody reacting specifically with the tyrosylated form of alpha-tubulin. I. Biochemical characterization, effects on microtubule polymerization in vitro, and microtubule polymerization and organization in vivo. *J Cell Biol* 97: 1467–1475.
- Rabinowitz M (1941) Studies on the cytology and early embryology of the egg of *Drosophila melanogaster*. *J Morphol* 69: 1–49.
- Fernandon D, Epluch L, Nüsslein-Volhard G, St Johnston D (1994) Staufen protein associates with the 3'UTR of bicoid mRNA to form particles that move in a microtubule-dependent manner. *Cell* 79: 1221–1232.
- Foe VE, Odell GM, Edgar BA (1993) Mitosis and morphogenesis in the *Drosophila* embryo: point and counterpoint. The Development of *Drosophila melanogaster*. Ed by Bate M and Martinez Arias A Cold Spring Harbor Laboratory Press 1: 149–300.
- Matthews KA, Rees D, Kaufman TC (1995) A functionally specialized alpha-tubulin is required for oocyte meiosis and cleavage mitoses in *Drosophila*. *Development* 117: 577–591.
- Venkai Z, Gaspar I, Toth G, Szabad J (2006) alpha2-Tubulin is involved in rapid formation of long microtubules to push apart the daughter centrosomes during early *Drosophila* embryogenesis. *J Cell Sci* 119: 3238–3248.
- Schejter ED, Wieschaus E (1993) Functional elements of the cytoskeleton in the early *Drosophila* embryo. *Annu Rev Cell Biol* 9: 67–99.
- Callaini G, Riparbelli MG (1996) Fertilization in *Drosophila melanogaster*: centrosome inheritance and organization of the first mitotic spindle. *Dev Biol* 176: 199–208.
- Matthews KA, Miller DF, Kaufman TC (1989) Developmental distribution of RNA and protein products of the *Drosophila* alpha-tubulin gene family. *Dev Biol* 132: 45–61.
- McQuilton P, St Pierre SE, Thurmond J (2012) FlyBase 101 the basics of navigating FlyBase. *Nucleic Acids Res* 40: D706–714.
- Mathies HJ, Messina LG, Namba R, Greer KJ, Walker MY, et al. (1999) Mutations in the alpha-tubulin 67C gene specifically impair achiasmatic segregation in *Drosophila melanogaster*. *J Cell Biol* 147: 1137–1144.
- Venkai Z, Szabad J (2005) The *Kavar(D)* dominant female-sterile mutations of *Drosophila* reveal a role for the maternally provided alpha-tubulin4 isoform in cleavage spindle maintenance and elongation. *Mol Genet Genomics* 273: 283–289.
- Gaspar I, Szabad J (2009) In vivo analysis of MT-based vesicle transport by confocal reflection microscopy. *Cell Motil Cytoskeleton* 66: 68–79.
- Endow SA, Chandra R, Komma DJ, Yamamoto AH, Salmon ED (1994) Mutants of the *Drosophila* ncd microtubule motor protein cause centrosomal and spindle pole defects in mitosis. *J Cell Sci* 107 (Pt 4): 859–863.
- Komma DJ, Endow SA (1995) Haploidy and androgenesis in *Drosophila*. *Proc Natl Acad Sci U S A* 92: 11884–11888.
- Komma DJ, Endow SA (1997) Enhancement of the ncd microtubule motor mutant by mutants of alpha-Tub67C. *J Cell Sci* 110 (Pt 2): 229–237.
- Komma DJ, Horne AS, Endow SA (1994) Separation of meiotic and mitotic effects of claret non-disjunctional on chromosome segregation in *Drosophila*. *EMBO J* 10: 419–424.
- Welte MA (2009) Fat on the move: intracellular motion of lipid droplets. *Biochem Soc Trans* 37: 991–996.
- Welte MA, Gross SP, Postner M, Block SM, Wieschaus EF (1998) Developmental regulation of vesicle transport in *Drosophila* embryos: forces and kinetics. *Cell* 92: 547–557.
- Janke C, Bulinski JC (2011) Post-translational regulation of the microtubule cytoskeleton: mechanisms and functions. *Nat Rev Mol Cell Biol* 12: 773–786.
- Lemos CL, Sampaio P, Maisto H, Costa M, Omezyanchuk LV, et al. (2000) Mast, a conserved microtubule-associated protein required for bipolar mitotic spindle organization. *EMBO J* 19: 3668–3682.
- Inoue YH, do Carmo Avides M, Shiraki M, Deak P, Yamaguchi M, et al. (2000) Orbit, a novel microtubule-associated protein essential for mitosis in *Drosophila melanogaster*. *J Cell Biol* 149: 153–166.
- Spiegelman BM, Lopata MA, Kirschner MW (1979) Multiple sites for the initiation of microtubule assembly in mammalian cells. *Cell* 16: 239–252.
- Bre MH, Kreis TE, Karsenti E (1987) Control of microtubule nucleation and stability in Madin-Darby canine kidney cells: the occurrence of noncentrosomal, stable deorganized microtubules. *J Cell Biol* 105: 1283–1296.

50. Khodjakov A, Cole RW, Oakley BR, Rieder CL (2000) Centrosome-independent mitotic spindle formation in vertebrates. *Curr Biol* 10: 59–67.
51. Sawin KE, Fran PT (2006) Cytoplasmic microtubule organization in fission yeast. *Yeast* 23: 1001–1014.
52. Rogers CG, Russa NM, Peifer M, Rogers SL (2008) A multicomponent assembly pathway contributes to the formation of acentrosomal microtubule arrays in interphase *Drosophila* cells. *Mol Biol Cell* 19: 3163–3178.
53. Efimov A, Kharitonov A, Efimova N, Loncarek J, Miller PM, et al. (2007) Asymmetric CLASP-dependent nucleation of acentrosomal microtubules at the trans-Golgi network. *Dev Cell* 12: 917–929.
54. Bobiniec Y, Marcellou C, Morin X, Debrec A (2003) Dynamics of the endoplasmic reticulum during early development of *Drosophila melanogaster*. *Cell Motil Cytoskeleton* 54: 217–225.
55. Ripoché J, Link B, Yucel JK, Tokoyasu K, Malhotra V (1994) Location of Golgi membranes with reference to dividing nuclei in syncytial *Drosophila* embryos. *Proc Natl Acad Sci U S A* 91: 1878–1882.
56. Little SC, Tkacik G, Kneeland TB, Wieschaus EF, Gregor T (2011) The formation of the *Bicoid* morphogen gradient requires protein movement from anteriorly localized mRNA. *PLoS Biol* 9: e1000596.
57. Baker J, Theurkauf WE, Schubiger G (1993) Dynamic changes in microtubule configuration correlate with nuclear migration in the preblastoderm *Drosophila* embryo. *J Cell Biol* 122: 113–121.
58. Salles FJ, Lieberfarb ME, Wreden C, Gergen JP, Strickland S (1994) Coordinate initiation of *Drosophila* development by regulated polyadenylation of maternal messenger RNAs. *Science* 266: 1996–1999.
59. Cui J, Sartain CV, Pleiss JA, Wolfner MF (2013) Cytoplasmic polyadenylation is a major mRNA regulator during oogenesis and egg activation in *Drosophila*. *Dev Biol* 383: 121–131.
60. Rasset A, Spadola L, Ratih O (2004) OsiX: an open-source software for navigating in multidimensional DICOM images. *J Digit Imaging* 17: 203–216.
61. Foe VE, Alberts BM (1983) Studies of nuclear and cytoplasmic behaviour during the five mitotic cycles that precede gastrulation in *Drosophila* embryogenesis. *J Cell Sci* 61: 31–70.
62. Warn RM, Harrison A, Planques V, Robert-Nicoud N, Wehland J (1990) Distribution of microtubules containing post-translationally modified alpha-tubulin during *Drosophila* embryogenesis. *Cell Motil Cytoskeleton* 17: 34–45.

Supporting Information

Figure S1.

bed mRNA gradients in Diptera. (A) a *Drosophila* embryo at fertilization hybridised with a bed probe and alkaline phosphatase to reveal the strict accumulation of the mRNA at the anterior pole. (B) a *Drosophila* nc 14 embryo hybridised with a bed probe and alkaline phosphatase showing an extended gradient. (C) a *Lucilia sericata* nc 14 embryo hybridised with a bed probe and alkaline phosphatase showing an extended gradient. (D) a *Lucilia sericata* nc 14 embryo hybridised with a bed probe using fluorescence. Methods and colour conversion as in Fig. 1A, B and [3].

<https://doi.org/10.1371/journal.pone.0112053.s001>

Figure S2.

Mislocalization of the bed mRNA in α Tub67C and motor protein mutants. (A) a nc 1 α Tub67C1/ α Tub67C1 embryo, stained for the bed mRNA (green) along with DAPI (blue) to reveal a streak of the mRNA. (B) a nc 5 α Tub672/ α Tub67C2 embryo, stained for the bed mRNA (green), along with DAPI (blue). (C) 3-D reconstruction of the tip of a nc 5 α Tub67C3/ α Tub67C3 embryo, stained with mab YL1,2 (red) and DAPI (blue) to reveal a dense MT network and aster-like MT bundles without nuclei (asterisks). The positions of the nuclei are indicated with yellow arrows, one normal metaphase nucleus is indicated with a white arrow. A movie of this 3-D construction is available as Video S4. (D) a nc 5 Kavar21G/+ embryo, stained for the bed mRNA (green), along with DAPI (blue). (E) a nc 1 Kavar18C/+ embryo, stained for the bed mRNA (green), along with DAPI (blue). (F) a nc 3 ncd05884/ncd05884 embryo, stained for the bed mRNA (green) along with DAPI (blue). (G) wild-type stage 10 oocyte, stained for the bed mRNA (green), along with DAPI (blue). (H) kavarnull/Df(3L)55 stage 10 oocyte, stained for the bed mRNA (green), along with DAPI (blue). The anterior localization is largely normal.

<https://doi.org/10.1371/journal.pone.0112053.s002>

Figure S3.

Specificity of Tubulin antibodies. Western analysis of 0–2 h embryonic extracts (Fig. S3) showed that mab YL1,2 detected two Tubulin bands, in accordance with previous reports [62]. The upper band corresponded to α Tub67C, while the lower band corresponded to both α Tub84B and α Tub84D [31]. mab DM1A, another α Tubulin-specific mab specifically detected the lower α Tub84B/D band, in accordance with [31], while the α Tub67C-specific-antibody detected exclusively the upper band.

<https://doi.org/10.1371/journal.pone.0112053.s003>

Video S1.

An exclusive anterior MT network. Video of the 3D-reconstruction of the confocal stack used in Fig. 1C to reveal the MT network exclusively in the anterior half of a nc 1 embryo.

<https://doi.org/10.1371/journal.pone.0112053.s004>

(ZIP)

Video S2.

Independence of the early MT network from the actin sheet in a nc 2 embryo. Video of the 3D-reconstruction of the confocal stack used in Fig. 2A–C, G. The MT network (red) is not in contact with the actin sheet (green) of a nc 2 embryo.

<https://doi.org/10.1371/journal.pone.0112053.s005>

(ZIP)

Video S3.

Independence of the early MT network from the actin sheet in a nc 6 embryo. Video of the 3D-reconstruction of the confocal stack used in Fig. 2D–F, H. The MT network (red) is not in contact with the actin sheet (green) of a nc 6 embryo.

<https://doi.org/10.1371/journal.pone.0112053.s006>

(ZIP)

Video S4.

Asters and intensive MT network activity at the cortex of α Tub67C3 embryos. Video of the 3D-reconstruction of the confocal stack used in Fig. S2C. An intense MT activity with huge asters and a dense network is observed (red). Note that the internal nuclei (blue) are not associated with the asters.

<https://doi.org/10.1371/journal.pone.0112053.s007>

(ZIP)

Figure s1

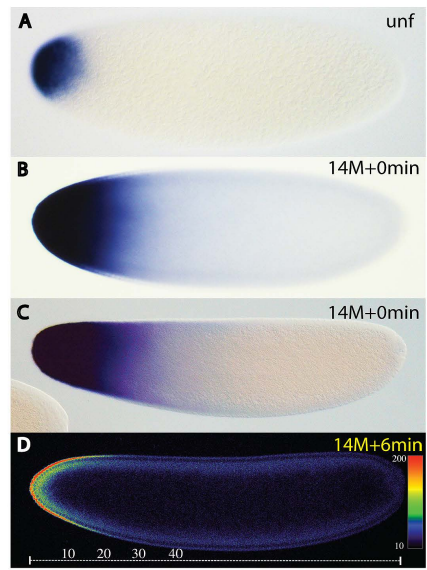


Figure S2

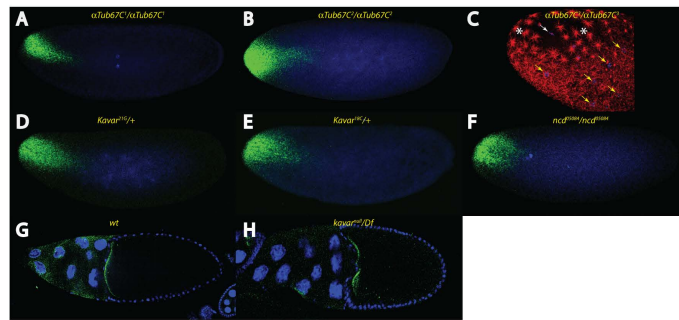
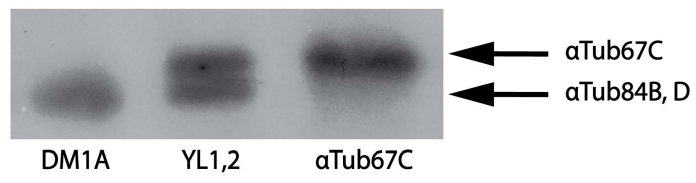


Figure S3



Paper II



RESEARCH ARTICLE

Cortical movement of Bicoid in early *Drosophila* embryos is actin- and microtubule-dependent and disagrees with the SDD diffusion model

Xiaoli Cai¹, Mira Akber¹, Alexander Spirov², Stefan Baumgartner^{1*}

1 Department of Experimental Medical Sciences, Lund University, Lund, Sweden, **2** Computer Science Department, Stony Brook University, Stony Brook, NY, United States of America and Sechenov Institute of Evolutionary Physiology and Biochemistry, St. Petersburg, Russia

* Stefan.Baumgartner@med.lu.se

OPEN ACCESS

Citation: Cai X, Akber M, Spirov A, Baumgartner S (2017) Cortical movement of Bicoid in early *Drosophila* embryos is actin- and microtubule-dependent and disagrees with the SDD diffusion model. PLoS ONE 12(10): e0185443. <https://doi.org/10.1371/journal.pone.0185443>

Editor: Sang-Chul Nam, Texas A&M International University, UNITED STATES

Received: June 20, 2017

Accepted: September 12, 2017

Published: October 3, 2017

Copyright: © 2017 Cai et al. This is an open access article distributed under the terms of the [Creative Commons Attribution License](https://creativecommons.org/licenses/by/4.0/), which permits unrestricted use, distribution, and reproduction in any medium, provided the original author and source are credited.

Data Availability Statement: All relevant data are within the paper and its Supporting Information files.

Funding: This work was supported by the Swedish Research Council (<https://www.vr.se/>) (Stefan Baumgartner: study design, data collection and analysis, decision to publish, or preparation of the manuscript); Eric Philipp Sörensen Stiffelse (Stefan Baumgartner: study design, data collection and analysis, decision to publish, or preparation of the manuscript); Byggmästare Olle Engkvist Stiffelse

Abstract

The Bicoid (Bcd) protein gradient in *Drosophila* serves as a paradigm for gradient formation in textbooks. The SDD model (synthesis, diffusion, degradation) was proposed to explain the formation of the gradient. The SDD model states that the *bcd* mRNA is located at the anterior pole of the embryo at all times and serves as a source for translation of the Bicoid protein, coupled with diffusion and uniform degradation throughout the embryo. Recently, the ARTS model (active RNA transport, synthesis) challenged the SDD model. In this model, the mRNA is transported at the cortex along microtubules to form a mRNA gradient which serves as template for the production of Bcd, hence little Bcd movement is involved. To test the validity of the SDD model, we developed a sensitive assay to monitor the movement of Bcd during early nuclear cycles. We observed that Bcd moved along the cortex and not in a broad front towards the posterior as the SDD model would have predicted. We subjected embryos to hypoxia where the mRNA remained strictly located at the tip at all times, while the protein was allowed to move freely, thus conforming to an ideal experimental setup to test the SDD model. Unexpectedly, Bcd still moved along the cortex. Moreover, cortical Bcd movement was sparse, even under longer hypoxic conditions. Hypoxic embryos treated with drugs compromising microtubule and actin function affected Bcd cortical movement and stability. Vinblastine treatment allowed the simulation of an ideal SDD model whereby the protein moved throughout the embryo in a broad front. In unfertilized embryos, the Bcd protein followed the mRNA which itself was transported into the interior of the embryo utilizing a hitherto undiscovered microtubular network. Our data suggest that the Bcd gradient formation is probably more complex than previously anticipated.

(Stefan Baumgartner: study design, data collection and analysis, decision to publish, or preparation of the manuscript); Russian Foundation for Basic Research (Alexander Spirov: study design, data collection and analysis). A.V.S. is partially supported by RFBR grants 15-04-07800 and 15-04-06480. The funders had no role in study design, data collection and analysis, decision to publish, or preparation of the manuscript.

Competing interests: The authors have declared that no competing interests exist.

Introduction

The maternal *bicoid* (*bcd*) gene in *Drosophila* is described a paradigm in textbooks for gradient formation. To date, there are two prevailing models describing how the gradient is established in the first 3 hours of embryonic development. The first one, termed SDD model, after synthesis, diffusion and uniform degradation [1] states that the *bcd* mRNA stays at the anterior tip at all stages and that, upon translation of the protein, Bcd diffuses to the posterior, followed by uniform degradation. It is noted that diffusion has not been demonstrated experimentally, nor has it been shown in which path of the early embryo Bcd chooses to move to the posterior. In essence, the SDD model was proclaimed as a dogma without experimental evidence and has stayed in textbooks for more than two decades as a paradigm for gradient formation. The SDD model was challenged in 2009 with a report showing that the Bcd protein movement is not the cause for gradient formation, but rather the existence of a *bcd* mRNA gradient which serves as template for Bcd a gradient protein translation [2–5]. Later, in 2011, the SDD model was modified to the “extended SDD model” by [6] whereby a small mRNA gradient reaching about 80% egg length would contribute, but would not fully account for Bcd protein gradient formation, concluding that the major cause for gradient formation would still be Bcd protein movement.

To validate the diffusion model whose basic assumption had never been rigorously tested since its establishment in 1988 [1], fluorescent dextran particles were injected at the very tip of the embryo leading the author to conclude that the motion of the dextran particles fits the diffusion equation well [7]. Most importantly, the particles spread uniformly over the whole inner area leading to the final conclusion that the movement of Bcd would conform to the same diffusion properties as dextran particles.

Bcd protein distribution and posterior migration in early nuclear cycle (nc) 2–6 embryos was analyzed in detail by [8]. In addition to the posterior movement, a deep internal plume of Bcd was detected during nuclear cycles 4–6 enwrapping internal nuclei, thus recapitulating the expression of the *bcd* mRNA in a plume at nc 4 [3, 6, 8]. This observation led [8] to propose two models of Bcd gradient formation during early nuclear cycles. The first, termed “the continuous model”, would allow a continuous redistribution of both the mRNA and the protein entirely at the cortex, while the second one, termed “2-step model”, would imply that the *bcd* mRNA and protein would generate an interior plume during nc 4–6, followed by the generation of a second gradient at the cortex during the blastoderm stages.

Exposure of *Drosophila* to hypoxia has been described in detail [9–15]. The majority of the studies were performed on adult flies, while only a few reports dealt with embryogenesis [9, 10, 16]. The first marked signs of oxygen deprivation exerted at early nuclear stages was a reversible developmental arrest, with younger embryos being more sensitive and less able to resume development than older embryos [9, 16]. An immediate reaction of internal nuclei to hypoxia was often, but not always, a characteristic condensation and movement of the DNA to the inner surface of the swollen nuclei, giving them a typical ring-like structure [9, S2 Fig]. Whether the nuclei adopted a ring-shaped configuration or not depended solely on whether nuclei arrest occurred at interphase or at metaphase where O₂ deprivation was induced [10]. Another marked feature of hypoxic embryos was the fast recovery to normal development, occurring within ~ 10 minutes [9, 10]. All these above aspects allowed us to study Bcd protein movement in an experimental set-up ideal for testing the SDD model.

It is well known that drugs can influence *bcd* localization in oocytes and embryos. Most studies with drugs were performed with the intention to study the behavior of the *bcd* mRNA in oocytes [17, 18] and to a lesser extent also in the embryo [5]. The most commonly used drugs were those directed against the two major cytoskeletal components, the microtubules

(MTs) and actin. To compromise the function of MTs, the MT-degrading drugs colchicine and colcemid were mostly used in the past [19]. If *Drosophila* oocytes were bathed in these drugs, the *bcd* mRNA did not localize properly to the anterior [18, 20, 21] which suggested that the MT-based transport of *bcd* mRNA was compromised. The drug vinblastine was shown to bind to a distinct site between Tubulin heterodimers [19], leading to the degradation of MTs, but was not used in *bcd* localization so far. Finally, taxol was described as a MT-stabilizing drug [19] used in the past to visualize MTs in early *Drosophila* embryos [22–25]. However, taxol elicited artefacts and thus did not reveal the true architecture of early cortical MTs, leading to alteration of the appearance of the anterior cortical network [5].

Actin was shown to be crucial for anterior *bcd* mRNA tethering at the end of oogenesis. If oocytes were incubated in the actin-depolymerizing drug cytochalasin D, *bcd* mRNA localization at the anterior end was compromised and stable actin-dependent anchoring of the mRNA was no longer possible [17, 20]. Likewise, the actin cytoskeleton was shown to be required for the maintenance of polar plasm components such as the *nanos* or *oskar* mRNA [26]. Other actin-targeting drugs exist [27, 28], such as the latrunculins, an actin-destabilizing drug similar to cytochalasin D which was used in the past to disrupt filamentous actin (F-actin) in the early embryo [29]. Another is the F-actin-stabilizing drug phalloidin which is mostly used as a tool to visualize F-actin in combination with fluorescent phalloidin-derivatives.

To monitor Bcd movement in early nc embryos, we developed a sensitive assay, coupled with the ability to apply drugs that influence Bcd movement. We demonstrate that the Bcd protein migrates along the outermost cortex. Furthermore, Bcd migration is microtubule- and actin-dependent, suggesting that the Bcd gradient formation is probably more complex than previously anticipated.

Material and methods

Fly stocks

To ensure high levels of Bcd protein, the P (*bcd*⁺⁵⁺⁸) / FM7 stock was used (T301, Tübingen stock list, gift of Tom Kornberg). Unfertilized eggs in larger quantities were obtained from females transgenic for the male sex peptide, P[rye[+t7.2] = Acp70A[g.Yp1.hs]]G10 (Bloomington stock number 4365). In all cases, pre-collections were used to ensure correct age of the laid embryos. *bcd* mRNA patterns in those G10 embryos were indistinguishable from those of unfertilized wild-type embryos.

Hypoxia and drug treatment

Embryos were collected at 25° (using precollection) in 1 hour intervals and were exposed to hypoxia with or without drug treatment for the time indicated. The assay was as follows: After dechorionation and rinsing with tap water, embryos were transferred to a cap which was cut off from an Eppendorf vial and filled with 200 µl PBT, supplemented by 1/100 volume of embryo permeabilization buffer [52]. The solution was evacuated with a water vacuum pump to remove any oxygen, and drugs were added to the final concentration: 50 µg/ml colchicine / 20 µg/ml colcemid mixture, 10 µM taxol, 10 µM vinblastine, 20 µg/ml latrunculin B and 20 µg/ml phalloidin. Embryos were transferred to the cap using a brush, aided by a fine forceps to remove embryos from the brush tip. All embryos sank down to the bottom despite the fact that they still harbored the vitelline membrane. Embryos were incubated for the indicate time interval in a moisture chamber at 25°C. Addition of heptane was strictly avoided as it led to a substantial increase of background during immunofluorescence. Embryos were fixed using either 4% formaldehyde (for *in situ* hybridization and Bcd antibody staining in Fig 1), or using heat-fixation (for all other embryos). Molecular markers in S2 Fig were Hoechst 33342,

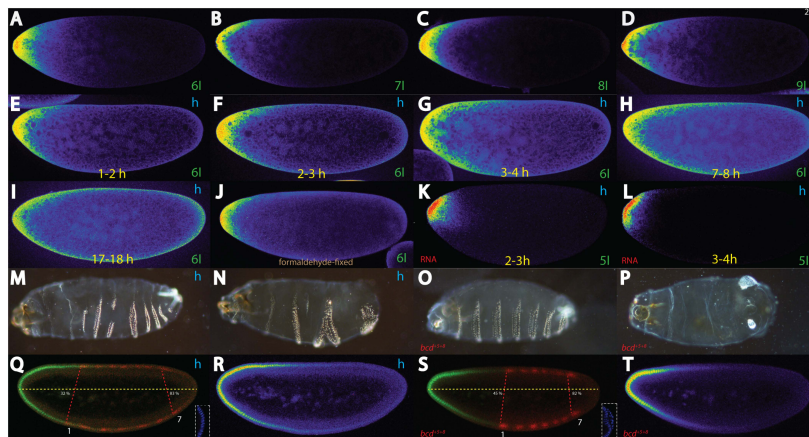


Fig 1. Cortical movement of Bcd in hypoxic embryos and effects of hypoxia on the segmental axis. Pictures represent midsagittal confocal planes of embryos oriented with their dorsal side up and anterior to the left, except for (M-P) which show cuticles. Relative intensities of the crude confocal pictures were converted to a color scale with values of 0–255 (8-bit), shown in (D), except for (M) to (Q) and (S). Nomenclature of nuclear cycles follows that of [46]. (A–D) untreated *bcd*⁵⁻⁸ embryos stained with Bcd antibodies. (A) interphase of nuclear cycle (nc) 6, (B) nc 7, (C) nc 8, (D) nc 9 embryos. Note the migration of the protein at the cortex of the embryo and not to the interior. (E–L) Relative Bcd intensities of nc 6 embryos in hypoxic *bcd*⁵⁻⁸ embryos and collected at different time intervals after hypoxia treatment: (E) 1–2 h, (F) 2–3 h, (G) 3–4 h, (H) 7–8 h, (I) 17–18 h. Note the movement of the Bcd protein in the “sleeping” embryos along the cortex. (J) Formaldehyde-fixed nc 6 embryo stained with Bcd antibodies. (K–L) distribution of the *bcd* RNA in *bcd*⁵⁻⁸ embryos after 2–3 h hypoxia (K) and 3–4 h hypoxia (L). Note the sparse movement of the mRNA. Weak (M) and strong cuticle phenotype (N) of wild-type (Oregon R) embryos collected in a 1 hour interval, subjected to 3 h hypoxia and recovered for 36 h. Weak (O) and strong cuticle phenotype (P) of *bcd*⁵⁻⁸ embryos. (Q) 0–1 h collected, 3 h hypoxia-treated and 3 h recovery nc 14 embryo, stained for Bcd protein (green) and Eve (red), percentages indicate position of Eve stripes 1 and 7 in % egg length, respectively. Insert in (Q) shows DAPI staining of the posterior end demonstrating lack of pole cells. (R) color conversion of the Bcd pattern in (Q). (S) nc 14 *bcd*⁵⁻⁸ embryo stained for Bcd protein (green) and Eve (red). Percentages indicate position of Eve stripes 1 and 7 in % egg length, respectively. (T) color conversion of the Bcd pattern in (S).

<https://doi.org/10.1371/journal.pone.0185443.g001>

used at 50 µg/ml, Sytox Green and TO-PRO3 (Molecular Probes), used at 20 µg/ml, respectively.

Antibodies and image recording

Rabbit antibodies against full-length Bcd were a gift from M. Biggin and were used at 1:500. Goat-anti Staufen antibodies (Santa Cruz Biotechnology) (used in S1 Fig) were used at 1:20. Rat antibodies against Staufen were a gift from A. Ephrussi and were used at 1:1000. mab JLA20 directed against actin (DHSB) was used at 1:50. All confocal pictures were recorded on a Zeiss LSM 710 at 8-bit resolution allowing 256 intensity values. Each embryo was recorded as a stack of 6–10 pictures from a start point before the middle of the embryo to an end point beyond the middle which then served as the basis to decide upon the mid-sagittal-most section. Care was taken to ensure that the gain of all recordings was adjusted to avoid saturation of the peak intensities by adjusting the gain of the LSM 710. For color conversion and interpretation of signal intensities, the OsiriX DICOM program was used [33].

Data acquisition

Intensity graphs (Fig 2) were obtained from an ellipsoid area moved along the dorsal cortex of midsagittal sections, as illustrated in Fig 2G [53]. A detailed description of used algorithms, scripts, and tools is available on request.

In situ hybridization

Fluorescent *in situ* hybridization (FISH) was used according to [3], except that RNA probes were used, combined with a home-made Alexa Fluor 555 Signal-Amplification Kit, using identical steps as the commercially-available Alexa Fluor 568 Signal-Amplification Kit (Thermo Fisher A11066).

Results

Bcd moves at the cortex and not to the interior during early nuclear cycles

To analyze Bcd movement during early nuclear cycles combined with the ability to use drugs that perturb Bcd migration, we tested numerous fixation and antibody staining protocols that would allow the combination of both approaches with an adequate signal-to-noise ratio. Since the formaldehyde fixation conditions as described in [8] constantly led to unwanted noise in combination with hypoxia and drug treatment (see below), we used heat-fixation instead. This fixation method was shown to work reliably in the past for Bcd antibody staining [3, 30]. To increase the sensitivity, we utilized a strain which produces 3 times more Bcd protein than wild-type, bcd^{+5+8} [8, 31, 32]. Moreover, the increased levels of Bcd permitted the analysis of single confocal midsagittal sections that allowed a precise analysis of the spatial pattern of Bcd. bcd^{+5+8} embryos are known to generate a distinct Bcd gradient which differs from that of wild-type embryos [1]. We monitored the distribution of Bcd in bcd^{+5+8} embryos in early cleavage staged embryos and used single confocal pictures derived from midsagittal stacks. To

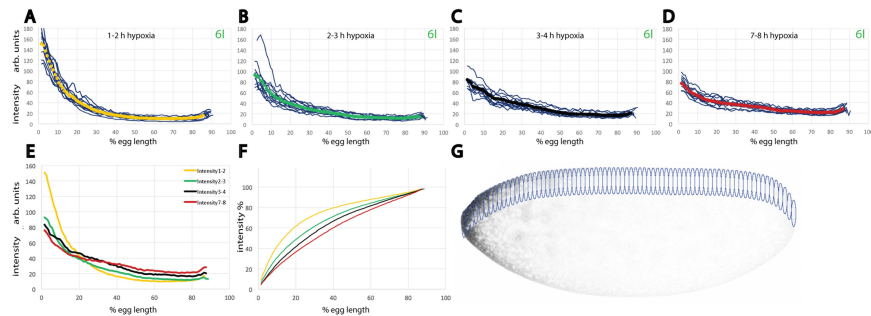


Fig 2. Batch analysis of hypoxic embryos demonstrates that the extent of Bcd movement changes with time. (A-D) Bcd protein profiles of embryos at different hypoxia durations. (A) 12 embryos exposed to hypoxia for 1 h and shown along with a yellow line as mean profile, (B) 12 embryos exposed to hypoxia for 2 h and shown along with a green line as mean profile, (C) 12 embryos exposed to hypoxia for 3 h and shown along with a black line as mean profile, (D) 12 embryos exposed to hypoxia for 6 h and shown along with a red line as mean profile. Profiles were measured as illustrated in Fig 2G and shown as intensities with arbitrary units. (E) Superimposition of all 4 mean profiles from (A-D), shown as intensities with arbitrary units. (F) Plots of (E) shown as percentage of the total Bcd protein content at a given point of the A-P axis. (G) Overview of an embryo, illustrating positions at which Bcd protein levels were measured in overlapping ellipsoid discs along the dorsal cortex of embryos.

<https://doi.org/10.1371/journal.pone.0185443.g002>

monitor the relative distribution without the necessity to graph the intensities along the A-P axis, we converted the intensities from the crude confocal file to a color scale [3, 33] allowing us to monitor the spatial distribution of Bcd. *bcd*⁵⁺⁸ embryos produce about three times more Bcd protein than wild-type embryos (S1A, S1B, S1D and S1E Fig), but the appearance of the initial gradient of Bcd in *bcd*⁵⁺⁸ embryos is retarded at nc 6 compared to an identical nc 6 wild-type embryo. This was evident from comparing the heat maps of the respective caps (S1D and S1E Fig). This observation suggests that the system for transporting the mRNA is not scaled up to accommodate for the transport of the high amount of *bcd* mRNA in *bcd*⁵⁺⁸ embryos. In a nc 6 embryo (Fig 1A), Bcd is strongly concentrated at the tip with some posterior migration on the dorsal and ventral side, recapitulating the distribution of the mRNA, also confirmed in [6, 8] at nc 4. At nc 7, however, this distribution changes dramatically and the protein covers an anterior cap with little Bcd in the inside (Fig 1B) and a smaller gradient extending to about 15% of the egg length. During the next two nuclear cycles (Fig 1C and 1D), the cap with the gradient expands to the posterior reaching about 25% at nc 9 (Fig 1D). To rule out that the heat-fixation procedure would extract Bcd protein such that only a subset of Bcd was revealed, we stained a formaldehyde-fixed nc 6 embryo (Fig 1J) that showed a staining pattern comparable to that of a heat-fixed nc 6 embryo (Fig 1A).

Hypoxia and uptake of smaller molecules

To further investigate the movement and the path of the Bcd protein along the cortex, we decided to inactivate the mRNA transportation system without affecting the viability of the embryo. We had previously shown that the *bcd* mRNA is transported along cortical MTs in the early embryo [5]. Hence, it would be desirable to selectively inactivate cortical MTs without affecting the interior MT network involved in nuclear division and migration, a technically-challenging scenario, as any disturbance of the function of MTs has deleterious effects on the viability of the embryo.

To overcome the above constraints, we noted that embryos exposed to hypoxia arrest growth and are virtually “sleeping”, but are readily reactivated once oxygen is supplied [9, 10]. To this end, we developed an assay to submerge embryos into water-based buffer systems rather than expose them to argon as in other studies [9, 10]. Our approach also allowed drugs to move into the embryo. Other drug deliver assays into embryos have been previously described [34, 35] using detergents to help to permeabilize the embryo. The disadvantage was that many of the embryos suffered from the treatment. In contrast, our simple assay allowed for the simultaneous application of any drug in the hypoxic state, despite the presence of the water-repelling wax layer and the robust vitelline membrane [36].

To illustrate movement of smaller substances through the membranes, we assayed embryos under hypoxia by adding fluorescent substances up to a molecular weight of 1500 (S2 Fig). During hypoxia for 2 hours and simultaneous incubation with nuclear staining tools coupled to fluorochromes, we were able to detect fluorescence from the DNA stain Hoechst 33342 (S2A and S2E Fig), the DNA marker Sytox Green (S2B and S2F Fig) and the DNA marker TO-PRO3 (S2C and S2G Fig), all associated with the ring-type chromatin (S2D and S2H Fig). In many cases, strong fluorescence was observed at the anterior end (data not shown), suggesting that the most likely point of entry is at the micropyle, the location where the sperm enters the egg.

Bicoid movement without mRNA gradient still occurs at the cortex

We reasoned that the sleeping period would allow us to monitor the movement of the Bcd protein and to assess how fast and how far the Bcd protein can move in the time where gradient formation was predicted to occur.

We chose the 6th nuclear cycle, i. e. embryos with 32 nuclei as a reference time point to evaluate Bcd protein migration from the position where hypoxia was applied. To this end, *bcd⁺⁵⁺⁸* embryos were collected during 1 hour intervals, incubated under hypoxic conditions and fixed. Only embryos at the 6th nuclear division were recorded. In 1–2 h embryos (1 hour collecting, 1 hour hypoxia, Fig 1E), little movement of the protein was observed, compared to an untreated embryo (Fig 1A). In 2–3 h (2 hours-hypoxic) embryos (Fig 1F), the protein migrated to about 30% egg length (EL), but still the majority of the protein remained at the tip. In 3 hours-hypoxic embryos (Fig 1G), movement continued to about 50% EL, but the bulk was still detected at the tip. In 7 hours-hypoxic embryos (Fig 1H), Bcd protein has reached about 70% EL, revealing a flat gradient. After 17 hours of induced hypoxia, some Bcd protein has reached the posterior end, barely showing a gradient. Under these conditions, we can conclude one important finding: Bicoid protein does not move throughout the whole embryo, but rather follows a discrete path along the outmost part of the embryonic cortex, as it does under normal conditions (Fig 1A–1D).

To investigate if the *bcd* mRNA is the cause for the Bcd protein movement, we stained *bcd⁺⁵⁺⁸* embryos that were exposed to hypoxia for the presence of *bcd* mRNA. To account for the time that is needed to synthesize Bcd protein, about 2 minutes [3, 37], we chose hypoxic not 5 embryos, instead. In 2–3 h hypoxic embryos (Fig 1K), *bcd* mRNA was tightly located to the tip and very little movement was seen, consistent with its expression in wild-type embryos at a similar stage including the plume of interior mRNA [3, 6, 8]. In a 3–4 h hypoxic embryo (Fig 1L), little change was observed and the mRNA was still located at the tip. From these two time points, we can conclude, that 1) oxygen deprivation has an impact on the localization of the mRNA, i. e. it does not move in comparison with wild-type embryos, and 2) the mRNA is not the cause for the protein movement seen in Fig 1E–1I.

Developmental consequences of hypoxia on segmental anlagen

To investigate the developmental consequences of hypoxia and the impact of Bicoid movement, we subjected wild-type Oregon-R embryos to 3 h hypoxia and allowed recovery for 36 hours in order to analyze the developmental consequences based on the cuticular pattern. The majority of the embryos (71%, S1 Table) showed the A-P axis affected, with an enlargement of the anterior segments and compression of the posterior segments, including head defects with shortened mouth hooks (Fig 1M). A lower portion of the embryos (24%, S1 Table) showed more severe A-P axis defects with several segments missing (Fig 1N). To compare the above effects to embryos exposed to high levels of Bcd, we monitored the cuticles of *bcd⁺⁵⁺⁸* larvae. Since *bcd⁺⁵⁺⁸* is a living stock, the majority (58%) of the offspring survive without any noticeable effect on A-P axis, also noted by [32]. The remaining 42% can be divided into mild defects (39%, S1 Table), where 2 thoracic segments, T2 and T3 were lacking, associated with defects in head-involution (Fig 1O). The remaining fraction (3%, S1 Table) contained embryos which showed a severely-affected A-P axis (Fig 1P) revealing no abdominal segments at all, while the head part was only mildly affected, revealing defects in head involution only. This data is consistent with results from *6x bcd* embryos [32]. To corroborate the cuticle defects caused by hypoxia, we stained embryos that were exposed to hypoxia for 3 hours followed by recovery for another 3 hours, with Bcd and Eve antibodies. While Bcd staining at first sight revealed a rather normal-looking gradient (Fig 1Q and 1R), Eve staining showed that all bands appeared stretched to the posterior (Fig 1Q), starting from 32% for stripe 1 to 83% to stripe 7, while in untreated wild-type embryos the stripes appeared from 32% to 75% [38–40]. Most conspicuously, however, no pole cells were observed (Fig 1Q, insert), suggesting that the fraction of posteriorly-migrated Bcd within the extra 3 hours was sufficient to suppress pole cell determination, indicative of

altered fate of posterior nuclei. In comparison, the Bcd and Eve pattern in bcd^{+5+8} embryos showed a steep Bcd gradient (Fig 1S and 1T) while Eve stripes appeared compressed, starting from 45% to 82% (Fig 1S). In contrast to the hypoxic embryos, however, bcd^{+5+8} embryos still revealed pole cells (Fig 1S, insert). We can conclude that the migration of Bcd protein during 3 hours of hypoxia causes posterior defects not associated with bcd^{+5+8} embryos. Possibly, a distinct fraction of Bcd molecules may be transported to the posterior leading to suppression of pole cell formation.

Quantitative analysis of cortical Bcd movement

To visualize cortical movement more precisely, we used the crude confocal data from larger batches of midsagittal sections from the time intervals as seen in Fig 1E–1L and analyzed the intensities by sliding an ellipsoid area along the dorsal side (Fig 2G). In contrast to the pictures in Fig 1 where the gain of the confocal microscope was individually adjusted to avoid saturation, the embryos of the batch series of Fig 2 were processed, collected and stained in the same experiment, and 12 nc 6 embryos from each hypoxic series were recorded in a single confocal session using identical intensity condition adjusted to the strongest signal of 1–2 h embryos. In 1–2 h hypoxic embryos (Fig 2A), the effect of extra Bcd movement appears minimal and the gradient looks similar to that of untreated bcd^{+5+8} embryos [1]. In 2–3 h hypoxic embryos (Fig 2B), however, a portion of the anteriorly-located Bcd protein has moved posteriorly, making the plot markedly flatter. This tendency continues in 3–4 h hypoxic embryos (Fig 2C). In 7–8 h hypoxic embryos (Fig 2D), the change of the shape of the plot is remarkably little compared to that of 3–4 h embryos (Fig 2C) suggesting that Bcd movement has come to a halt. Possibly, the embryo suffers from the prolonged hypoxia, associated with a high degree of lethality which is inherent to young embryos [9]. When the mean curves of Fig 2A–2D were compared (Fig 2E), 1–2 h hypoxic embryos (yellow) revealed a distinct curve compared to the remaining 3 curves whose slopes decreased the longer the embryos were exposed to hypoxia. This observation prompted us to monitor the percentage distribution of Bcd in relation to the A-P axis after the different hypoxic incubations (Fig 2F). After 1–2 h hypoxia, still about 80% of Bcd was contained within the first 40.5% of the embryos. A marked change took place in 2–3 h embryos where 80% of the protein was contained within the first 52.5% of the embryo, representing a change of 12% during one hour. In 3–4 h embryos, the value was at 57.5% indicating a reduced movement in comparison to the previous interval. Most notably, during the following 3 hours (i. e. in 7–8 h embryos), only another 5% of Bcd moved to the posterior. From this experiment, we can conclude that Bcd movement was strongest during the early phases of hypoxia, but decreased substantially during the subsequent time intervals.

Cortical movement of Bcd is microtubule-dependent

To investigate whether Bcd movement is dependent on cytoarchitectural changes of the egg, we combined our water-based hypoxia assay with drug application. To this end, we added the drugs directly to the buffer for the hypoxia-treated embryos and exposed them for the time interval indicated.

[5] exposed early nc embryos to the MT-stabilizing drug mixture colchicine/colcemid (CC) and could demonstrate that the anterior cortical MT network implicated in *bcd* mRNA transport was degraded. This data showed that drugs could enter the egg despite the water-repelling wax layer and the vitelline membrane, and that the MT network responded to the application.

Embryos exposed for 1 hour to hypoxia and CC exhibited subtle changes to the Bcd distribution pattern (Fig 3A), compared to untreated embryos (Fig 1E). Some protein moved more

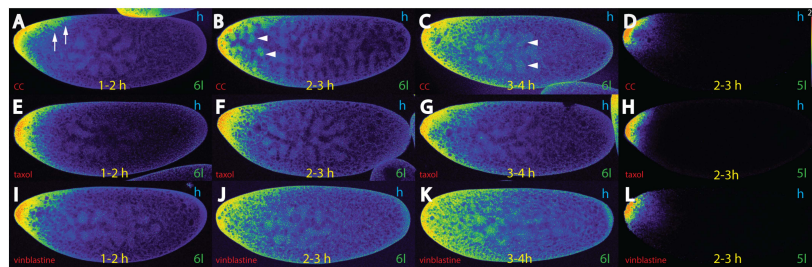


Fig 3. Bcd movement in hypoxia-treated embryos depends on microtubules. Pictures represent midsagittal confocal planes of embryos oriented with their dorsal side up and anterior to the left. Relative intensities of the crude confocal pictures were converted to a color scale with values of 0–255 (8-bit), shown in (D). (A–C) nc 6 *bcd*^{5/8} embryos treated with colchicine/colcemid (“CC”) for 1–2 h (A), 2–3 h (B) and 3–4 h (C), and stained for Bcd. (D) nc 5 *bcd*^{5/8} embryo treated with CC for 2–3 h, and stained for the *bcd* RNA. (E–G) nc 6 *bcd*^{5/8} embryos treated with taxol for 1–2 h (E), 2–3 h (F) and 3–4 h (G), and stained for Bcd. (H) nc 5 *bcd*^{5/8} embryo treated with taxol for 2–3 h, and stained for the *bcd* RNA. (I–K) nc 6 *bcd*^{5/8} embryos treated with vinblastine for 1–2 h (I), 2–3 h (J) and 3–4 h (K), and stained for Bcd. (L) nc 5 *bcd*^{5/8} embryo treated with vinblastine for 2–3 h, and stained for the *bcd* RNA. Note that destabilization of microtubules compromises the cortical path in favor of a more ubiquitous path. Note that the movement in (K) corresponds to the one predicted by the ideal SDD model where the protein will move in a broad front throughout the entire embryo.

<https://doi.org/10.1371/journal.pone.0185443.g003>

posteriorly (Fig 3A, arrows). If treated for 2–3 hours (Fig 3B), marked changes were observed. Parts of the protein migrated to the interior of the egg and some protein entered the energids, an actin-rich area surrounding the nuclei [24], as well as the nuclei (Fig 3B, arrowheads). Of note, in CC-treated hypoxic embryos, the chromatin never formed the typical rings (S2 Fig). In embryos treated for 3–4 hours (Fig 3C), the situation was even more pronounced with more Bcd migrating to the interior. Some Bcd even reached the nuclei in the middle of the embryo (Fig 3C, arrowheads). To exclude the possibility that the mRNA was the cause for this movement, we stained 2–3 hours-treated embryos for the presence of *bcd* mRNA (Fig 3D) which exhibited a distribution similar to that of hypoxia-only treated embryos (Fig 1K). This data demonstrated that Bcd movement was dependent on an intact MT network.

Hypoxia combined with taxol treatment revealed subtle changes in Bcd movement when exposed for 1–2 hours (Fig 3E) compared to the reference without drugs (Fig 1E). In 2–3 hours-treated embryos (Fig 3F), there was little change observed except that the protein as a bulk moved to the interior (Fig 3F). In 3–4 hours-treated embryos (Fig 3G), some posterior Bcd movement was observed, comparable to the reference (Fig 1G). If assayed for *bcd* mRNA distribution, taxol-treated embryos were almost indistinguishable from the reference (Fig 1K). We can conclude that taxol did not have a deleterious effect on Bcd movement, nor did it promote it substantially.

Vinblastine treatment allows to simulate the SDD model

Vinblastine has been shown to affect MT growth, but has been shown to bind to a distinct site between heterodimers which are different to those by colchicine/colcemid and taxol (Florian and Mitchison, 2016). When vinblastine was applied during a 1–2 hour interval (Fig 3I), protein movement began in all directions, and became more obvious during the 2–3 h interval (Fig 3J). Here, the protein distributed equally over the whole inner part. In 3–4 hours-treated embryos (Fig 3K), the situation was even more pronounced. Protein distribution moved to the posterior in a broad front, and thus seemingly conforming to the SDD model. This data allows

two interpretations: 1) Bcd protein movement requires an intact MT network in the yolk to prevent Bcd movement to the interior, 2) the cortical MT network no longer restricts Bcd protein movement to the cortex. To rule out that the cause for this massive migration being attributed to the mRNA, vinblastine-treated embryos were stained for the *bcd* mRNA revealing that *bcd* mRNA remained at the tip (Fig 3L), as observed in CC- or taxol-treated embryos (Fig 3D and 3H).

Actin is indispensable for Bcd stability and cortical movement

To investigate whether actin is involved in the movement, we subjected *bcd⁺⁵⁺⁸* embryos to drugs such as phalloidin that prevents F-actin degradation (S3A and S3B Fig), or to latrunculin B that disrupts the formation of actin bundles (S3C and S3D Fig). In phalloidin-treated embryos, long cortical microfilaments (MFs) were observed (S3B Fig), consistent with a stabilization of F-actin [41]. In contrast, latrunculin B-treated embryos revealed absence of long MFs, and only globular actin particles were detected, instead (S3D Fig), demonstrating that these drugs can efficiently alter the actin cytoarchitecture. In 1–2 hours latrunculin B-treated embryos (Fig 4A), initial movement of Bcd was indistinguishable from the reference (Fig 1E), while in 2–3 hours-treated embryos, sparse cortical movement and fewer Bcd protein particles were observed (Fig 4B), in comparison to the reference (Fig 1F). In 3–4 hours-treated embryos, no further movement occurred, but considerably lower amount of Bcd protein was observed, suggesting that the degradation of Bcd has commenced (Fig 4C). As for the mRNA was concerned, *bcd⁺⁵⁺⁸* embryos treated for 2–3 h with latrunculin B did not show any mRNA movement nor were fewer mRNA molecules detected (Fig 4D), in comparison to the reference (Fig 1K). This suggests that the movement and the stability of Bcd protein was not dependent on the status of the mRNA. This data proposes that an intact actin network at the cortex is critically important for both Bcd movement and stability.

When the existing actin filaments were prevented from degradation, i. e. after exposure to phalloidin, we noted that Bcd movement initially (at the 1–2 hours interval) behaved like in a wild-type embryo, with the exception of a small fraction of the protein moving to the interior (Fig 4E, arrow). In 2–3 hours-exposed embryos, this behavior continued, resulting in Bcd staining in energids and interior nuclei (Fig 4F, arrows). Concurrently, a greater proportion of the Bcd protein followed the cortical pathway similar to control hypoxic embryos (Fig 1F). Longer exposure (3–4 hours interval) revealed further streaming of Bcd to the interior, and

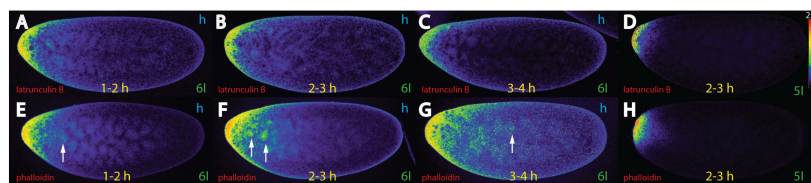


Fig 4. Bcd movement and stability in hypoxia-treated embryos depends on actin. Pictures represent midsagittal confocal planes of embryos oriented with their dorsal side up and anterior to the left. Relative intensities of the crude confocal pictures were converted to a color scale with values of 0–255 (8-bit), shown in (D). (A–C) nc 6 *bcd⁺⁵⁺⁸* embryos treated with latrunculin B for 1–2 h (A), 2–3 h (B), 3–4 h (C) and stained for Bcd. (D) nc 5 embryo treated for 2–3 h with latrunculin B and stained for the *bcd* mRNA. Note that the Bcd protein does not move anymore along the cortex. (E–G) nc 6 *bcd⁺⁵⁺⁸* embryos treated with phalloidin for 1–2 h (E), 2–3 h (F) and 3–4 h (G) and stained for Bcd. (H) nc 5 embryo treated for 2–3 h with phalloidin and stained for the *bcd* mRNA. Arrows in (E–G) denote interior nuclei, as well as energids revealing accumulation of Bcd protein. Note the decreased stability of Bcd in latrunculin B-treated embryos (A–C).

<https://doi.org/10.1371/journal.pone.0185443.g004>

nuclei and organelles showed staining with Bcd (Fig 4G, arrow), similar to embryos treated with CC (Fig 3C). However, it was not as extensive as that seen in vinblastine-treated embryos (Fig 3K). Again, the *bcd* mRNA did not move from the tip (Fig 4H), suggesting that cortical actin does not impede movement of Bcd.

Bcd movement in unfertilized embryos is strictly dependent on the *bcd* mRNA which utilizes a MT pathway into the interior

It is well documented that unfertilized eggs synthesize Bcd protein and that the process of fertilization is not a prerequisite for the initiation of Bcd translation [1, 8]. A recent study monitored Bcd movement in unfertilized embryos [42] showing that the Bcd gradient appeared longer and less steep compared to fertilized embryos of the same stage. The data was then interpreted in support of the SDD model. We therefore analyzed the patterns of Bcd and Staufer protein (as a read-out system for the *bcd* mRNA) in unfertilized embryos during short time intervals to monitor their movement. During the first hour, there was little diffusion of Bcd (Fig 5A) away from the source of the *bcd* mRNA template (Fig 5B). During the next hour (hours 1–2), Bcd showed expansion towards the posterior, with the bulk of protein associated in a region slightly shifted posterior from the tip (Fig 5E), congruent with the template which showed similar posterior movement (Fig 5F). In 2–3 hours old embryos, weak and uniform Bcd covered the anterior third of the embryo likely representing freely-moving Bcd, while the bulk of Bcd stayed localized to the anterior-most 20% of the embryo (Fig 5I), consistent with

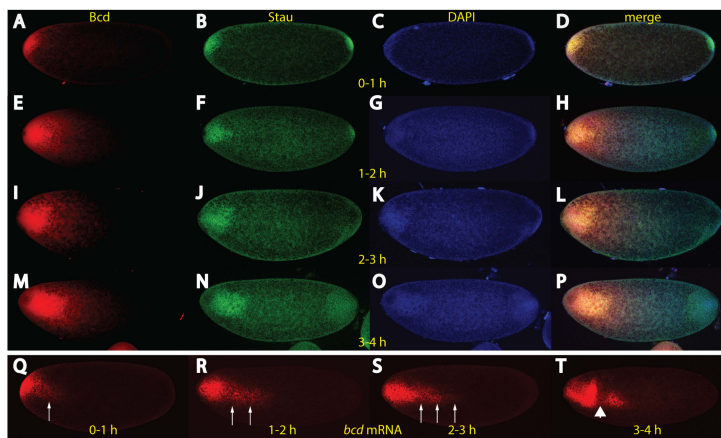


Fig 5. In unfertilized embryos, *bcd* mRNA and Bcd protein move to the interior. Unfertilized eggs collected from different time intervals, 0–1 h (A–D), 1–2 h (E–H), 2–3 h (I–L), 3–4 h (M–P), stained for Bcd protein (A, E, I, M), Staufer protein (B, F, J, N) and DAPI (C, G, K, O). The merge of all staining patterns is revealed in (D, H, L, P). Note the weak diffusion of the Bcd protein away from the bulk (A, E, I, M), which is always congruent to the Staufer protein (B, F, J, N). (Q–T) *in situ* hybridization of *bcd* mRNA of 0–1 h (Q), 1–2 h (R), 2–3 h (S) and 3–4 h (T) old unfertilized embryos. Arrows in (Q, R, S) denote fast movement of a portion of mRNA particles, apparently not associated with Staufer (compare to B, F, J). Time intervals and proteins are indicated in yellow.

<https://doi.org/10.1371/journal.pone.0185443.g005>

the template (Fig 5). In late embryos (3–4 hours), Bcd showed further axial expansion of movement, including the bulk which also moved towards the interior (Fig 5M) consistent with the data of [8]. Concurrently, the Stauf protein has now migrated deeply into the interior of the embryo (Fig 5N), where it showed co-localization with the bulk of Bcd (Fig 5P). Another interesting feature was that Staufen disappeared rapidly at the posterior pole, while it persisted at the anterior pole (Fig 5B, 5F, 5J and 5N), suggesting distinct degradation mechanisms.

Our data on Bcd protein distribution in unfertilized embryos were in agreement with data of [8, 42]. However, our data on the behavior of Staufen was in true conflict with the interpretation of the SDD model in [42] which implied that the mRNA stayed anchored at the anterior tip at all times. We sought to resolve this apparent discrepancy and analyzed the *bcd* mRNA pattern in subsequent stages of unfertilized eggs. The fragile embryos were fixed well to survive the harsh treatment during *in situ* hybridization. As expected and in agreement with Fig 5B, the mRNA moved away from the tip during the early stages (Fig 5Q). More importantly, subsequent stages showed that the mRNA moved to the center of the embryo as a streak (Fig 5R and 5S, arrows) and not to the cortex, implying that the cortical network was not established. Furthermore, the streak mRNA did not seem to involve Staufen (compare Fig 5R and 5S with Fig 5F and 5J), suggesting that the *bcd* mRNA utilizes another adapter protein than Staufen for the transport along the streak. At late stages (3–4 hours), *bcd* mRNA encountered a barrier (Fig 5T, arrowhead) which prevented further transport towards the posterior. Our data demonstrates the presence of an internal MT network in unfertilized eggs, which serves as a path for migration of the mRNA, however, the cortical network is only built up upon fertilization [5]. Occasionally, in about 1–2% of fertilized wild-type embryos, a thin mRNA streak was observed, where the direction of the streak was always pointing towards the dividing nuclei (unpublished).

Discussion

The present study sheds light onto the movement of the Bcd protein and demonstrates that the Bcd protein follows a discrete pathway at the cortex during early cleavage stages. The movement of Bcd during the early stages was never investigated experimentally until recently [8], but rather relied on assumptions based on the dogma of *bcd* gradient formation [1], the proposals of the SDD model, and on the simulation of protein movement by injecting dextrane particles [7].

Several assumptions were put forward in the past [6, 43–45] that should explain the apparent paradox of a diffusion coefficient of Bcd which was two orders of magnitude too low. Summarized in [44] were: 1) diffusion might be much higher in other compartments, for example within the center; 2) diffusion might be faster during nc 1–9, i. e. at a time when Bcd could not be observed by live imaging; 3) several fractions of Bcd molecules exist that have different diffusion properties; 4) active transport of Bcd.

For the first two assumptions, our data provides evidence that neither assumptions mentioned above can account for the diffusion properties as they were revealed. This for the following reasons: 1) the underlying cause for the protein gradient is the mRNA gradient [2, 3], 2) the protein moves along the cortex (this report).

The yolk, a non-permissive-territory for Bcd movement

The cortical movement of Bcd in wild-type embryos revealed that the inner yolk mass was a non-permissive territory for Bcd movement (Fig 1). In the past, the yolk was considered to be a compartment where Bcd could diffuse fast enough to explain the apparent low diffusion constant [43]. Our data in Fig 1 refutes this possibility. In line with our observations for a distinct

regionalization of Bcd movement, [46] described the inner yolk mass as an ellipsoid entity which morphologically behaved as a distinct unit during each syncytial nuclear cycle, while the cortex was described as a completely different entity.

Data about the content and structure of the inner yolk is sparse, mostly due to the inability of the laser of a confocal microscope to penetrate the dense yolk layer. Actin microfilaments in the deep yolk were described [47, 48], but require a more detailed description. As far as MTs are concerned, only the spindle apparatus during the nuclear cycles were bright enough to become visible [5].

Our drug treatment data demonstrated that the yolk became permissive for Bcd if embryos were treated with CC, vinblastine (Fig 3) or with phalloidin (Fig 4). The most pronounced of these cases was with vinblastine-treated embryos (Fig 3I–3K). The protein behaved exactly as the SDD model would have predicted, it moved to the posterior in a broad front (Fig 3K), while the mRNA remained at the tip.

In unfertilized eggs, the Bcd protein was also found in the yolk, but this observation was not the result of movement from the cortex, rather it represented *de novo* synthesis of Bcd from the template which was translocated to the yolk (Fig 5). During longer incubations, we observed some movement of the protein away from the source (Fig 5I and 5M), indicating that the yolk became "permissive" for Bcd movement under these conditions. Possibly, in an unfertilized embryo, the components of the yolk alter with time, making it permissive for Bcd.

The role of actin for Bcd stability and movement

In the past, it was shown that actin was instrumental in anchoring *bcd* mRNA to the anterior of stage 14 oocytes [17, 20], while only sparse information was available on actin's role for the Bcd protein in the early embryo.

For the first time, we could demonstrate that actin has a profound impact on Bcd stability and movement in the embryo (Fig 4). Particular that actin-dependent, Bcd-stabilizing function (Fig 4A–4C), may constitute an undiscovered means to fine-tune Bcd gradient formation and nuclear filling, as actin is predominant at the cortex where gradient formation actually takes place. We noted that Bcd was particularly enriched around the energids under circumstances where actin was stabilized, i. e. upon phalloidin-treatment (Fig 4F and 4G). During MT-drug treatment, i. e. when actin function was not compromised, a similar enrichment of Bcd in energids was observed (Fig 3B, 3C, 3J and 3K). This observation suggests that Bcd tends to accumulate in territories where there is high levels of actin. Similar observations were made by [49]. Possibly, the energids could serve as a reservoir for Bcd to quicken the step of nuclear filling after the nuclear membrane has formed again.

In cases, where F-actin was destroyed (Fig 4A–4C, S3C and S3D Fig), we also noted a second function of F-actin: aiding Bcd movement to the posterior. While degradation could contribute to a general picture that there was less posterior migration due to a lack of signal, increase of the gain during the confocal analysis confirmed that Bcd movement is indeed impeded (not shown). While actin-dependent long-range movement of Bcd is an unlikely process to occur in wild-type embryos, it suggests that actin may play a role for short range movement of Bcd, e. g. from the site of synthesis to the energids or directly to the nuclei.

Interior transport of *bcd* mRNA

In unfertilized eggs, the cortical MT network for *bcd* mRNA transport was not activated [5] and hence the *bcd* mRNA was not transported along the cortex (Fig 5). Instead, the mRNA was transported, presumably via MTs in the yolk into the middle of the embryo. Concomitantly, the Bcd protein was translated and was confined to the interior of the egg (Fig 5A, 5E,

51 and 5M). Although we could confirm the data of [42], i. e. that a longer, shallower Bcd gradient was observed compared to fertilized embryos of the same age, we could not support their claim that the SDD model was the basis for their observation. Our results demonstrated active transport of the mRNA into the interior of the egg, followed by translation [1]. The weakness of the conclusions drawn by [42] was that they were based on the assumption that the mRNA would stay anchored at the tip which was not the case (Fig 5Q–5T). Our observations were not consistent with an involvement of the SDD model to explain the apparent extended range of Bcd diffusion. Another striking observation was that the inward migration of the mRNA in unfertilized embryos was faster than cortical transport in fertilized embryos (Fig 5R and 5S), raising the possibility that 1) either the tubulin composition of the two MT networks was different from that at the cortex; 2) the interior MT network was oriented more parallel to the A-P axis than the cortical one; 3) the internal MT persisted during all nuclear cycles.

Conclusions

Why does localization and movement of the Bcd protein at the cortex make sense? In the past, we and others have shown that the mRNA gradient follows a similar discrete cortical path as the protein [2, 3, 5, 8]. Hence, the protein as a direct consequence of its template is located in close proximity to the mRNA. Since the egg undergoes strong periplasmic contractions during each nuclear cycle [46], any protein gradient generated by free movement from the tip would suffer from unwanted turbulence. However, since the information of the gradient is already stored at the level of the mRNA [2, 3, 5], the mRNA associated with microtubules is much more resistant against cytoplasmic turbulences than the freely floating Bcd protein. Another feature is that local Bcd synthesis and the shuffling activity of Bcd between the periplasm and the nucleus might be under intricate control. Reported as a rather intriguing result, the concentration of Bcd in nuclei after every mitosis is surprisingly constant, taking into account that number and volume of nuclei vary with each nuclear cycle [43]. Here, we wish to add a rather simple explanation for this seemingly intriguing result: Since each point along the A-P axis experiences an increase of *bcd* mRNA concentration during each nuclear cycle, the number of templates for the translation of Bcd are adjusted for the need of each nuclear cycle. This model could be extended by proposing that during each nuclear cycle, the Bcd protein could be degraded, facilitated by the presence of the PEST domain [45, 50, 51]. This model has barely been taken into consideration in the past, except in [43]. *De novo* synthesis of Bcd takes maximally 2 minutes [3, 37], permitting enough time to fill the nuclei with the correct amount of Bcd, based on the mRNA template. Moreover, since Bcd is translated locally, we envision that there might be tightly-adjusted control mechanisms linking the process of translation to nuclear translocation, thereby allowing to adjust intricately the concentration of Bcd within the nuclei.

Supporting information

S1 Fig. Comparison of Bcd patterns of *bcd*⁺⁵⁺⁸ and wild-type embryos. (A), (D), (G) nc 6 *bcd*⁺⁵⁺⁸ embryo stained for Bcd (A) using saturation of intensities at the tip, color conversion (D) from 0–255 (8 bit), and Staufen (G). (B), (E), (H) nc 6 wild-type embryo stained for Bcd (B) and analyzed using identical confocal parameters as for (A), color conversion (E) with a maximum scale of 1/3 of (D), i. e. from 0–85, and Staufen (G). (C), (F), (I) identical nc 6 wild-type embryo as in (B), recorded using confocal parameters for saturation of intensities at the tip, color conversion (F) with maximum scale of 255, and DAPI to reveal nuclei (I). Note that *bcd*⁺⁵⁺⁸ embryos express about 3 times more Bcd than wild-type embryos, best seen at color conversion between (D) and (E). Likewise, Staufen as a read-out for *bcd* mRNA is equally

stronger in *bcd*⁺⁵⁺⁸ embryos (G), compared to wild-type embryos (H).
(TIF)

S2 Fig. Movement of small molecules into *Drosophila* embryos. (A-D) nc 8 embryo exposed for 2 hours to hypoxia, simultaneously incubated with 3 molecular markers and recorded as a single stack in different channels, revealing Hoechst 33342 (A), Sytox Green (B), TO-PRO3 (C) and merge of (A-C) in (D). (E-H), high magnification of a single stack recording of the embryo in (A-D) showing Hoechst 33342 (E), Sytox Green (F), TO-PRO3 (G) and merge of (E-F) in (H). Note the condensation of the chromatin under hypoxic conditions at the inner surface of nuclei, first described by [9].
(TIF)

S3 Fig. Effect of phalloidin and latrunculin B on cortical actin microfilaments. (A-D) nc 6 embryos exposed for 2 hours to hypoxia and to phalloidin (A, B) and to latrunculin B (C, D). (A) sagittal confocal section, actin staining as revealed with mab JLA20 (red) together with DAPI (blue). (B) cortical confocal section of the anterior tip at high magnification of the same embryo as in (A), stained for actin (red). (C) sagittal confocal section, actin staining as revealed with mab JLA20 (red), together with DAPI (blue). (D) cortical confocal section of the anterior tip at high magnification of the same embryo as in (C), stained for actin (red). Note the extended actin microfilaments upon phalloidin-treatment (B), compared to the globular actin appearance upon latrunculin B-treatment (D).
(TIF)

S1 Table. *bcd*⁺⁵⁺⁸ phenotypes. Percentages of cuticular phenotypes of 3 h hypoxic and 36 h recovered embryos (left) and *bcd*⁺⁵⁺⁸ embryos (right). 3 classes were compared, normal cuticle (blue), mild cuticle phenotype (red) and severe cuticle phenotype (green).
(TIF)

Acknowledgments

We thank Anne Ephrussi for providing rat anti-Staufen antibodies, Mark Biggin for providing rabbit anti-Bicoid antibodies, Tom Kornberg for the *bcd*⁺⁵⁺⁸ stock and Catarina Rippe for the gift of latrunculin B. We also thank Sol Da Rocha for excellent technical assistance and Linda Wei and Thomas Blom for comments on the manuscript.

Author Contributions

Conceptualization: Xiaoli Cai, Alexander Spirov, Stefan Baumgartner.

Data curation: Alexander Spirov.

Formal analysis: Mira Akber, Alexander Spirov, Stefan Baumgartner.

Funding acquisition: Stefan Baumgartner.

Investigation: Xiaoli Cai, Stefan Baumgartner.

Project administration: Stefan Baumgartner.

Supervision: Stefan Baumgartner.

Validation: Xiaoli Cai.

Writing – original draft: Xiaoli Cai.

Writing – review & editing: Stefan Baumgartner.

References

1. Driever W, Nüsslein-Volhard C. A gradient of bicoid protein in *Drosophila* embryos. *Cell*. 1988; 54(1):83–93. PMID: 3383244.
2. Frigerio G, Burri M, Bopp D, Baumgartner S, Noll M. Structure of the segmentation gene paired and the *Drosophila* PRD gene set as part of a gene network. *Cell*. 1986; 47(5):735–46. PMID: 2877746.
3. Spirov A, Fahmy K, Schneider M, Frei E, Noll M, Baumgartner S. Formation of the bicoid morphogen gradient: an mRNA gradient dictates the protein gradient. *Development*. 2009; 136(4):605–14. <https://doi.org/10.1242/dev.031195> PMID: 19168676.
4. Lipshitz HD. Follow the mRNA: a new model for Bicoid gradient formation. *Nature reviews Molecular cell biology*. 2009; 10(8):509–12. <https://doi.org/10.1038/nrm2730> PMID: 19626044.
5. Fahmy K, Akber M, Cai X, Koul A, Hayder A, Baumgartner S. alphaTubulin 67C and Ncd are essential for establishing a cortical microtubular network and formation of the Bicoid mRNA gradient in *Drosophila*. *PLoS one*. 2014; 9(11):e112053. <https://doi.org/10.1371/journal.pone.0112053> PMID: 25390693; PubMed Central PMCID: PMC4229129.
6. Little SC, Tkacik G, Kneeland TB, Wieschaus EF, Gregor T. The formation of the Bicoid morphogen gradient requires protein movement from anteriorly localized mRNA. *PLoS Biol*. 2011; 9(3):e1000596. Epub 2011/03/11. <https://doi.org/10.1371/journal.pbio.1000596> PMID: 21390295; PubMed Central PMCID: PMC3046954.
7. Gregor T, Bialek W, de Ruyter van Steveninck RR, Tank DW, Wieschaus EF. Diffusion and scaling during early embryonic pattern formation. *Proc Natl Acad Sci U S A*. 2005; 102(51):18403–7. <https://doi.org/10.1073/pnas.0509483102> PMID: 16352710; PubMed Central PMCID: PMC1311912.
8. Ali-Murthy Z, Kornberg TB. Bicoid gradient formation and function in the *Drosophila* pre-synctial blastoderm. *Elife*. 2016; 5. <https://doi.org/10.7554/eLife.13222> PMID: 26883601; PubMed Central PMCID: PMC4786422.
9. Foe VE, Alberts BM. Reversible chromosome condensation induced in *Drosophila* embryos by anoxia: visualization of interphase nuclear organization. *J Cell Biol*. 1985; 100(5):1623–36. PMID: 3921555; PubMed Central PMCID: PMC2113892.
10. Douglas RM, Xu T, Haddad GG. Cell cycle progression and cell division are sensitive to hypoxia in *Drosophila melanogaster* embryos. *Am J Physiol Regul Integr Comp Physiol*. 2001; 280(5):R1555–63. PMID: 11294781.
11. Zhao HW, Haddad GG. Review: Hypoxic and oxidative stress resistance in *Drosophila melanogaster*. *Placenta*. 2011; 32 Suppl 2:S104–8. <https://doi.org/10.1016/j.placenta.2010.11.017> PMID: 21353099; PubMed Central PMCID: PMC3073591.
12. Azad P, Zhou D, Zarndt R, Haddad GG. Identification of genes underlying hypoxia tolerance in *Drosophila* by a P-element screen. *G3 (Bethesda)*. 2012; 2(10):1169–78. <https://doi.org/10.1534/g3.112.003681> PMID: 23050227; PubMed Central PMCID: PMC3464109.
13. Zhou D, Haddad GG. Genetic analysis of hypoxia tolerance and susceptibility in *Drosophila* and humans. *Annu Rev Genomics Hum Genet*. 2013; 14:25–43. <https://doi.org/10.1146/annurev-genom-091212-153439> PMID: 23808366.
14. Haddad GG, Sun Y, Wyman RJ, Xu T. Genetic basis of tolerance to O2 deprivation in *Drosophila melanogaster*. *Proc Natl Acad Sci U S A*. 1997; 94(20):10809–12. PMID: 9380715; PubMed Central PMCID: PMC23494.
15. Heinrich EC, Farzin M, Klok CJ, Harrison JF. The effect of developmental stage on the sensitivity of cell and body size to hypoxia in *Drosophila melanogaster*. *J Exp Biol*. 2011; 214(Pt 9):1419–27. <https://doi.org/10.1242/jeb.051904> PMID: 21490250; PubMed Central PMCID: PMC3076073.
16. Zalokar M, Erk I. Division and migration of nuclei during early embryogenesis of *Drosophila melanogaster*. *J Microscopie Biol Cell*. 1976; 25(97–106).
17. Weil TT, Parton R, Davis I, Gavis ER. Changes in bicoid mRNA anchoring highlight conserved mechanisms during the oocyte-to-embryo transition. *Curr Biol*. 2008; 18(14):1055–61. <https://doi.org/10.1016/j.cub.2008.06.046> PMID: 18639459.
18. Weil TT, Xanthakis D, Parton R, Dobbie I, Rabouille C, Gavis ER, et al. Distinguishing direct from indirect roles for bicoid mRNA localization factors. *Development*. 2010; 137(1):169–76. <https://doi.org/10.1242/dev.044867> PMID: 20023172; PubMed Central PMCID: PMC2796925.
19. Florian S, Mitchison TJ. Anti-Microtubule Drugs. *Methods Mol Biol*. 2016; 1413:403–21. https://doi.org/10.1007/978-1-4939-3542-0_25 PMID: 27193863.
20. Weil TT, Forrest KM, Gavis ER. Localization of bicoid mRNA in late oocytes is maintained by continual active transport. *Dev Cell*. 2006; 11(2):251–62. <https://doi.org/10.1016/j.devcel.2006.06.006> PMID: 16890164.

21. Parton RM, Hamilton RS, Ball G, Yang L, Cullen CF, Lu W, et al. A PAR-1-dependent orientation gradient of dynamic microtubules directs posterior cargo transport in the *Drosophila* oocyte. *J Cell Biol.* 2011; 194(1):121–35. <https://doi.org/10.1083/jcb.201103160> PMID: 21746854; PubMed Central PMCID: PMC3135408.
22. Callaini G, Riparbelli MG. Fertilization in *Drosophila melanogaster*: centrosome inheritance and organization of the first mitotic spindle. *Dev Biol.* 1996; 176(2):199–208. Epub 1996/06/15. <https://doi.org/10.1006/dbio.1996.0127> PMID: 8660861.
23. Callaini G, Riparbelli MG. Patterns of microtubule assembly in taxol-treated early *Drosophila* embryo. Cell motility and the cytoskeleton. 1997; 37(4):300–7. Epub 1997/01/01. [https://doi.org/10.1002/\(SICI\)1097-0169\(1997\)37:4<300::AID-CM2>3.0.CO;2-8](https://doi.org/10.1002/(SICI)1097-0169(1997)37:4<300::AID-CM2>3.0.CO;2-8) PMID: 9258503.
24. Karr TL, Alberts BM. Organization of the cytoskeleton in early *Drosophila* embryos. *J Cell Biol.* 1986; 102(4):1494–509. PMID: 3514634.
25. Schejter ED, Wieschaus E. Functional elements of the cytoskeleton in the early *Drosophila* embryo. Annual review of cell biology. 1993; 9:67–99. Epub 1993/01/01. <https://doi.org/10.1146/annurev.cb.09.110193.000435> PMID: 8280474.
26. Lantz VA, Clemens SE, Miller KG. The actin cytoskeleton is required for maintenance of posterior pole plasm components in the *Drosophila* embryo. *Mech Dev.* 1999; 85(1–2):111–22. PMID: 10415352.
27. Spector I, Braet F, Shochet NR, Bubb MR. New anti-actin drugs in the study of the organization and function of the actin cytoskeleton. *Microsc Res Tech.* 1999; 47(1):18–37. [https://doi.org/10.1002/\(SICI\)1097-0029\(19991001\)47:1<18::AID-JEMT3>3.0.CO;2-E](https://doi.org/10.1002/(SICI)1097-0029(19991001)47:1<18::AID-JEMT3>3.0.CO;2-E) PMID: 10506759.
28. Allingham JS, Kienchin VA, Rayment I. Actin-targeting natural products: structures, properties and mechanisms of action. *Cell Mol Life Sci.* 2006; 63(18):2119–34. <https://doi.org/10.1007/s00018-006-6157-9> PMID: 16909206.
29. Mavrakīs M, Rikhy R, Lippincott-Schwartz J. Plasma membrane polarity and compartmentalization are established before cellularization in the fly embryo. *Dev Cell.* 2009; 16(1):93–104. <https://doi.org/10.1016/j.devcel.2008.11.003> PMID: 19154721; PubMed Central PMCID: PMC2684963.
30. Houchmandzadeh B, Wieschaus E, Leibler S. Establishment of developmental precision and proportions in the early *Drosophila* embryo. *Nature.* 2002; 415(6873):798–802. <https://doi.org/10.1038/415798a> PMID: 11845210.
31. Frohnhöfer HG, Nüsslein-Volhard C. Organization of anterior pattern in the *Drosophila* embryo by the maternal gene bicoid. *Nature.* 1986; 324:120–5.
32. Namba R, Pazdera TM, Cerrone RL, Minden JS. *Drosophila* embryonic pattern repair: how embryos respond to bicoid dosage alteration. *Development.* 1997; 124(7):1393–403. PMID: 9118810.
33. Rosset A, Spadola L, Flatib O. OsiriX: an open-source software for navigating in multidimensional DICOM images. *J Digit Imaging.* 2004; 17(3):205–16. <https://doi.org/10.1007/s10278-004-1014-6> PMID: 15534753.
34. Schulman VK, Folker ES, Baylies MK. A method for reversible drug delivery to internal tissues of *Drosophila* embryos. *Fly.* 2013; 7(3):193–203. <https://doi.org/10.4161/fly.25438> PMID: 23846179; PubMed Central PMCID: PMC34049853.
35. Rand MD. A method of permeabilization of *Drosophila* embryos for assays of small molecule activity. *J Vis Exp.* 2014;(89). <https://doi.org/10.3791/51634> PMID: 25046169; PubMed Central PMCID: PMC34049853.
36. Papassideri I, Margaritis LH, Gulik-Krzywicki T. The egg-shell of *Drosophila melanogaster*. VI. Structural analysis of the wax layer in laid eggs. *Tissue & cell.* 1991; 23(4):567–75. PMID: 1926139.
37. Petkova MD, Little SC, Liu F, Gregor T. Maternal origins of developmental reproducibility. *Curr Biol.* 2014; 24(11):1283–8. <https://doi.org/10.1016/j.cub.2014.04.028> PMID: 24856210; PubMed Central PMCID: PMC4061740.
38. Frasnich M, Hoey T, Rushlow C, Doyle H, Levine M. Characterization and localization of the even-skipped protein of *Drosophila*. *EMBO J.* 1987; 6(3):749–59. PMID: 2884106; PubMed Central PMCID: PMC34049853.
39. Driever W, Nüsslein-Volhard C. The bicoid protein determines position in the *Drosophila* embryo in a concentration-dependent manner. *Cell.* 1988; 54(1):95–104. PMID: 3383245.
40. Lucchetta EM, Lee JH, Fu LA, Patel NH, Ismagilov RF. Dynamics of *Drosophila* embryonic patterning network perturbed in space and time using microfluidics. *Nature.* 2005; 434(7037):1134–8. <https://doi.org/10.1038/nature03509> PMID: 15858575; PubMed Central PMCID: PMC2656922.
41. Riparbelli MG, Callaini G, Schejter ED. Microtubule-dependent organization of subcortical microfilaments in the early *Drosophila* embryo. *Dev Dyn.* 2007; 236(3):662–70. Epub 2007/02/03. <https://doi.org/10.1002/dvdy.21062> PMID: 17266137.

42. Drocco JA, Wieschaus EF, Tank DW. The synthesis-diffusion-degradation model explains Bicoid gradient formation in unfertilized eggs. *Physical biology*. 2012; 9(5):055004. Epub 2012/09/27. <https://doi.org/10.1088/1478-3975/9/5/055004> PMID: 23011646; PubMed Central PMCID: PMC3540996.
43. Gregor T, Wieschaus EF, McGregor AP, Bialek W, Tank DW. Stability and nuclear dynamics of the bicoid morphogen gradient. *Cell*. 2007; 130(1):141–52. <https://doi.org/10.1016/j.cell.2007.05.026> PMID: 17632061.
44. Grimm O, Coppey M, Wieschaus E. Modelling the Bicoid gradient. *Development*. 2010; 137(14):2253–64. <https://doi.org/10.1242/dev.032409> PMID: 20570935; PubMed Central PMCID: PMC2889599.
45. Grimm O, Wieschaus E. The Bicoid gradient is shaped independently of nuclei. *Development*. 2010; 137(17):2857–62. <https://doi.org/10.1242/dev.052589> PMID: 20699297; PubMed Central PMCID: PMC2939918.
46. Foe VE, Alberts BM. Studies of nuclear and cytoplasmic behaviour during the five mitotic cycles that precede gastrulation in *Drosophila* embryogenesis. *J Cell Sci*. 1983; 61:31–70. PMID: 6411748.
47. Warn RM, Magrath R, Webb S. Distribution of F-actin during cleavage of the *Drosophila* syncytial blastoderm. *J Cell Biol*. 1984; 98(1):156–62. PMID: 6423648; PubMed Central PMCID: PMC2113007.
48. Hatanaka K, Okada M. Retarded nuclear migration in *Drosophila* embryos with aberrant F-actin reorganization caused by maternal mutations and by cytochalasin treatment. *Development*. 1991; 111(4):909–20. PMID: 1879360.
49. Lucchetta EM, Vincent ME, Ismagilov RF. A precise Bicoid gradient is nonessential during cycles 11–13 for precise patterning in the *Drosophila* blastoderm. *PloS one*. 2008; 3(11):e3651. <https://doi.org/10.1371/journal.pone.0003651> PMID: 18989373; PubMed Central PMCID: PMC2578877.
50. Gregor T, McGregor AP, Wieschaus EF. Shape and function of the Bicoid morphogen gradient in diplopteran species with different sized embryos. *Dev Biol*. 2008; 316(2):350–8. <https://doi.org/10.1016/j.ydbio.2006.01.039> PMID: 18328473.
51. Berleth T, Burri M, Thoma G, Bopp D, Fichstein S, Frigerio G, et al. The role of localization of bicoid RNA in organizing the anterior pattern of the *Drosophila* embryo. *Embo J*. 1988; 7(6):1749–56. PMID: 2901954.
52. Rand MD, Kearney AL, Dao J, Clason T. Permeabilization of *Drosophila* embryos for introduction of small molecules. *Insect biochemistry and molecular biology*. 2010; 40(11):792–804. <https://doi.org/10.1016/j.ibmb.2010.07.007> PMID: 20727969; PubMed Central PMCID: PMC269133.
53. Alexandrov T, Golyandina N, Spirov A. Singular Spectrum Analysis of Gene Expression Profiles of Early *Drosophila* embryo: Exponential-in-Distance Patterns. *Res Lett Signal Process*. 2008; 2008. <https://doi.org/10.1155/2008/825758> PMID: 21152265; PubMed Central PMCID: PMC2997757.

Supplement Figure 1. Comparison of Bcd patterns of bcd+5+8 and wild-type embryos.

(A), (D), (G) nc 5 bcd+5+8 embryo stained for Bcd (A) using saturation of intensities at tip, color conversion (D) from 0-255 (8 bit), and Staufen (G). (B), (E), (H) nc 5 wild-type embryo stained for Bcd (B) and analyzed using identical confocal parameters for (A), color conversion (E) with a maximum scale of 1/3 of (D), i. e. from 0-85, and Staufen (G). (C), (F), (I) identical nc 5 wild-type embryo as in (B) recorded using confocal parameters for saturation at tip, color conversion (E) with maximum scale of 255, and DAPI to reveal nuclei (G). Note that bcd+5+8 embryos express about 3 times more Bcd than wild-type embryos, best seen at color conversion between (D) and (E). Likewise, Staufen as a read-out for bcd mRNA is equally stronger in bcd+5+8 embryos (G), compared to wild-type embryos (H).

Supplement Figure 2. Movement of small molecules into the Drosophila embryo.

(A)-(D) nc 7 embryo exposed for 2 hours to hypoxia, simultaneously incubated with 3 molecular markers and recorded as a single stack in different channels, revealing Hoechst 33342 (A), Sytox Green (B), TO-PRO3 (C) and merge of (A-C) in (D). (E)-(H), high magnification of a single stack recording of the embryo in (A-D) showing Hoechst 33342 (E), Sytox Green (F), TO-PRO3 (G) and merge of (E-F). Note the condensation of the chromatin under hypoxic conditions at the inner surface of nuclei, first described by [13].

Supplement Figure 3. Effect of phalloidin and latrunculin B on cortical actin microfilaments.

(A-D) nc 6 embryos exposed for 2 hours to hypoxia and to phalloidin (A, B) and to latrunculin B (C, D). (A) sagittal confocal section, actin staining as revealed with mab JLA20 (red) together with DAPI (blue). (B) cortical confocal section of the anterior tip at high magnification of the same embryo as in (A), stained for actin (red). (C) sagittal confocal section, actin staining as revealed with mab JLA20 (red), together with DAPI (blue). (D) cortical confocal section of the anterior tip at high magnification of the same embryo as in (C), stained for actin (**red**). **Note the**

extended actin microfilaments upon phalloidin-treatment (B), compared to the globular actin appearance upon latrunculin B-treatment (D).

Table 1.

Percentages of cuticular phenotypes in 3 h hypoxic embryos (left) and *bcd+5+8* embryos (right). 3 classes were compared, normal cuticle (blue), mild cuticle phenotype (red) and severe phenotype (green).

Figure S1

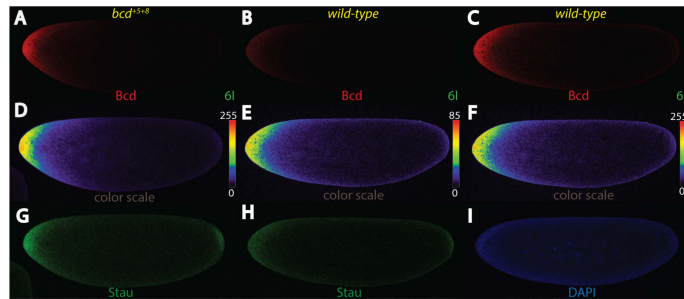


Figure S2

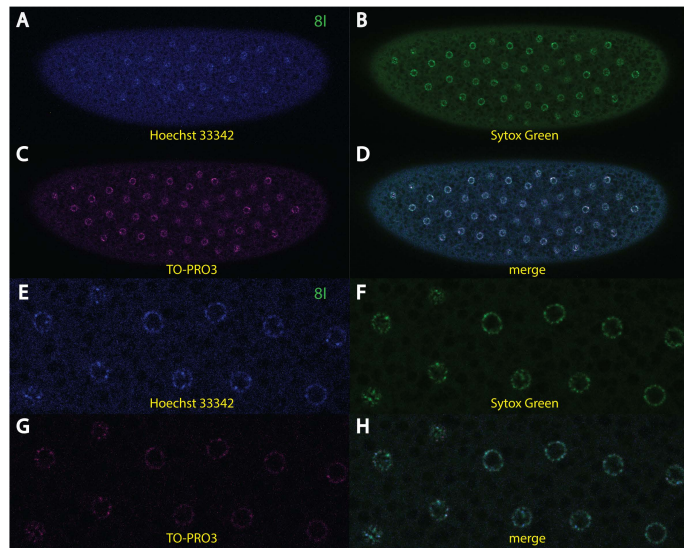


Figure S3

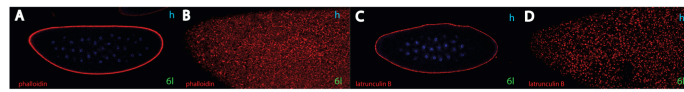
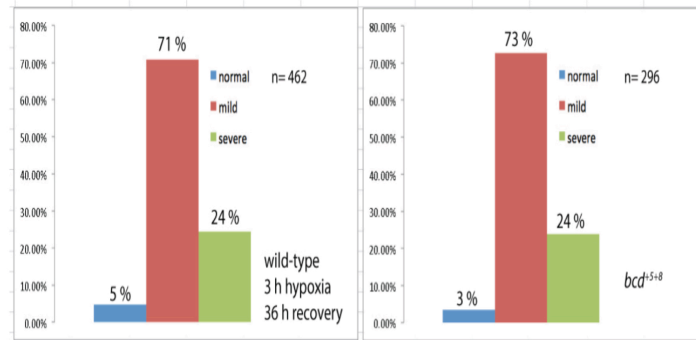
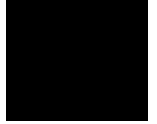


Table S1



Paper IV



Segmentation gene expression patterns in *Bactrocera dorsalis* and related insects: regulation and shape of blastoderm and larval cuticle

WORRAMIN SUKSUWAN[†], XIAOLI CAI, LERTLUK NGERNSIRI[‡] and STEFAN BAUMGARTNER*

Dept. of Experimental Medical Sciences, Lund University, Lund, Sweden

ABSTRACT The oriental fruit fly, *Bactrocera dorsalis*, is regarded as a severe pest of fruit production in Asia. Despite its economic importance, only limited information regarding the molecular and developmental biology of this insect is known to date. We provide a detailed analysis of *B. dorsalis* embryology, as well as the expression patterns of a number of segmentation genes known to act during patterning of *Drosophila* and compare these to the patterns of other insect families. An anterior shift of the expression of gap genes was detected when compared to *Drosophila*. This shift was largely restored during the step where the gap genes control expression of the pair-rule genes. We analyzed and compared the shapes of the embryos of insects of different families, *B. dorsalis* and the blow fly *Lucilia sericata* with that of the well-characterized *Drosophila melanogaster*. We found distinct shapes as well as differences in the ratios of the length of the anterior-posterior axis and the dorsal-ventral axis. These features were integrated into a profile of how the expression patterns of the gap gene *Krüppel* and the pair-rule gene *even-skipped* were observed along the A-P axis in three insect families. Since significant differences were observed, we discuss how *Krüppel* controls the *even-skipped* stripes. Furthermore, we discuss how the position and angles of the segmentation gene stripes differed from other insects. Finally, we analyzed the outcome of the expression patterns of the late acting segment polarity genes in relation to the anlagen of the naked-cuticle and denticle belt area of the *B. dorsalis* larva.

KEY WORDS: *Bactrocera dorsalis*, segmentation, *Krüppel*, *even-skipped*

The oriental fruit fly *Bactrocera dorsalis* (Hendel) (Diptera: Tephritidae) is a major cause of damage of fruit production in tropical and sub-tropical regions, often leading to a total failure of crop production (Vargas *et al.*, 2015). It has in fact been classified as belonging to the most destructive category of insects (category A pests) (Vargas *et al.*, 2015). *B. dorsalis* is widely prevalent in many countries in Asia, but also in the U.S. state of Hawaii. Since accidental introduction in the 1940's, *B. dorsalis* has established itself as a common pest. The insects have also occasionally been detected in the U. S. mainland, e. g. in California and Florida. Attempts have been made to eradicate the pest during four major infestations between 1960 and 1997. In Asia, eradication was not possible for monetary reasons initially. Consequently, damage on crop production was so severe that eradication programs were ultimately implemented to combat this insect.

Phylogenetically, Tephritidae is a family of fruit flies, located immediately adjacent of that of Drosophilidae (Yong *et al.*, 2016). Both families belong to the sub-section Acalypterae, and are referred to as "fruit flies", while the Drosophilidae are often referred to as "the common fruit fly". To make Tephritidae more distinct from Drosophilidae, they are often called "peacock flies". Both families maintain a similar body shape, however, Tephritidae are usually larger than Drosophilidae and are often more colorful with pictured wings. The third family that will be described below is Calliphoridae, a family that is phylogenetically even closer to Tephritidae than to Drosophilidae (Anderer *et al.*, 2016). Within the Calliphoridae, we will focus on the blow fly *Lucilia sericata*.

Abbreviations used in this paper: En, engrailed; Eve, even-skipped; Hb, hunchback; Kr, Krüppel; otd, orthodenticle.

*Address correspondence to: Stefan Baumgartner, Dept. of Experimental Medical Sciences, Lund University, BMC D10, S-22184 Lund, Sweden.
e-mail: Stefan.Baumgartner@med.lu.se • <http://orcid.org/0000-0000-0000-0000>

[†]Present address: Department of Genetics, Faculty of Science, Kasetsart University, Bangkok, Thailand.

Submitted: 4 August, 2016; Accepted: 17 March, 2017.

ISSN: Online 1696-3547, Print 0214-6282
© 2017 UPV/EHU Press
Printed in Spain

Within the family of *Tephritidae*, several other insect members have been described to some detail such as *Ceratitis capitata* (the Mediterranean fruit fly) (Scolari et al., 2014) and *B. oleae* (the olive fly; Mavragani-Tsipidou, 2002). Common to this family is that all three fly species represent the most destructive of fruit pests. *Ceratitis capitata*, in particular, because of its wide distribution over the world, its ability to tolerate cooler climates better than most other species of tropical fruit flies and its wide range of hosts is ranked first among economically important fruit fly species.

The body of the adult *B. dorsalis* is about 8 mm in length, with a wingspan of about 7 mm. Its body color is quite variable: the thorax is mainly dark brown with yellow stripes, while the abdomen is light brown with two black stripes perpendicular to the anterior-posterior (A-P) axis, and a black stripe along the midline. More than 150 kinds of fruits and vegetables are known to be attacked by *B. dorsalis*. Mango, papaya and avocado are the preferred food sources (Leblanc et al., 2012).

Embryogenesis and the formation of segments in insects follows two modes: in short-germband development, segments are added sequentially by adding them to the posterior of a growing embryo (reviewed by Davis and Patel, 2002). The blastoderm embryo occupies only a small fraction of the egg (the remainder consists of yolk and extra-embryonic tissue). Anterior segments are already determined during the blastoderm stage, while posterior segments are added only after gastrulation. In contrast, in insects using long-germband development (where *B. dorsalis* belongs to), the body axis is established already during oogenesis and segments are formed through subdividing the embryo into equally-sized subdomains (Davis and Patel, 2002). Most long-germband embryos take up a large proportion of the egg, and segments are already determined before gastrulation begins. No tissue growth is involved in this process. The morphological formation of segments occurs much later in development; segmental boundaries are visible only at the extended germband stage.

In *Drosophila*, the process of segmentation was described in detail and revealed that at the molecular level, a hierarchy of segmentation genes was crucial for setting up the anterior-posterior axis (Peel et al., 2005). Since segmentation is the common denominator of all insects, attempts have been made to integrate segmentation gene expression patterns of different insects into gene network models to detect common modes of regulation and to explain differences that were observed. The best defined gene regulation model is the gap-gene network model analyzed in dipteran insects (Crombach et al., 2016; Jaeger, 2011) which states that early activation and placement of gap gene expression domains show significant quantitative differences, yet the final patterning output of the system, i. e. the expression of pair-rule genes, is essentially identical in the species investigated, referred to as "system drift" (Crombach et al., 2016). However, information is still limited in regard to comparative gene expression sets in insect families which would allow to test this network model.

An important question is how do the gap genes regulate the pair-rule genes and is this regulation conserved between insect families? For the former question, some progress was made, mainly in *Drosophila*, due to the availability of mutants and the possibility of manipulating this insect. Major focus was on the gap genes *Krüppel*, *hunchback*, *giant* and *knirps*, and how these genes regulated the different stripes of the pair-rule gene *even-skipped* (Goto et al., 1989; Harding et al., 1989; Stanojević et al., 1991; Small et

al., 1996). These reports extended our understanding how the interplay of gap genes control the different *even-skipped* stripes, and defined an initial set of transcriptional activators and repressors for each of the *even-skipped* stripe enhancers. For example, *even-skipped* stripe 2 appeared because it was activated by the *bicoid* and *hunchback* gradients, but repressed by *giant* anteriorly to its margin and by *Krüppel* posteriorly to its margin, giving rise to a 4-cell-wide expression of *even-skipped* stripe 2 (Small et al., 1996). To further understanding as to whether or not *even-skipped* enhancers were conserved between insect families, *even-skipped* enhancers were identified in scavenger flies, *Sepsidae* (Hare et al., 2008), but the sequence identity of the enhancers to those of *Drosophila* was unexpectedly low. This report demonstrated that the identification of regulatory sequence by simple sequence comparison in other insects would not be successful, unless yet-unestablished functional studies would be performed as well. To circumvent this issue, *in silico* approaches were developed to model the transcription of *Drosophila even-skipped* stripe 2 (Ilsley et al., 2013). To date, the only method to reliably detect similarities or differences of how gap genes activate the pair-rule genes in different insect families is to compare the relative positions of gap genes and pair-rule gene stripes along the AP-axis and to determine whether or not a particular gap gene can exert control on a particular pair-rule gene stripe.

As far as the analyses of expression patterns of segmentation genes in *Tephritidae* is concerned, only limited information is available. One report identified plasticity in expression with *orthodenticle* (*otd*), an early segmentation gene in the medfly, *Ceratitis capitata* and the caribfly, *Anastrepha suspensa* (Schetelig et al., 2008), suggesting that changes in *otd* expression can occur even in closely related taxa. Another report showed that the maternal gene *nanos* of the medfly was expressed in a similar pattern as *Drosophila* forming a posterior mRNA gradient, but not identifying plasticity between the two families (Ogaugwu and Wimmer, 2013).

Despite its significant impact on the world-wide fruit market, little is known about the molecular and developmental biology of *B. dorsalis*. Recently, some progress was made in developing genomic resources for this species after the complete sequencing of the genome and some detailed analysis (Calla and Geib, 2015; Geib et al., 2014; Sirm et al., 2015). In addition, RNA sequencing of the transcriptome of genes involved in sexual maturation and mating led to the identification of important genes involved in the sexual development of the *B. dorsalis* female, which consequently may help to develop sterility programs (Zheng et al., 2016). Concurrently, a draft sequence of a relative of *B. dorsalis*, *B. tryoni*, was made available in 2014 (Gilchrist et al., 2014). However, only limited information on the embryology and developmental biology of *Bactrocera* is available, with the exception of a superficial description of the biology of *B. tau* (Singh, 2010) and that of another *Tephritid*, *B. tryoni* (Anderson, 1964).

To supplement the information currently available in describing *B. dorsalis* embryology, we have characterized its embryonic development in detail. We describe the embryonic development of this species, present a panel of expression patterns of early segmentation genes and compare these to the known expression patterns of other established model insects. To address the question whether or not the control of the pair-rule genes by the gap genes is conserved between three insect families, we superimposed the expression patterns of the gap gene *Krüppel* to those of the pair-

rule gene *even-skipped* and draw conclusions how *Krüppel* can control the *even-skipped* stripes in the different insect families. We also noted that the angle and behavior of the *even-skipped* stripes are distinct from those of previously characterized insects with respect to the A-P axis. Furthermore, we show that the shape of the *B. dorsalis* egg and the behavior of the nuclei during the blastoderm stage is considerably different from that of previously characterized insects. Lastly, we analyzed the outcome of the expression patterns of the late acting segment polarity genes in relation to the anlagen of the naked-cuticle and denticle belt area of the *B. dorsalis* larva.

Results

Embryogenesis of *B. dorsalis*

To date, only sparse information of *B. dorsalis* embryogenesis and postembryonic development exists. Some information exist for two closely-related species, *B. tau* (Singh, 2010) and *B. tryoni* (Anderson, 1964), respectively. For this reason, we have analyzed and summarized relevant stages of the *B. dorsalis* life cycle in Fig. 1. We refer to the nomenclature of the stages of *Drosophila* embryogenesis as previously described (Campos-Ortega and Hartenstein, 1985) and also to those of the blow fly *Lucilia sericata* (Mellenthin *et al.*, 2006; Blechert *et al.*, 2011). Embryonic development of *B. dorsalis* proceeds as a long germband insect (Davis and Patel, 2002). As in most insects, the egg is surrounded by a vitelline

membrane and a chorion, however, in contrast to *Drosophila*, no dorsal appendages are observed. Once the chorion is removed, an egg is revealed which is about 0.8 mm long and 0.3 mm in diameter (Fig. 1). The ratio of the length to width, however, is quite different from that of *Drosophila* rendering the egg prone to pressure and physical manipulations. The ventral side as well as the dorsal side are usually curved, a feature not found in *Drosophila*. The posterior tip is often pointed (Fig. 1D) giving the egg a distinct form, compared to those of *Drosophila* or *Lucilia* (Fig. 7B).

After fertilization, the first nuclear cleavages are very similar to those of *Drosophila* where the nuclei divide in the interior of the yolk (Fig. 1 A,B) until they migrate to the periphery to form a syncytial blastoderm (Fig. 1B). In contrast to *Drosophila* where the pole cells (the future germ cells) are formed at nuclear cycle (nc) 10 at the posterior pole, the pole cells are only formed at nc 12 in *B. dorsalis* (Fig. 1C). As in *Drosophila*, after nc 10, four more nuclear cycles follow until the stage of cellular blastoderm is reached (Fig. 1 C,D). Interestingly, during nc 14, no elongation of nuclei occurs as is observed in *Drosophila*, hence nuclei remain rather round during this nc (Fig. 1D). At about 6 hours after egg deposition, the first signs of gastrulation become obvious (Fig. 1E). However, the shape of the cells still does not change and they remain round. Anteriorly, a prominent circumferential furrow is observed which corresponds to the cephalic furrow in *Drosophila*. Ventrally, the mesoderm starts to invaginate (Fig. 1E). On the lateral side, up to 4 folds are observed. This is due to the fact that the radius of the

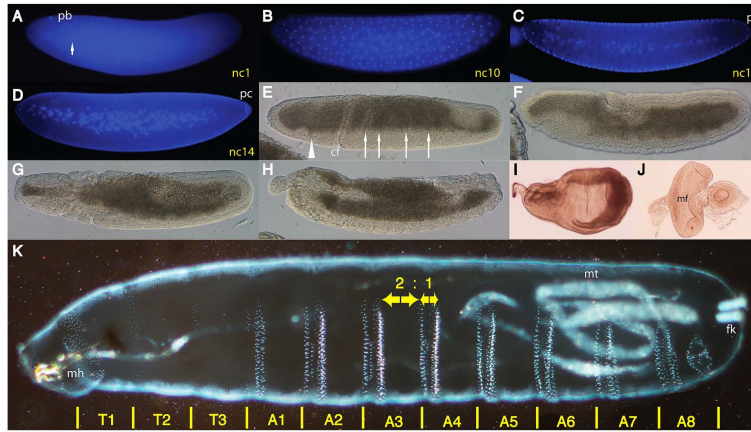


Fig. 1. Embryogenesis and imaginal discs of *B. dorsalis*. (A-K) All embryos are oriented anterior to the left and dorsal side up, unless otherwise noted. (A-D) DAPI staining, nuclear cycles (nc) are indicated in yellow. (A) Nuclear cycle (nc) 1 embryo staining showing the polar body (pb) and the zygotic nucleus (arrow). (B) Nc 10 embryo. Note absence of pole cells. (C) Nc 12 embryo. Note the presence of the pole cells (pc) as a small number of cell at the posterior tip. (D) Nc 14 showing the pole cells (pc). (E-J) Bright field microscopy. (E) Gastrulating embryo showing the cephalic furrow (cf) and up to 4 posterior transverse fold (arrows). Anteriorly, an anterior fold is observed (arrowhead). (F) Extended germband embryo. (G) Embryo during germband retraction. (H) Germband retracted embryo. (I) 3rd instar wing disc. (J) 3rd instar eye-antennal disc showing the morphogenetic furrow (mf). (K) Dark field picture of a 1st instar larva with annotation of the segments and segmental borders (in yellow). The ratio of the distance of naked cuticle versus denticle belts is indicated above A3. Abbreviations: mh, mouth hook; mt, malpighian tubules; fk, filzkörper.

curve leading to germband extension is smaller in *Bactrocera* than in *Drosophila* with respect to the dimension of the body axes. 10 hours into development, the germband is fully extended (Fig. 1F), and its shape appears quite similar to that of *Drosophila* or *Lucilia*. At approximately 14 hours of development, the germband starts to retract (Fig. 1G) taking about 10 hours to complete retraction (Fig. 1H). The following morphogenetic movements such as head involution or dorsal closure proceed as they do in *Drosophila*, however, the speed by which they progress is considerably slower, as noted by (Vargas, 2000; Anderson, 1964). Only after approximately 48 hours at 25°C, the larva hatches (Fig. 1K) showing an identical number of segments compared to *Drosophila* or *Lucilia*, a head, 3 thoracic segments, 8 abdominal segments and a tail (Jurgens, 1987; Martinez Arias, 1993; Mellenthin et al., 2006). The patterns of the denticle bands are distinct from that of *Drosophila* (Moline et al., 1999) or that of *Lucilia* (Mellenthin et al., 2006), showing a gap between weaker anterior rows and stronger posterior rows (Fig. 1K), the latter caused by thicker individual denticle hairs. The ratio of the distance of naked cuticle to that of the denticle bands was about 2:1, a feature distinct from other insects (Fig. 1K; Mellenthin et al., 2006).

B. dorsalis undergoes 3 larval stages, as does *Drosophila* and *Lucilia*. The larval stages last about 8 days at 24°C (Vargas, 2000). These values are also larger than those of *Drosophila* or *Lucilia*. During the end of the 3rd instar larval stage, *B. dorsalis* larvae show a peculiar behavior inherent to most *Tephritidae*: the larvae bend their body by arresting their muscles and releasing the tension which enables them to jump as far as 50 centimeters and as high as 30 centimeters. This behavior is interpreted as an attempt to leave the habitat and to find a secluded place for pupation. The pupal stage takes about 12 days at 24°C (Vargas, 2000). Hence, the complete life cycle of *B. dorsalis* can take as long as 19 days at 24°C (Vargas, 2000), 40-50% longer than in *Drosophila*, mostly due to the prolonged larval and pupal stage.

To determine if *B. dorsalis* utilizes imaginal discs to form the precursors for the adult structures, 3rd instar larvae were dissected

to look for conspicuous discs such as wing and an eye-antennal discs to investigate if they resemble those of *Drosophila* (Fig. 1I, J). A wing disc is similar in shape to that of *Drosophila* (Fig. 1I) and so is an eye-antennal disc (Fig. 1J). Photoreceptor cells follow a similar developmental fate as in *Drosophila* or *Lucilia*, as revealed by the existence of a morphogenetic furrow (Fig. 1J). Altogether, this data demonstrates that imaginal disc development of *B. dorsalis* and probably that of most *Tephritidae* resembles strongly that of *Drosophilidae* or *Calliphoridae*.

B. dorsalis segmentation genes

In order to analyze *Bactrocera* segmentation gene expression, we first screened a database (Geib et al., 2014) for the presence of orthologous segmentation genes of the prime model system *Drosophila melanogaster*. In *Drosophila*, the process of segmentation was described in detail showing that a hierarchy of segmentation genes is crucial for setting up the anterior-posterior axis (Peel et al., 2005). In *Bactrocera*, not all genes of this hierarchy were found (Geib et al., 2014). For example, the maternal gene *bicoid* (*bcd*), shown to be a feature of higher Diptera only, is not present in the *Bactrocera* genome. In *Drosophila*, *bicoid* is expressed in a protein gradient along the A-P axis (Driever and Nüsslein-Volhard, 1988), preceded by the formation of a mRNA gradient (Frigerio et al., 1986; Spirov et al., 2009; Fahmy et al., 2014). The protein gradient serves as morphogen gradient to pattern the anterior-posterior axis. In insects where *bicoid* is lacking, it was proposed that two genes described in *Drosophila* as gap genes, the *hunchback* (*hb*) and the *orthodenticle* (*otd*) act cooperatively to pattern the anterior-posterior axis, instead (Peel et al., 2005; Schetelig et al., 2008).

With this in mind, we have analyzed the expression patterns of important *Bactrocera* members of the segmentation gene hierarchy (Nüsslein-Volhard and Wieschaus, 1980). Of the class of genes at the top of the hierarchy, we analyzed the *hb* and *otd* gene, followed by a member of the gap gene class, the *Krüppel* (*Kr*) gene. The pair-rule gene class is represented by the *even-skipped* (*eve*) gene, while the segment polarity gene class by the *engrailed* (*en*) gene.

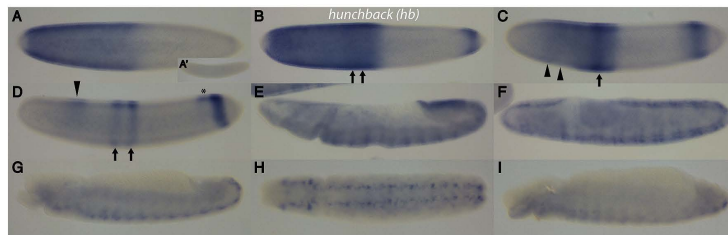


Fig. 2. Embryonic expression of *B. dorsalis* hunchback (*hb*). (A-I) All embryos are oriented anterior to the left and dorsal side up, unless otherwise noted. (A) Nc 13 embryo, *hb* expression is in a broad anterior domain. (A*) Early cleavage stage embryo, no maternal *hb* expression is detected. (B) Early nc 14 embryo, an additional posterior band emerges. In the anterior broad band, the posterior end increases transcription (arrows). (C) Late nc 14 embryo, the anterior end of the broad domain loses transcripts (arrowheads). In the posterior part, a distinct band becomes visible (arrow). (D) Early gastrulation embryo, the broad anterior band has resolved into a dorsal band (arrowhead) and two adjacent bands (arrows), while the posterior band shows a dorsally-expressed spot (asterisk) and the residual strong posterior band. (E) Germband extension, a repetitive pattern of ectodermal stripes emerges. (F) Extended germband, transcripts are in a segment-specific pattern in specific neuroblasts. (G,H) Germband retracted embryo, lateral (G) and ventral (H) view, respectively, a repetitive segmental pattern in neuroblasts is observed. (I) Late embryogenesis, transcripts persist mainly in the ventral chord.

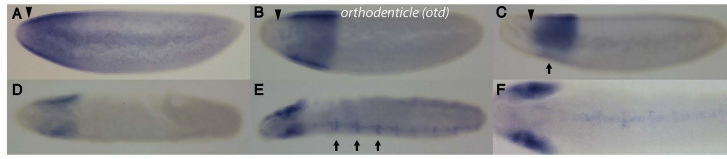


Fig. 3. Embryonic expression of *B. dorsalis orthodenticle (otd)*. (A-F) All embryos are oriented anterior to the left and dorsal side up, unless otherwise noted. (A) Early nc 14 embryo, *otd* is expressed in a broad domain, leaving the anterior-most tip free (arrowhead). (B) Late nc 14 embryo, a large area of the tip does no longer show *hb* transcripts (arrowhead). (C) Early gastrula embryo, anteriorly, transcripts disappear (arrowhead), as well as in the ventral-most region (arrow). (D) Embryo during germband extension, *hb* transcripts are detected in two large lateral patches. (E) Extended germband embryo, the anterior patches remain, while midline cells show transcripts with a segmental pattern (arrows). (F) Extended germband, ventral view; the lateral patches remain as well as expression in midline cells.

Expression of hunchback (*hb*)

Expression of *Bactrocera hb* commenced at nuclear cycle (nc) 13 where a broad domain extending was detected from about 5% to 55% egg length (EL, where the anterior tip is defined as 0% and the posterior tip as 100%; Fig. 2A). In *Drosophila*, this expression is similar, although the anterior domain included the whole anterior tip (Bender *et al.*, 1988; Tautz and Pfeifle, 1989), FlyBase (Attrill *et al.*, 2016). In contrast to *Drosophila*, however, no ubiquitous maternal *hb* contribution in *Bactrocera* was detected during the early nuclear stages (Fig. 2A). At early nc 14, the posterior end of the broad *hb* domain showed increased levels of transcription (Fig. 2B, arrow), while at the posterior end a posterior stripe appeared. During later stages of nc 14, the anterior end of the broad domain showed decreased levels of *hb* (Fig. 2C, arrowheads) and the posterior band increased in intensity. At early gastrula (Fig. 2D), expression of the anterior domain almost completely ceased, with the exception of two distinct stripes in the middle (Fig. 2D, arrows) and an anterior dorsal patch (Fig. 2D, arrowhead). The posterior band remained strong with the anterior end showing expression

only dorsally (Fig. 2D, asterisk). In *Drosophila*, a similar pattern was observed (Attrill *et al.*, 2016), however, only one stripe was found in the middle and the stripe was shown shifted to the anterior, in comparison to *Bactrocera*. During germband extension (Fig. 2E), a repetitive pattern of *hb* stripes evolved, with the posterior-most expression showing strongest expression. At extended germband (Fig. 2F), strong expression was observed in neuroblasts in a segmented pattern. During germband retraction (Fig. 2 G,H), *hb* expression was observed in neuroblasts. During late embryogenesis (Fig. 2I), many neurons in the ventral nerve chord showed strong *hb* expression.

Expression of orthodenticle (*otd*)

Expression of *otd* initiated as a broad circumferential anterior domain at early nc 14, ranging from 2% to 34% EL (Fig. 3A) and leaving the tip free (Fig. 3A, arrowhead), thus clearly later than *B. dorsalis hb* (Fig. 2A) and making *otd* a possible target of regulation by *hb*. During nc 14 (Fig. 3B), the anterior edge shifted to about 11% EL (Fig. 3B, arrowhead), while the posterior edge remained

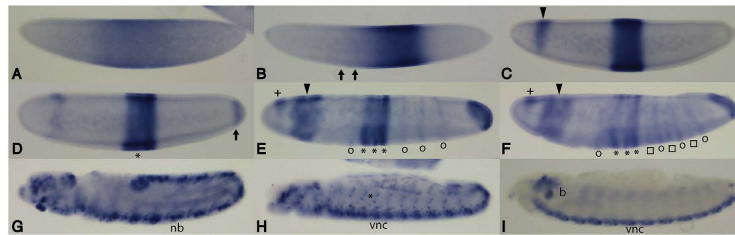


Fig. 4. Embryonic expression of *B. dorsalis Krüppel (Kr)*. (A-I) All embryos are oriented anterior to the left and dorsal side up, unless otherwise noted. (A) Nc 13 embryo, a broad *Kr* band is observed. (B) Early nc 14 embryo, *Kr* transcripts disappear at the anterior end of the broad band (arrows). (C) Late nc 14 embryo, a central domain has emerged and anteriorly, a dorsal "cap" appears (arrowhead). (D) Early gastrula embryo, a posterior band appears (arrow). The middle band begins to split up (asterisk). (E) Embryo at beginning of germband extension, the band in the middle shows clear splitting into 3 bands (asterisk) and 3 new weak bands appear posteriorly and one anteriorly to the central band (open circles). Anteriorly, the dorsal cap becomes stronger (arrowhead). Even more anteriorly, a new cap band appears (+). (F) Embryo during germband extension, slightly older than that in (E), posterior to the middle band which remains split as 3 separate bands, a series of new bands (squares) appear posteriorly which alternate with those marked by open circles making a total of 10 consecutive bands with alternate intensities. (G) Extended germband embryo, strong transcription is observed in neuroblasts (nb). (H) Retracted germband embryo, *Kr* transcripts are seen in the ventral nerve cord (vnc) and in certain muscle precursor cells (asterisk). (I) Embryo shortly before hatching, transcripts are detected in the ventral nerve chord (vnc) and in the brain (b).

constant. During early gastrula (Fig. 3C), transcripts disappeared further from the anterior edge (Fig. 3C, arrowhead) and comprised a band from 17–34% EL. At the ventral side, the presumptive mesodermal anlagen was devoid of any transcripts (Fig. 3C, arrow), similar to that in *Drosophila* (Finkelstein et al., 1990; Attrill et al., 2016). During germband extension (Fig. 3D), the anterior domain remained. At extended germband (Fig. 3E,F), a two-cell wide stripe with lateral extensions emerged (Fig. 3E, arrows). These cells corresponds to the midline cells that marked the outermost cells of the invaginating mesoderm. A similar expression in midline cells was also observed in *Drosophila* (Finkelstein and Perrimon, 1990; Attrill et al., 2016). However, while transcription of *otd* continues in *Drosophila*, *otd* transcripts in *B. dorsalis* ceased after the extended germband stage. Contrary to our expectation, we noted that in two other *Tephritidae*, the medfly *Ceratitis capitata* and the caribfly *Anastrepha suspensa*, maternal *otd* expression was observed (Schetelig et al., 2008). Moreover, medfly *otd* showed a wide band of expression at the early blastoderm expression, and only at cellular blastoderm, all three *Tephritidae* *otd* patterns

converged to an identical broad anterior band of about 17–34% EL. Therefore, there is considerable plasticity of *otd* gene regulation between close relatives within the same family, also noted by (Schetelig et al., 2008).

Expression of Krüppel (Kr)

Kr expression in *B. dorsalis* started with a broad band in the middle of the embryo from about 30% EL to 75% EL with tapered expression on either side at nc 13 (Fig. 4A). Its occurrence paralleled that of *hb* (Fig. 2A). At early nc 14, the anterior-most part of the band diminished (Fig. 4B, arrows) and transcripts were observed in a band from 45% to 70% with a sharp posterior boundary. At late nc 14 (Fig. 4C), a band from 45% to 60% with sharp anterior and posterior boundaries emerged, while anteriorly, a new band appeared whose width tapered off on the ventral side (Fig. 4C, arrowhead). At early gastrula stage (Fig. 4D), a posterior band appeared and the broad middle band began to split (Fig. 4D, asterisk). Slightly later, at the anterior end, another band appeared (Fig. 4E, marked with +), while the initial anterior bands broadened and segregated.

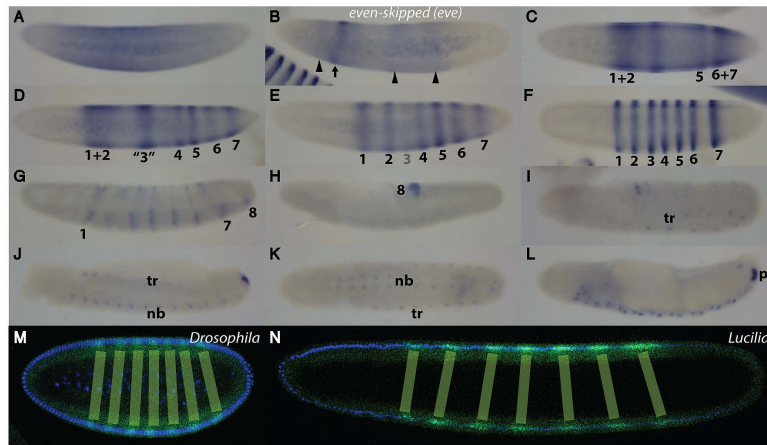


Fig. 5. Embryonic expression of *B. dorsalis* even-skipped (*eve*). (A–N) All embryos are oriented anterior to the left and dorsal side up, unless otherwise noted. (A) Early nc 14 embryo, *eve* is expressed in a broad central domain with diffuse ends. (B) Early nc 14 embryo slightly later than in (A), an anterior band (arrow) appears, along with further weak bands (arrowheads). (C) Mid nc 14 embryo, the weak bands become stronger and anteriorly, another broad band appears, forming bands 1, 2, 5, 6 and 7 (D) Mid nc 14, slightly older than (C), 6 bands with different widths and intensities evolve. Bands 4–7 have final width and positions, bands 1–3 are still not determined. Numbering of stripes according to the final 7 stripe-pattern in (F). (E) Nc 14 embryo close to cellularization, all bands are established, band 3 is considerably weaker. (F) Early gastrula embryo, 7 bands with equal intensity have evolved. (G) Embryo during germband extension, posterior to band 7, band 8 appears. Bands 1–7 become weaker. (H) Extended germband embryo, only the posteriormost band 8 remains. (I) Embryo at beginning of germband retraction, the posterior band is still visible. Single cells, presumably in tracheal precursors (tr), start to express *eve*. (J) Germband retracted embryo, a repetitive pattern in certain neuroblasts (nb) and tracheal cells (tr) emerges. (K) Ventral of a similar staged embryo as in (J), expression is conspicuous in neuroblasts and tracheal cells. (L) Late embryogenesis, *eve* expression is in the ventral nerve chord in neuroblasts and the posterior spiracle (ps). (M) Confocal picture of a late nc 14 of a *D. melanogaster* embryo. *Eve* protein expression is in green, along with DAPI (blue) to reveal the nuclei. The angle of the 7 stripes with respect to the A–P axis is indicated in shaded green. (N) Confocal picture of a late nc 14 *L. sericata* embryo. *Eve* protein expression is in green, along with DAPI (blue) to reveal the nuclei. The angle of the 7 stripes with respect to the A–P axis is indicated in shaded green.

The band in the middle divided into 3 bands (Fig. 4E, marked by asterisk). Posterior to the middle bands, 3 weak new stripes appeared and anteriorly one additional band was detected (Fig. 4E, marked by "o"). During germband extension (Fig. 4F), a faint set of stripes (Fig. 4F, marked by squares) appeared between the 3 posterior bands marked with "o". Hence, at this stage, a row of 10 distinct bands with different intensities emerged, subdividing the region at 40% to 80% EL of the embryo into a striped pattern, reminiscent of segment polarity gene expression (Fig. 6). During extended germband (Fig. 4G), all segments exhibited strong *Kr* expression, mainly in specific neuroblasts (nb). During germband retraction (Fig. 4H), strong *Kr* expression was in neuroblasts of the ventral nerve cord (vnc) and in certain muscle precursor cells (asterisk). During late embryogenesis (Fig. 4I), *Kr* was strongly expressed in the brain (b) and the ventral nerve cord (vnc).

Kr expression has been analyzed in a variety of insects: *Drosophila melanogaster* (Jaekle *et al.*, 1986; Gaul *et al.*, 1987), *Musca domestica* (Sommer and Tautz, 1991), *Clogmia albipunctata* (Rohr *et al.*, 1999; Garcia-Solache *et al.*, 2010), *Oncopeltus fasciatus* (Liu and Kaufman, 2004), *Tribolium castaneum* (Bucher and Klingler, 2004), *Nasonia vitripennis* (Olesnick *et al.*, 2006), *Episyrphus balteatus* (Lenke *et al.*, 2010), *Apis mellifera* (Wilson *et al.*, 2010), *Lucilia sericata* (Blechert *et al.*, 2011) and *Bombyx mori* (Nakao, 2015). In comparison to the aforementioned insects, the evolution of the complex *B. dorsalis Kr* expression pattern at blastoderm and early gastrulation resembled that of *L. sericata Kr* (Blechert *et al.*, 2011), as similar banding patterns were seen in the anterior, middle (Fig. 4D) and biphasic onset of the posterior weak stripes (Fig. 4E, F).

Expression of even-skipped (*eve*)

Expression of *eve* began at early nc 14 (Fig. 5A) revealing a broad band with diffuse ends. At early nc 14 (Fig. 5B), an anterior

strong band was visible (Fig. 5B, arrow), along with some minor bands (Fig. 5B, arrowheads). At mid nc 14 (Fig. 5C), a more defined banding pattern appeared with broad anterior and posterior bands, respectively. In the middle, a strong but transitional band appeared. Thereafter, but still during mid nc 14 (Fig. 5D), the posterior broad band split up, and a new band, band 4, appeared. Anteriorly, the broad band (band 1+2) remained together, while the identity of the middle band (referred to as "3") still remained obscured. Close to cellularization (Fig. 5E), all bands resolved, with the exception of band 3 which was still weak. At early gastrulation (Fig. 5F), 7 bands with a width of 3 cells evolved without regular spacing. Notably, band 7 was more posteriorly-located. During germband extension (Fig. 5G), a new band 8 appeared which was the only one to remain at extended germband (Fig. 5H). During germband retraction (Fig. 5I), a segmental pattern at certain tracheal cells emerged while the posterior band remained defined. At retracted germband (Fig. 5 J,K), the pattern remained unchanged in the tracheal cells, while neuroblasts showed *eve* transcripts in a repetitive pattern. During late embryogenesis (Fig. 5L), *eve* transcription remained high in neuroblasts and the posterior spiracles.

To compare the relative position along the A-P axis and the spatial geometry of the *eve* stripes in some related phyla, *D. melanogaster* and *L. sericata* embryos were stained with monoclonal antibody 2B8, known to detect the Eve protein in distant insect families. While 2B8 did not detect Eve in *B. dorsalis* (data not shown), it revealed 7 stripes in *D. melanogaster* (Fig. 5M) and *L. sericata* (Fig. 5N). Interestingly, in comparison to *B. dorsalis* (Fig. 5F) where the stripes were perpendicular to the A-P axis, the angles of the anterior-most and posterior-most stripes were tilted towards the dorsal side, respectively (Fig. 5 M,N). While this could easily be explained in the case of *D. melanogaster* by the fact that the dorsal side was rather straight and the ventral side rounded (Fig.

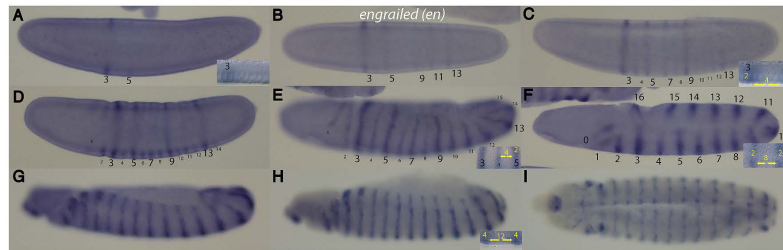


Fig. 6. Embryonic expression of *B. dorsalis engrailed (en)*. (A-I) All embryos are oriented anterior to the left and dorsal side up, unless otherwise noted. Numbering of stripes is according to the final 17 stripe-pattern in (F). (A) Late nc 14 embryo, *en* transcripts are detected in a 2-cell wide stripe 3 and posteriorly a weaker stripe 5. Insert shows width of 2 cells in stripe 3. (B) Nc14, cellular blastoderm embryo, posterior to stripe 5, stripes 9, 11 and 13 appear. Stripe 7 is delayed. (C) Early gastrula embryo, odd-numbered stripes 3-13 become established. In between, even-numbered stripes 4-12 appear with the exception of stripe 10 which is delayed. Insert shows the width of stripe 3 of 2 cells, as well as the interstripe section of 4 cells (indicated by arrows) and stripe 4. (D) Early gastrula embryo, slightly later than in (C), stripes 1, 2 and 14 appear. The stripe intensity is not equal, the odd-numbered ones are stronger than the even-numbered ones. (E) Germband extension embryo, posterior to stripe 14, stripe 15 appears. The intensity of the stripes is still not equal. Insert shows the area of stripe 3 to 5 with width of 2 cells for the stripes and 4 cells for the interstripe region. (F) Extended germband embryo, 16 stripes with equal intensity have evolved. Insert shows the area of stripe 4 to 5 with width of 2 cells for the stripes and 8 cells for the interstripe region. (G) Embryo during germband retraction, the number of stripes remains identical. (H,I) Germband retracted embryos, lateral and ventral view, respectively. Insert in (H) shows the area of stripe 8 to 9 with a width of 4 cells for the stripes and 12 cells for the interstripe region. All stripes are close to the posterior border of each segment.

5M), difficulties arose to explain the observation in the case of *L. sericata* (Fig. 5N) which has a similar body shape and A-P/D-V axis ratio as *B. dorsalis* (Fig. 5F).

Expression of engrailed (en)

B. dorsalis *en* expression was first detected at late nc 14 in a two-cell wide stripe and a posterior weaker stripe (Fig. 6A). The stripes correspond to stripes 3 and 5 and were within the position of the first appearance of the striped expression of *eve* (insert of Fig. 6A). Shortly thereafter, at cellularization (Fig. 6B), stripes 9, 11 and 13 emerged, comprising the first wave of *en* expression in odd-numbered bands. During early gastrula (Fig. 6C), the odd-numbered stripes were complemented by weaker even-numbered stripes in between, a pattern which progressed through germband extension (Fig. 6 D,E) with 2 cells expressing *en* followed by a gap of 4 cells, making a total of 6 cells/segment (insert in Fig. 6E). At extended germband, even- and odd-numbered stripes reached identical intensities (Fig. 6F). Anteriorly, stripes 0 and posteriorly stripes 15 and 16 became visible, making a total of 17 stripes. The width of the *en* bands was 2 cells and the interstripe region 8 cells (insert in Fig. 6F). Hence, one segment comprised of about 10 cells at this stage. During germband retraction (Fig. 6G), a striped pattern in the ectoderm in the posterior of each segment was visible, which persisted during the remaining stages of embryogenesis (Fig. 6 H,I). The number of *en*-expressing cells increased to 4 cells and the interstripe region to 12 cells, making a total of 16 cells/segment (insert in Fig. 6H).

Evo-Devo: comparative expression analysis reveals distinct interpretation of the gap signal at the pair-rule level

A survey in the literature revealed that the expression of *Kr* was investigated in many insects, a comprehensive list is presented above. Hence, it serves as a prime marker to understand how gene expression correlates with the geometry and layout of the insect embryo. Of these aforementioned insects, only a handful were long germband insects: *Drosophila melanogaster* (Gaul et al., 1987), *Musca domestica* (Sommer and Tautz, 1991), *Episyrphus balteatus* (Lemke et al., 2010) and *Lucilia sericata* (Blechert et al., 2011). This collection of data nevertheless permitted the establishment of a map of their expression domains with respect to the A-P axis (Fig. 7A). This comparative map revealed that the majority of long germband insects showed *Kr* expressed in a band between 40-53/57% EL, with *L. sericata* showing a distinct anterior shift (30-45% EL, (Blechert et al., 2011) and *B. dorsalis* a marginal posterior shift (45-60% EL).

Surprisingly, when *eve* banding patterns were compared (Fig. 7B), these considerable differences at the gap-gene level were almost completely restored: The anterior *L. sericata* *eve* bands were still more anterior compared to the "reference" bands of *D. melanogaster* and

B. dorsalis, however, the percentage of the difference compared to *Kr* diminished. Interestingly, the posterior-most bands were at similar levels, despite the difference of 12-15% at the posterior end of the *Kr* bands. We conclude that a compensation of the relative position of the segmental anlagen must have occurred during the stage from the gap gene to the pair-rule gene level which is more pronounced at the posterior part of the embryo.

To address the question if gap genes showed a conserved behavior of controlling the pair-rule genes between the three insect families, we superimposed the *Kr* expression domains to the *eve* stripes (Fig. 7B). We noted significant differences: in *Drosophila*, the anterior margin of the *Kr* band is congruent to the posterior margin of *eve* stripe 2, consistent with the notion that *Kr* demarcates the posterior end of *eve* stripe 2 (Small et al., 1996). In *Lucilia*, we noted the dramatic anterior shift of the *Kr* domain (Blechert et al., 2011), but when this domain was superimposed to that of *eve*, the anterior margin of the *Kr* band was congruent to the posterior margin of *eve* stripe 1, and not to that of stripe 2. In *Bactrocera*, however, the anterior margin of the *Kr* band was congruent to the posterior margin of *eve* stripe 2, as in *Drosophila*, suggesting a similar control. What was common to all three insect families was the fact that the *Kr* band straddled two adjacent *eve* stripes. Data

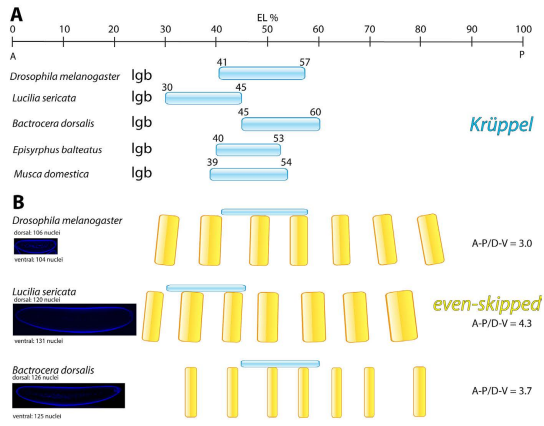


Fig. 7. Schematic representation of relative expression domains of Krüppel and even-skipped in long germband insects. (A) Expression domains in regard to the A-P axis in percentage of egg length (% EL) of *Kr* (blue) in insect families, as reported (Gaul et al., 1987; Rohr et al., 1999; Sommer and Tautz, 1991; Lemke et al., 2010; Blechert et al., 2011) along with those of *B. dorsalis*. Note the distinct anterior shift in *L. sericata* (Blechert et al., 2011) and *B. dorsalis* a marginal posterior shift (45-60% EL). *lgb* indicates "long germband insect". **(B)** Expression domains of even-skipped (yellow) and superimposed Krüppel (blue) in regard to the A-P axis in % EL in *D. melanogaster* (Fig. 5M), *L. sericata* (Fig. 5N) and *B. dorsalis* (Fig. 5F). Representative nuclear DAPI stainings of embryos are indicated and are shown to scale. The number of nuclei on the dorsal as well as ventral side is indicated. Angles of the bands regarding the A-P axis are indicated in yellow as they appear in the respective insect. The ratio of the A-P/D-V axis is indicated on the right side. Note the perfect perpendicularity of the bands in *B. dorsalis* with respect to the A-P axis, compared to the other insects.

from *Episyrphus balteatus* indicated that the *eve* stripes were at similar positions as those of *Drosophila* (Lemke and Schmidt-Ott, 2009), but since the *Kr* band was narrower in comparison to that of *Drosophila* (Fig. 7A), it did not encompass *eve* stripe 4 as in *Drosophila* and consequently, only a single stripe, *eve* stripe 3 was contained within the *Kr* domain.

Evo-Devo: comparative analysis of the shape of the embryos and consequences for the segmentation gene expression at blastoderm stage

Insect embryos have distinct overall shapes where the primary determinant of the shape is the ratio of the A-P axis versus that of the dorsal-ventral (D-V) axis. To investigate the cause for this, the number of cells for the A-P axis on the dorsal and ventral side were counted in 3 insect systems, *D. melanogaster*, *L. sericata* and *B. dorsalis*. It should be noted that not only the cell number, but also the size and shape of the individual cells contribute to the overall shape of the insect eggs (Blechert *et al.*, 2011, Mellenthin *et al.*, 2006). For *Drosophila*, on average 106 ± 3 nuclei on the dorsal side versus 104 ± 3 nuclei on the ventral side were counted, for *Lucilia* 120 ± 4 nuclei on the dorsal side versus 131 ± 5 nuclei on the ventral side, and for *Bactrocera* 126 ± 4 on the dorsal side and 125 ± 3 nuclei on the ventral side (Fig. 7B). The ventral side of the *Drosophila* egg was more rounded, despite the fact that both sides have similar numbers of cells. At close examination, this difference is due to the fact that dorsal cells are highly columnar and the amount of lateral cytoplasm is small, enabling a straight dorsal surface (Fig. 7B). Conversely, ventral cells were slightly constricted at the basal side which enabled a rounded surface. The form of the insect embryo is already determined during the late stages of oogenesis, an observation extended to all long-germband insects. Furthermore, the migration of the nuclei to the periphery during nc 9-10 is a microtubule-driven process not involving changes to the shape of the embryo. Hence, the nuclei of the *Drosophila* embryo adapted to their environment once they have reached their final position at the cortex. The situation in the *Lucilia* egg, however, which also shows a rounded ventral surface, is not as pronounced as in *Drosophila*. Due to its elongated shape, it appears to follow another strategy. The number of nuclei on the ventral side is larger than that of the dorsal side, consequently, leading to almost even spacing on both sides. *Bactrocera* embryos have similar numbers of nuclei on either side and a slightly rounded ventral side which appears to be controlled in a similar way as in *Drosophila*.

To address the question whether the different number of cells on the dorsal and ventral side have implications for the expression patterns, a comparison of the angles of the *eve* stripes with respect to the A-P axis in all 3 insects was conducted. It was noted that the *eve* stripes in *Drosophila* and *Lucilia* were not always perpendicular to the A-P axis, particularly the first and the last stripes. While this behavior can be explained by the curved nature of the ventral side in *Drosophila* (Fig. 5M), a reasonable explanation could not be given for the elongated *Lucilia* egg (Fig. 5N). In contrast, a similarly shaped egg such as the *Bactrocera* egg revealed almost perfectly arranged perpendicular stripes (Fig. 5 D-F). Notably, all *B. dorsalis* segmentation genes analyzed exhibited this behavior at blastoderm stage (Fig. 2-6).

As far as the overall shape of the embryos, there were distinct A-P/D-V ratios between the insects. *Drosophila*, a relatively compact insect egg showed a ratio of 3.0, while *Bactrocera* showed a

ratio of 3.8 and *Lucilia* as the largest of the 3 eggs had a ratio of 4.3 (Fig. 7). It is important to note that the ratio has an impact on the mechanical stability of the egg: rounder eggs are more stable than elongated eggs. This fact becomes an issue when the egg is manipulated, e.g. by pricking it with a needle during genetic transformation where *Lucilia* and *Bactrocera* are particularly vulnerable, compared to *Drosophila* (unpublished observations).

Discussion

We have analyzed the expression of some of the important early A-P axis patterning genes in *B. dorsalis* and found some similarities to known expression patterns in *Drosophila*, but also some distinct features associated with this oriental fruit fly. Furthermore, we described, in detail, its embryogenesis and imaginal disc development.

We noted some similarities of the appearance of the *B. dorsalis* egg to that of *L. sericata* or *D. melanogaster*. All three insects showed an identical number of segments, including a head, 3 thoracic segments, 8 abdominal segments, and a tail (Fig. 1K). The *engrailed* gene was an excellent marker for segment number as well as identity, hence, comparison of the *en* stripe numbers and position might give some clues as to the subdivision of the insect. As evident from Fig. 6, *B. dorsalis* revealed more *en* stripes than *L. sericata* (Mellenthin *et al.*, 2006) or *D. melanogaster* (Attrill *et al.*, 2016). This is due to a stripe in the head, designated "0" (Fig. 6F) and stripe 16 at the posterior end, while the number and position of the stripes in the trunk seemed constant. These different numbers of stripes may be attributed to different functions of tissues. For example, *B. dorsalis* females harbor an ovipositor while a true equivalent of this organ is not found in *L. sericata* or *D. melanogaster*.

It is important to note that in *Drosophila*, not all cells of the cellular blastoderm contribute to the later larval body structure, referred to as the "fate map of the blastoderm" (Technau and Campos-Ortega, 1985). The precursor cells of T1 (Fig. 1K) were located at about 35% EL, and A8 at ~ 80% EL, while regions more anterior were precursors for head structures and elements of the internal digestive system such as anterior midgut or esophagus. At the molecular level, parasegments were defined as the metameric units to subdivide the blastoderm embryo, whereby the *eve* stripes define all odd-numbered parasegments (Martinez-Arias and Lawrence, 1985). In this respect, it is noteworthy that in *Drosophila*, parasegment 3 which is defined by *eve* stripe 2 or *en* stripe 3 corresponds to the anterior half of T1. Hence, neither *eve* stripe 1 nor *en* stripes 1 & 2 contribute to the cuticle pattern, but rather to head structures. Likewise, at the posterior end, *eve* stripe 7 and *en* stripe 15 constitute A8. When looking at the relative position of the *eve* stripes among the 3 different insects, it became evident that the anlagen of the larval cuticle cells were located at distinct regions of the blastoderm (Fig. 7B). In this respect, if the *eve* stripes serve as a landmark to what extent the blastoderm cells will become progenitors for the exoskeleton of the larva, only about 45% of the surface of the *Bactrocera* blastoderm cells (Fig. 6F) will contribute to the exoskeleton which is lower than in *Drosophila* (56%) or *Lucilia* (53%).

As far as the major toolkit of segmentation genes was concerned, *Bactrocera* lacked maternal *bcd* which is a major player on the top of the hierarchy of segmentation genes in many insects. It is a

generally accepted view that in higher Dipterans, *bcd* arose through a duplication of an ancestral *Hox3/zerknüllt* gene. In more basal Diptera where *bcd* is lacking, it was suggested that the function of *bcd* is exerted by a maternally - as well as zygotically-expressed *Hox3/zerknüllt* gene (Stauber et al., 2002). In higher Dipterans, these functions are now separated into two functions exerted by maternally-expressed *bcd* and a zygotically-expressed *zerknüllt* gene (Stauber et al., 2002). In short germband insects such as *Tribolium* where *bcd* is lacking as well, it was proposed that *hb* and *otd* together exert the function of *bcd* (Schroeder, 2003).

Very recently, a report in the midge *Chironomus* showed that *panish*, a protein containing a cysteine-clamp DNA-binding motif, can exert similar functions as does *bcd* in *Drosophila* (Klomp et al., 2015). Like *bcd*, *panish* was strongly expressed at the anterior tip of the fertilized embryo as a result of maternal deposition, and like *bcd* formed a mRNA gradient at blastoderm stage. RNAi-mediated knock-down of *panish* revealed a bicaudal phenotype similar to strong *bcd* mutations. These results showed that evolution possibly established further systems that enabled patterning the anterior end and that *bcd* and *panish* were limited to specific families of flies. Of note, *panish* was not found in the *Bactrocera* genome nor was it detectable in two closely-related chironomid species which suggested that *panish* arose only very recently (Klomp et al., 2015).

The next class of genes in the hierarchy of the segmentation, the gap gene class showed both *hb* and *Kr* genes conserved. Compared to *Drosophila* where the first expression was observed during nc 12 (Knipple et al., 1985; Bender et al., 1988), *Bactrocera hb* and *Kr* showed expression from nc 13 on, suggesting that blastoderm identity followed a distinct regulation. During later embryogenesis, however, identical organs were labeled suggesting that the later functions of both genes were retained. The third gap gene, *otd*, also showed its expression delayed by one nc, compared to *Drosophila* (Finkelstein and Perrimon, 1990).

Down the hierarchy follows the pair rule gene class (Nüsslein-Volhard and Wieschaus, 1980) where the *eve* gene was analyzed. Compared to *Drosophila*, the number of *eve* stripes remained conserved, however, it was the evolution of the stripes that was clearly different in the two insects (MacDonald et al., 1988; Fig. 5). Again, transcription of *eve* in *Bactrocera* was delayed by one nc, compared to *Drosophila* (Macdonald et al., 1986). In addition, eye-catching was the fact how these 7 stripes were aligned along the A-P axis between the two insects at cellular blastoderm (Fig. 5F vs. Fig. 5M). These appeared oblique at either end in *Drosophila* or *Lucilia* (Fig. 5 M, N), while in *Bactrocera*, all segmentation genes were expressed perpendicular to the A-P axis (Fig. 2-6). We should also bear in mind that the number of cells on the dorsal versus the ventral side was only marginally different in all 3 insects, hence the outcome in the perpendicularity of the stripes must have a different origin.

Our comparative analysis in Fig. 7, demonstrates that there are marked differences across insect families of how the gap genes exert their control on pair-rule genes, evidenced by the position of the *Kr* band along the AP axis in comparison to the *eve* stripes. *eve* stripe 2 is a paradigm of how the maternal input, together with the gap genes, control the pair-rule genes (Small et al., 1996). While *Bactrocera* and *Drosophila* showed similar overlap of the *Kr* bands with reference to the *eve* stripes where the anterior border of the *Kr* band was precisely adjacent to the posterior border of *eve* stripe 2 (Fig. 7B), the position of the *Lucilia Kr* band was distinct and was

moved exactly one *eve* stripe unit to the anterior. Moreover, *eve* stripe 4 which in *Drosophila* and *Bactrocera* is probably activated by *Kr* (Fig. 7B) does not overlap any longer with the *Kr* band in *Lucilia*. Likewise, in *Episyrphus balteatus*, *eve* stripe 4 does not seem to involve *Kr* regulation either, as the posterior part of the *Kr* band does no longer overlap with *eve* stripe 4 (Lemke et al., 2010; Lemke and Schmidt-Ott, 2009). From this comparative analysis, we can conclude that regulation of *eve* stripes 2-4 by *Kr* is not conserved among insect families.

During blastoderm stage at nc 14, we noted a particular behavior for *B. dorsalis* nuclei, as they did not undergo an elongation step as in *L. sericata* or *D. melanogaster*. In *Drosophila*, elongation of the nuclei is initiated by the formation of an inverted basket of microtubules that originate from the centrosomes that are located in the periplasm next to the nuclei (Foe et al., 2000; Foe et al., 1993). These microtubules guide the invagination of a furrow which migrates from the apical to the basal side of the nuclei, until they wrap the nuclei into a cell. The leading edge of the furrow is driven by an actin-myosin interaction that migrates, from the apical to the basal side, along the microtubules, until the cellular membrane encapsulates the nucleus fully, thus forming a cell. The elongated form of the cells at cellular blastoderm allow cellular constrictions which are one of the driving forces for gastrulation. In contrast, the *B. dorsalis* cells hardly elongated during nc 14 and instead stayed largely round (Fig. 1D). This was true even for gastrulation which creates difficulties for cells to change the cellular morphology and to assign constrictions that are important for gastrulation. We presume that in *Bactrocera*, the mechanisms leading to the driving forces for ventral furrow formation or germband extension must be different ones, compared to *D. melanogaster* or *L. sericata*.

During the analysis of segmentation genes in *Lucilia* (Mellenthin et al., 2006), we noticed that the ratio of the area of naked cuticle to that of the denticle bands varied dramatically when comparing the large *Lucilia* fly to that of the small *Drosophila*. In *Lucilia*, we measured a ratio of 3:1, while the one in *Drosophila* was 1.5:1 (Mellenthin et al., 2006). We also noted that the naked cuticle area was particularly dependent on the patterning activity of the segmentation gene *wingless* which in *Lucilia* showed signaling activity over 3 times the distance compared to *Drosophila* (Mellenthin et al., 2006). Further, using mathematical calculations, it was shown that a 20-fold increase of the *Wingless* producing cells still was not enough to compensate for the larger distance between the sender and receiver cell, unless a facilitated movement of the *Wingless* protein was allowed (Mellenthin et al., 2006). In the case of the *Bactrocera* cuticle, we noted that the ratio was 2:1 (Fig. 1K) which was closer to that of the small *Drosophila*, and not in the range of the larger *Lucilia*. Hence, the ratio of the naked cuticles/denticle belts does not increase linearly with the size of the insect. Rather, these ratios likely represent adaptations of the systems to their habitat or their ability to exert movements. We therefore reasoned that these differences in these ratios should immediately be reflected in the expression patterns of the naked cuticle-patterning genes of these biological systems. In this case, the *en* gene is good marker gene, as it allows to define several issues important for insect segmentation, this for the following reasons: (i) its anterior expression border defines the parasegmental border, a feature which is conserved across most insect phyla (Mellenthin et al., 2006), (ii) the number of *en*-expressing cells is a good estimate how large the naked cuticle will be (Mellenthin et al., 2006), (iii)

the number of *en* bands is a good marker for estimation of how many segments a fly has (Baumgartner *et al.*, 1987; Mellenthin *et al.*, 2006). When compared to *Lucilia* where 6 cells were reported to show *en* expression at extended germband (Mellenthin *et al.*, 2006), *Bactrocera en* was expressed in a much less wider band, comprising only 2 cells (Fig. 6 F). Hence, the capacity to pattern the cuticle is limited, taken into account the size of the insect. In fact, the much smaller *Drosophila* embryo also revealed 2 cells expressing *en* which corroborated the notion that size did not matter.

Materials and Methods

Maintenance of *B. dorsalis*

B. dorsalis flies were maintained in 25 x 50 cm round Plexiglas cages and fed with a constant source providing 3 parts of sugar, 1 part of yeast hydrolysate and water. For larval stages, a mixture 1000 g, sugar, 100 g yeast hydrolysate, 50 g yeast extract and 50 g peptone, supplemented by banana or apple pieces was used. To prevent escape of larvae during the "jumping phase" of larval stages, containers were always covered with a cover during this time.

Embryo collection

Bactrocera flies were exposed to standard food for 10 days. For embryo collection, a smaller plastic beaker was prepared with many small holes (diameter > 1 mm) which was positioned over a freshly-cut apple piece. To enable a precise embryo collection, a pre-collection phase of 2 hours was employed where eggs that were deposited were discarded. In some cases, an apple, cut into a halves, was used for embryo collection, where the embryos were collected by removal of the shell and collecting the embryos from the inner surface of the shell.

Identification of orthologous genes in *B. dorsalis*

The *Bactrocera* orthologues of segmentation genes were identified through standard BLAST searches of a database where access was provided by Scott Geib. This database is accessible via the NCBI *Bactrocera dorsalis* Annotation Release 100. Note: the maternal *bicoid* gene is not present in the *Bactrocera* genome. *B. dorsalis hunchback* has accession number XM_011208844, *orthodenticle* XM_011202351.1, *Krüppel* XM_011207908.1, *even-skipped* XM_011210455.1 and *engrailed* XM_011216118.1. *hunchback* was amplified by PCR primers GCGAAATCACTACAAGATCAG (forw) and TAAATCTTAGGAACGTAAACC (rev), *orthodenticle* with CTCGACAGAAGCCCTAATGGC (forw) and TTATTCGATTGGCTCCAGCG (rev), *Krüppel* with ACCCCATAACCGTGC-CGATG (forw) and CTACTCCATTAGGGTGGTTG (rev), *even-skipped* with GCGATCAATTGACACGTCTGG (forw) and AAGACTCGGTTTGTAGGGCT (rev), *engrailed* with CTCGCGTTTACTACAACGCC (forw) and GGGACGATCGCTGTAGCGGT (rev). Each PCR fragment was sequenced to verify its origin.

In situ hybridization

Templates for Riboprobes were generated using a 0-4 h *B. dorsalis* cDNA library (L. Ngernsiri, unpublished) as templates and T7 RNA polymerase-binding sites on the reverse primer from the above identified *B. dorsalis* segmentation genes. These DNA templates were purified, sequenced and used as templates using a DIG-labeling kit (Roche) as described (Fahmy *et al.*, 2014). A non-related sense probe was used as a negative control. *In situ* hybridization followed a protocol according to (Fahmy *et al.*, 2014).

Immunohistochemistry

D. melanogaster and *L. sericata* embryos were heat-fixed and stained with a monoclonal antibody against the Even-skipped protein, (mab 2B8, DSHB) at a concentration of 1:250, counterstained with DAPI and monitored on a Zeiss LSM 710 confocal microscope.

Acknowledgements

S. B. thanks the Swedish Research Council, the Olle Engkvist Byggnästande Foundation, the Kock Foundation and the Eric Philip Sörensen Foundation for support. We thank Kasetsart University for the Student Exchange Fellowship to W. S. to work at Lund University. We wish to thank Scott Geib for access to his *B. dorsalis* database prior to publishing their data, Sol Da Rocha for excellent technical assistance and Linda Wei for comments on the manuscript.

References

- ANDERE, A.A., PLATT, R.N., RAY, D.A. and PICARD, C.J. (2016). Genome sequence of *Phormia regina* Meigen (Diptera: Calliphoridae): Implications for medical, veterinary and forensic research. *BMC Genomics* 17: 842.
- ANDERSON, D.T. (1964). The Embryology of *Dacus Tryoni* (Diptera). 3. Origins of Imaginal Rudiments Other Than the Principal Discs. *J Embryol Exp Morphol* 12: 65-75.
- ATTRILL, H., FALLS, K., GOODMAN, J.L., MILLBURN, G.H., ANTONAZZO, G., REY, A.J., MARYGOLD, S.J. and FLYBASE, C. (2016). FlyBase: establishing a Gene Group resource for *Drosophila melanogaster*. *Nucleic Acids Res* 44: D796-792.
- BAUMGARTNER, S., BOPP, D., BURRI, M. and NOLL, M. (1987). Structure of two genes at the gooseberry locus related to the paired gene and their spatial expression during *Drosophila* embryogenesis. *Genes Dev* 1: 1247-1267.
- BENDER, M., HORIKAMI, S., CRIBBS, D. and KAUFMAN, T.C. (1988). Identification and expression of the gap segmentation gene *hunchback* in *Drosophila melanogaster*. *Dev Genet* 9: 715-732.
- BLECHERT, C., DOUGLAS, D. and BAUMGARTNER, S. (2011). Conserved function of the *Kruppel* gap gene in the blowfly *Lucilia sericata*, despite anterior shift of expression. *Insect Mol Biol* 20: 257-265.
- BUCHER, G. and KLINGLER, M. (2004). Divergent segmentation mechanism in the short germ insect *Tribolium* revealed by giant expression and function. *Development* 131: 1729-1740.
- CALLA, B. and GEIB, S.M. (2015). MicroRNAs in the oriental fruit fly, *Bactrocera dorsalis*: extending *Drosophila* miRNA conservation to the Tephritidae. *BMC Genomics* 16: 740.
- CAMPOS-ORTEGA, J.A. and HARTENSTEIN, V. (1985). *The Embryonic Development of Drosophila melanogaster*. Springer, Berlin.
- CROMBACH, A., WOTTON, K.R., JIMENEZ-GURI, E. and JAEGER, J. (2016). Gap Gene Regulatory Dynamics Evolve along a Genotype Network. *Mol Biol Evol* 33: 1298-1307.
- DAVIS, G.K. and PATEL, N.H. (2002). Short, long, and beyond: molecular and embryological approaches to insect segmentation. *Annu Rev Entomol* 47: 669-699.
- DRIEVER, W. and NÜSSLEIN-VOLHARD, C. (1988). A gradient of *bicoid* protein in *Drosophila* embryos. *Cell* 54: 83-93.
- FAHMY, K., AKBER, M., CAI, X., KOUL, A., HAYDER, A. and BAUMGARTNER, S. (2014). α -Tubulin 67C and Nod are essential for establishing a cortical microtubular network and formation of the *Bicoid* mRNA gradient in *Drosophila*. *PLoS One* 9: e112053.
- FINKELSTEIN, R. and PERRIMON, N. (1990). The *orthodenticle* gene is regulated by *bicoid* and *torso* and specifies *Drosophila* head development. *Nature* 346: 485-488.
- FINKELSTEIN, R., SMOUSE, D., CAPACI, T.M., SPRADLING, A.C. and PERRIMON, N. (1990). The *orthodenticle* gene encodes a novel homeo domain protein involved in the development of the *Drosophila* nervous system and ocellar visual structures. *Genes Dev* 4: 1516-1527.
- FOE, V.E., FIELD, C.M. and ODELL, G.M. (2000). Microtubules and mitotic cycle phase modulate spatiotemporal distributions of F-actin and myosin II in *Drosophila* syncytial blastoderm embryos. *Development* 127: 1767-1787.
- FOE, V.E., ODELL, G.M. and EDGAR, B.A. (1993). Mitosis and morphogenesis in the *Drosophila* embryo: point and counterpoint. *The Development of Drosophila melanogaster* (Bate M. and Martinez Arias A., eds.) Cold Spring Harbor Laboratory Press: 1: 149-300.
- FRIGERIO, G., BURRI, M., BOPP, D., BAUMGARTNER, S. and NOLL, M. (1986). Structure of the segmentation gene *paired* and the *Drosophila* PRD gene set as part of a gene network. *Cell* 47: 735-746.

- GARCIA-SOLACHE, M., JAEGER, J. and AKAM, M. (2010). A systematic analysis of the gap gene system in the moth midge *Clogmia albipunctata*. *Dev Biol* 344: 306-318.
- GAUL, U., SEIFERT, E., SCHUH, R. and JACKLE, H. (1987). Analysis of Kruppel protein distribution during early *Drosophila* development reveals posttranscriptional regulation. *Cell* 50: 639-647.
- GEIB, S.M., CALLA, B., HALL, B., HOU, S. and MANOUKIS, N.C. (2014). Characterizing the developmental transcriptome of the oriental fruit fly, *Bactrocera dorsalis* (Diptera: Tephritidae) through comparative genomic analysis with *Drosophila melanogaster* utilizing modENCODE datasets. *BMC Genomics* 15: 942.
- GILCHRIST, A.S., SHEARMAN, D.C., FROMMER, M., RAPHAEL, K.A., DESHPANDE, N.P., WILKINS, M.R., SHERWIN, W.B. and SVED, J.A. (2014). The draft genome of the pest tephritid fruit fly *Bactrocera tryoni*: resources for the genomic analysis of hybridising species. *BMC Genomics* 15: 1133.
- GOTO, T., MACDONALD, P. and MANIATIS, T. (1989). Early and late periodic patterns of even-skipped expression are controlled by distinct regulatory elements that respond to different spatial cues. *Cell* 57: 413-422.
- HARDING, K., HOEY, T., WARRIOR, R. and LEVINE, M. (1989). Autoregulatory and gap gene response elements of the even-skipped promoter of *Drosophila*. *EMBO J* 8: 1205-1212.
- HARE, E.E., PETERSON, B.K., IYER, V.N., MEIER, R. and EISEN, M.B. (2008). Sepsid even-skipped enhancers are functionally conserved in *Drosophila* despite lack of sequence conservation. *PLoS Genet* 4: e1000106.
- ILSLEY, G.R., FISHER, J., APWEILER, R., DE PACE, A.H. and LUSCOMBE, N.M. (2013). Cellular resolution models for even-skipped regulation in the entire *Drosophila* embryo. *Elife* 2: e00522.
- JAECKLE, H., TAUTZ, D., SCHUH, R., SEIFERT, E. and LEHMANN, R. (1986). Cross-regulatory interactions among the gap genes of *Drosophila*. *Nature* 324: 668-670.
- JAEGER, J. (2011). The gap gene network. *Cell Mol Life Sci* 68: 243-274.
- JURGENS, G. (1987). Segmental organization of the tail region in the embryo of *Drosophila melanogaster*. *Roux's Arch Dev Biol* 196: 141-157.
- KLOMP, J., ATHY, D., KWAN, C.W., BLOCH, N.I., SANDMANN, T., LEMKE, S. and SCHMIDT-OTT, U. (2015). A cysteine-clamp gene drives embryo polarity in the midge *Chironomus*. *Science* 348: 1040-1042.
- KNIPPLE, D.C., SEIFERT, E., ROSENBERG, U.B., PREISS, A. and JACKLE, H. (1985). Spatial and temporal patterns of Kruppel gene expression in early *Drosophila* embryos. *Nature* 317: 40-44.
- LEBLANC, L., TORA VUETI, E., DREW, R.A.I. and ALLWOOD, A.J. (2012). Host plant records for fruit flies (Diptera: Tephritidae: Dactyn) in the Pacific Islands. *Proc. Hawaii. Entomol. Soc.* 44: 11-53.
- LEMKE, S., BUSCH, S.E., ANTONOPOULOS, D.A., MEYER, F., DOMANUS, M.H. and SCHMIDT-OTT, U. (2010). Maternal activation of gap genes in the hover fly *Episyrphus*. *Development* 137: 1709-1719.
- LEMKE, S. and SCHMIDT-OTT, U. (2009). Evidence for a composite anterior determinant in the hover fly *Episyrphus balteatus* (Syrphidae), a cyclorhaphan fly with an anterodorsal serosa anlage. *Development* 136: 117-127.
- LIU, P.Z. and KAUFMAN, T.C. (2004). Kruppel is a gap gene in the intermediate germ-band insect *Oncopeltus fasciatus* and is required for development of both blastoderm and germ band-derived segments. *Development* 131: 4567-4579.
- MACDONALD, P.M., INGHAM, P. and STRUHL, G. (1986). Isolation, structure, and expression of even-skipped: a second pair-rule gene of *Drosophila* containing a homeo box. *Cell* 47: 721-734.
- MARTINEZ-ARIAS, A. (1993). *Development and patterning of the larval epidermis of Drosophila*. Cold Spring Harbor Laboratory Press.
- MARTINEZ-ARIAS, A. and LAWRENCE, P.A. (1985). Parasegments and compartments in the *Drosophila* embryo. *Nature* 315: 639-642.
- MAVRAGANI-TSIPIDOU, P. (2002). Genetic and cytogenetic analysis of the olive fruit fly *Bactrocera oleae* (Diptera: Tephritidae). *Genetica* 116: 45-57.
- MELLENTHIN, K., FAHMY, K., ALL, R.A., HUNDING, A., DA ROCHA, S. and BAUMGARTNER, S. (2006). Wingless signaling in a large insect, the blowfly *Lucilia sericata*: a beautiful example of evolutionary developmental biology. *Dev Dyn* 235: 347-360.
- MOLINE, M.M., SOUTHERN, C. and BEJSOVEC, A. (1999). Directionality of wingless protein transport influences epidermal patterning in the *Drosophila* embryo. *Development* 126: 4375-4384.
- NAKAO, H. (2015). Analyses of interactions among pair-rule genes and the gap gene Kruppel in *Bombyx* segmentation. *Dev. Biol.* 405: 149-157.
- NÜSSLEIN-VOLHARD, C. and WIESCHAU, E. (1980). Mutations affecting segment number and polarity in *Drosophila*. *Nature* 287: 795-801.
- OGAUGWU, C.E. and WIMMER, E.A. (2013). Molecular cloning and expression of nanos in the Mediterranean fruit fly, *Ceratitis capitata* (Diptera: Tephritidae). *Gene Expr Patterns* 13: 188-188.
- OLESNICKY, E.C., BRENT, A.E., TONNES, L., WALKER, M., PULTZ, M.A., LEAF, D. and DESPLAN, C. (2006). A caudal mRNA gradient controls posterior development in the wasp *Nasonia*. *Development* 133: 3973-3982.
- PEEL, A.D., CHIPMAN, A.D. and AKAM, M. (2005). Arthropod segmentation: beyond the *Drosophila* paradigm. *Nat Rev Genet* 6: 905-916.
- ROHR, K.B., TAUTZ, D. and SANDER, K. (1999). Segmentation gene expression in the moth midge *Clogmia albipunctata* (Diptera, psychodidae) and other primitive dipterans. *Dev Genes Evol* 209: 145-154.
- SCHETELIG, M.F., SCHMID, B.G., ZIMOWSKA, G. and WIMMER, E.A. (2008). Plasticity in mRNA expression and localization of orthodenticle within higher Diptera. *Evol Dev* 10: 700-704.
- SCHROEDER, R. (2003). The genes orthodenticle and hunchback substitute for bicoid in the beetle *Tribolium*. *Nature* 422: 621-625.
- SCOLARI, F., GOMULSKI, L.M., GABRIELLI, P., MANNI, M., SAVINI, G., GASPERI, G. and MALACRIDA, A.R. (2014). How functional genomics will impact fruit fly pest control: the example of the Mediterranean fruit fly, *Ceratitis capitata*. *BMC Genet* 15 Suppl 2: S11.
- SIM, S.B., CALLA, B., HALL, B., DEREGO, T. and GEIB, S.M. (2015). Reconstructing a comprehensive transcriptome assembly of a white-pupal translocated strain of the pest fruit fly *Bactrocera cucurbitae*. *Gigascience* 4: 14.
- SINGH, S.K., KUMAR, D. and RAMAMURTHY, V. V. (2010). Biology of *Bactrocera* (*Zaenagda*) (*tau*) (Walker) (Diptera: Tephritidae). *Entomological Res.* 40: 259-263.
- SMALL, S., BLAIR, A. and LEVINE, M. (1996). Regulation of two pair-rule stripes by a single enhancer in the *Drosophila* embryo. *Dev Biol* 175: 314-324.
- SOMMER, R. and TAUTZ, D. (1991). Segmentation gene expression in the housefly *Musca domestica*. *Development* 113: 419-430.
- SPIROV, A., FAHMY, K., SCHNEIDER, M., FREI, E., NOLL, M. and BAUMGARTNER, S. (2009). Formation of the bicoid morphogen gradient: an mRNA gradient dictates the protein gradient. *Development* 136: 605-614.
- STANCOJEVIC, D., SMALL, S. and LEVINE, M. (1991). Regulation of a segmentation stripe by overlapping activators and repressors in the *Drosophila* embryo. *Science* 254: 1365-1367.
- STAUBER, M., PRELL, A. and SCHMIDT-OTT, U. (2002). A single Hox3 gene with composite bicoid and zerknullt expression characteristics in non-Cyclorhaphan flies. *Proc Natl Acad Sci USA* 99: 2714-2719.
- TAUTZ, D. and PFEIFLE, C. (1989). A non-radioactive *in situ* hybridization method for the localization of specific RNAs in *Drosophila* embryos reveals translational control of the segmentation gene hunchback. *Chromosoma* 98: 81-85.
- TECHNAU, G.M. and CAMPOS-ORTEGA, J.A. (1985). Fate-mapping in wild-type *Drosophila melanogaster*. *Wilhelm Roux Arch. Dev. Biol.* 194: 196-212.
- VARGAS, R.I., PINERO, J.C. and LEBLANC, L. (2015). An Overview of Pest Species of *Bactrocera* Fruit Flies (Diptera: Tephritidae) and the Integration of Biopesticides with Other Biological Approaches for Their Management with a Focus on the Pacific Region. *Insects* 6: 297-318.
- VARGAS, R.I., WALSH, W., KANEHISA, D., STARK, D. and NISHIDA, T. (2000). Comparative Demography of Three Hawaiian Fruit Flies (Diptera: Tephritidae) at Alternating Temperatures. *Ann. Entomological Soc. Am.* 90: 162-180.
- WILSON, M.J., HAVLER, M. and DEARDEN, P.K. (2010). Giant, Kruppel, and caudal act as gap genes with extensive roles in patterning the honeybee embryo. *Dev Biol* 339: 200-211.
- YONG, H.S., SONG, S.L., LIM, P.E., EAMSOBHANA, P. and SUANA, I.W. (2016). Complete Mitochondrial Genome of Three *Bactrocera* Fruit Flies of Subgenus *Bactrocera* (Diptera: Tephritidae) and Their Phylogenetic Implications. *PLoS One* 11: e0148201.
- ZHENG, W., LUO, D., WU, F., WANG, J. and ZHANG, H. (2016). RNA sequencing to characterize transcriptional changes of sexual maturation and mating in the female oriental fruit fly *Bactrocera dorsalis*. *BMC Genomics* 17: 194.